Politecnico di Milano

SCHOOL OF INDUSTRIAL AND INFORMATION ENGINEERING
Master of Science – Biomedical Engineering

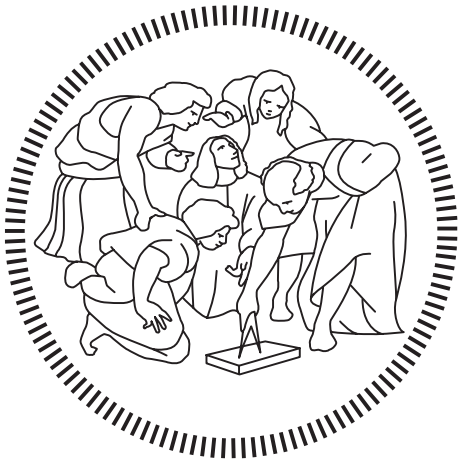

Analysis of upper-limb and trunk kinematic variability: accuracy and reliability of an RGB-D sensor

Supervisor
Prof. Pietro Cerveri

Co-Supervisor
Ing. Alessandro Scano, PhD

Candidate
Robert Mihai Mira – 905055

Academic Year 2019 – 2020

Acknowledgements

I would like to thank Prof. Pietro Cerveri and Eng. Alessandro Scano for their support in writing this document.
I would like to thank my parents and family who gave me the opportunity to embark on this adventure in the Politecnico di Milano and who have always supported me in my choices and activities.
I would like to thank all my friends for being by my side and for their support.

Abstract

Background: It is known that in the field of human motion acquisition, optoelectronic systems using surface markers are considered the gold standard. Despite them being very accurate, these systems are very expensive, require relatively demanding working environments and long preparation times. These characteristics make them unusable in small clinics and in other industrial applications. Thus, the need for cheaper devices, usable in general working environments and featuring faster setup, has become apparent. One appropriate alternative consists of RGB-Depth devices. This paper aims at providing an adequate comparison between the above-mentioned technologies. To that purpose, one representative for each of the two approaches was chosen. The Vicon system (Vicon Motion Systems, U.K.) was chosen as the gold standard system and the Kinect V2.0 (Microsoft, Redmond, USA) as the RGB-Depth sensor.

Methods: In order to achieve the proposed goal, the acquisition protocol was designed to perform two predefined movements in the right upper-limb's workspace (point-to-point and workspace exploration) and each gesture was repeated twice in three workspace sectors. Fifteen subjects were enrolled in the experiment. The motion was simultaneously surveyed by Vicon and Kinect devices. Eleven degrees of freedom (DoFs), describing the upper-limb and trunk kinematic model, were reconstructed and compared across the motion protocol.

Results: DOFs were tracked by the Kinect device with an average error (accuracy) of less than 10°, except for two angles (internal-external rotation of the shoulder and pronation-supination of the forearm). The best tracked workspace sector varied depending on the type of movement considered. For the point-to-point task, the best performance was obtained in the right sector with statistically significant differences to left and central sectors respectively ($p=0.012$ and $p=0.0053$). For the exploration task, the results showed no statistical difference (left-right $p=0.79$) (right-central $p=0.68$) (left-central $p=0.96$) between the sectors. The test-retest showed that the sensor's reliability is quite high in the central and right sector (ICC > 0.75), and lower for the left sector ($0.62<ICC<0.73$).

Conclusions: Commercial RGB-D sensors adequately track the upper limb for biomechanical assessments, even though limitations can be found in specific degrees of freedom and gestures.

Abstract

Contesto: È risaputo che nell'ambito dell'acquisizione del movimento umano, i sistemi di tracciamento basati su marker vengono considerati lo stato dell'arte. Sebbene siano molto precisi, questi sistemi sono molto costosi, richiedono ambienti di lavoro adeguati e lunghi tempi di preparazione. Queste caratteristiche li rendono inutilizzabili in piccole cliniche e in altre applicazioni industriali. Pertanto, è emersa la necessità di dispositivi più economici, applicabili a varie tipologie di scenari e tempi di preparazione più brevi. Un'alternativa appropriata sono i dispositivi RGB-Depth. Questo lavoro mira a fornire un confronto tra le tecnologie sopra menzionate. A tal fine abbiamo scelto un rappresentante per ciascun approccio. Il sistema Vicon (Vicon Motion Systems, Regno Unito) è stato scelto come sistema a stato d'arte e Kinect V2.0 (Microsoft, Redmond, USA) come sensore RGB-D.

Metodi: Al fine di raggiungere l'obiettivo proposto, è stato stabilito un protocollo, e sono stati reclutati 15 partecipanti. Ad ogni soggetto è stato richiesto di eseguire due gesti predefiniti nell'area di lavoro dell'arto superiore destro (punto-a-punto ed esplorazione dell'area di lavoro) e ogni gesto è stato ripetuto due volte in tre settori dell'area di lavoro. All'interno di questo protocollo, abbiamo testato l'accuratezza e l'affidabilità dei sensori RGB-D attraverso il confronto di undici gradi di libertà associati all'arto superiore e al tronco. L'esecuzione di ogni movimento è stata registrata con entrambi i dispositivi e confrontata attraverso la differenza angolare euclidea di ciascun grado di libertà comparata tra i due dispositivi.

Risultati: Le variabili relative all'arto superiore sono state monitorate con una differenza media (precisione) inferiore a 10°, tranne 2 angoli (rotazione interna-esterna della spalla e pronazione-supinazione dell'avambraccio). In generale, si è trovato che il settore dello spazio di lavoro in cui si riscontrano le prestazioni migliori, varia a seconda del tipo di movimento considerato. Per il movimento di punto-a-punto, abbiamo rilevato che le prestazioni migliori sono state ottenute nel settore destro con differenze statisticamente significative rispettivamente con i settori sinistro e centrale ($p = 0,012$ e $p = 0,0053$). Per il movimento di esplorazione, i risultati non hanno mostrato differenze statistiche tra i settori (sinistra-destra $p = 0,79$) (centro-destra $p = 0,68$) (centro-sinistra $p = 0,96$). Il test-retest ha dimostrato che l'affidabilità del sensore è piuttosto elevata nel settore centrale e destro ($ICC > 0,75$) e inferiore per il settore sinistro ($0,62 < ICC < 0,73$).

Conclusioni: I sensori RGB-D commerciali sono adeguati a tracciare l'arto superiore al fine di fornire valutazioni biomeccaniche, anche se si possono trovare limiti rilevanti in specifici gradi di libertà e gesti.

Table of Contents

List of Figures

List of Tables

Chapter 1 State of the art

1.1 Human Motion Analysis

Human motion analysis (HMA) is a domain in the biomechanics field aiming at quantitatively describing the human movement, which is traditionally acquired by means of motion tracking technologies. The applications of HMA span many areas ranging from clinics and motor rehabilitation to industrial and entertainment fields (Colyer S. L. et al. 2018).

During the last decades, many instruments and devices have been developed in order to objectively quantify the parameters of human motion, ranging from mechanical devices like protractors to more sophisticated inertial sensors and other technologies, such as optical tracking systems. Specifically, the gold standard in this field are considered to be marker-based optoelectronic tracking systems. By placing the markers on anatomical landmarks on the subject's body, such systems allow a precise reconstruction of the kinematic parameters. Many studies describe a variety of usages for optoelectronic tracking equipment, for example the estimation of position and orientation of bones based on the position of markers on the skin (Cappozzo A. et al. 1995), (Cappozzo A. et al. 1996), (Lu T. W. et al. 1999) or the estimation of joint-centers' position (Nussbaum M. A. et al. 2000). Certain studies developed methods to estimate muscle forces related to elbow flexion movement (Pontonnier C. et al. 2009). Other studies focused on the functional evaluation of the kinematics of the upper extremities (Roux E. et al. 2002), (Petuskey K. et al. 2007). However, the high performance of marker-based optical tracking systems is associated with time-consuming marker-positioning procedures, heavily constrained working environments, such as laboratories, and a high financial cost. These restraints limit the use of such systems in less controllable environments, such as in scientific research laboratories, hospitals, small clinics, and for home rehabilitation as well as industrial applications. These limitations have led to a need for systems with faster setup time, more flexible acquisition environments and lower financial costs (Colyer S. L. et al. 2018).

The development of inertial sensors and RGB/RGB-Depth sensors has aided in overcoming the limits imposed by marker-based optoelectronic systems. RGB-D sensors allow the reconstruction of human motion via video frame segmentation coupled with depth analysis (D'Orazio et al. 2016).

Certain low-cost devices which have overcome some limits of the state-of-the-art systems are already available. Devices such as Microsoft Kinect, Kinect V2, Asus Xtion, XSens, Intel Creative, Leap Motion, Nintendo Wii Balance Board, and Wiimote. All these devices permit the tracking of human motion with less preparation time in more relaxed settings. XSens technologies work by integrating inertial sensor data with GPS data to reconstruct human motion in three-dimensions. Leap motion technologies are specialized in VR rendering and tracking of smooth hand gestures. The full system works with 2 RGB cameras and 3 infrared LEDs to identify fine movements of the hand or of small objects, such as pens. The Nintendo Wii balance board tracks the

position of the person's center of pressure. The Wiimote tracks the motion of the hand through inertial sensors integrated in the remote. Kinect, Kinect V2 and Asus Xtion are devices which use a combination of RGB cameras as well as time-of-flight infrared cameras. Specific studies have compared the two generations of Kinect and presented the Kinect V2 as the better version of the two (Diaz M. G. et al. 2015), (Pagliari D. et al. 2015). The embedded joint tracking algorithms make the device one of the most valuable and affordable substitutes for marker-based systems. Microsoft's Kinect V2, compared to other technologies, has a faster set-up time, identifies larger range of motion and provides a better motion reconstruction.

1.2 Medical applications of low-cost devices

In the area of human motor rehabilitation, the data obtained from motion tracking systems are used for medical treatment plans and evaluations. With the technological development, improved ways to asses the kinematics of the human body were developed, integrating them to the already existing clinical scales (Zhou H. et al. 2008). These new technologies have been used to objectively asses the arm impairment of patients suffering from multiple sclerosis (Carpinella I. et al. 2014). Some of the most valuable devices have become the optoelectronic marker-based systems. Certain studies have tested the reliability of technologies in evaluating the kinematics of neurologic patients (Ferrarin M. et al. 2011). Specific studies explored these technologies in clinical contexts to compare the parameters of stand-up movements of healthy subjects versus hemiplegic patients (Galli M. et al. 2008). Other studies have conducted gait analysis tests on children with different types of cerebral palsy in order to compare their motor strategies with those of healthy children's (Galli M. et al. 2010).

With the advent of marker-less systems and improved wearable sensors, these technologies gained relevance within clinical settings. Devices such as Kinect and Kinect V2 have been tested and confirmed to be reliable for recording the kinematics of the upper limb when compared to marker-based systems (Kultu M. et al. 2017), (Bonnchere B. et al. 2014). Applications of low-cost RGB-D systems in the field of rehabilitation and health include a variety of studies, ranging from biomechanical assessments (Cruz L. et al. 2012), (Clark R. A. et al. 2015), (Yang Y. et al. 2014), (Yahya M. et al. 2019), translation of quantitative clinical scales (Scano A. et al. 2018), (Kim W. S. et al. 2016), (Fern'ndez-Baena A. et al. 2012), post-stroke patients' assessments (Morrow K. et al. 2006), (Moyà-Alcover G. et al. 2019), (Scano A. et al. 2015), (Scano A. et al. 2019), validation for their usage in home environments (Gu Y. et al. 2019), (Cameirão M. et al. 2016),) and ambient of assisted living (Mosca N. et al. 2017).

The first generation of Microsoft's Kinect was released in 2010 in the videogame industry. Since its release, Kinect's versatility has been put to the test in medical and rehabilitative environments. In certain cases, it was used as an aid in motor gestures performance of children or neurological patients (Chang Y. J. et al. 2011), (Chang Y. J. et al. 2013), in evaluation of cognition during training (González-Ortega D. et al. 2014), training of selective movements of the pelvis (Summa S. et al. 2015), and in other cases as support for virtual reality rehabilitative training sessions during the execution of functional motor tasks (Pedraza-Hueso M. et al. 2015), (Lange B. et al. 2011), (Mottura S. et al. 2014), (Gotsis M. et al. 2014), (Brokaw E. B. et al. 2015). A review concluded that Kinect can be considered as an adequate tool for supporting rehabilitation demands (Mousavi H. et al. 2014). Another review (Da Gama et al.2015) stated that possible future works using the Kinect in rehabilitative applications are extensive. According to (Bonnechere B. et al. 2014), even though there are

differences in the range of motion (ROM) of specific body articulations, such as shoulder, elbow, hip and knee, Kinect's reconstruction ability is comparable to that of marker-based systems. The accuracy of the device is very important when employing it for biomechanical evaluations, since clinicians must prescribe treatment plans based on reliable, repeatable and comparable data. A study (Kurillo G. et al. 2013) suggests that the 3D available workspace of the upper limb registered with the Kinect provides sufficiently accurate and reliable results compared to the one obtained through motion capture systems. Similar results were obtained by evaluating shoulder's range of motion (Lee S. H. et al. 2015). There are specific studies which highlight the existence of clinically significant discrepancies in the evaluation of shoulder angles. The authors suggest that more studies should be conducted on evaluating the limits of this device (Huber M. E. et al. 2015).

The second generation of Microsoft devices was released in 2014 under the name of Kinect V2, featuring a more precise 25-joint tracking. Some of the most common Kinect V2 applications follow the gaming paradigm (Cameirão M. S. et al. 2016), which tries to make training sessions more interactive and incentivize the patient to participate by designating objectives or assigning a score based on performance. These applications rely on the interaction with simple virtual environments or games that hide the purpose of functional rehabilitation (Vieira A. et al. 2016). Certain studies used the Kinect V2 to study postural control (Clark R. A. et al. 2015), concluding that the results were generally comparable to the ones obtained by marker-based systems. Further applications have seen this device used for gait analysis on healthy adults and it was demonstrated that the Kinect V2 recorded effectively the parameters of interest (Dolatabadi E. et al. 2016). According to a study (Darby J. et al. 2016), the Kinect V2 sensor was used for assessing the position and orientation of the head and was able to offer a state-of-the-art head pose estimation in real time and without any need for calibration.

Certain studies have used RGB-D sensors to create a database in order to support the evaluation of neurological patients (Scano A. et al. 2017), while others have evaluated the performance of the device in tracking the movements of impaired limbs of post stroke patients with respect to healthy subjects, finding no statistical differences between the two groups (Scano A. et al. 2019). Tests have been performed in order to determine the precision of upper limb tracking of this device, concluding that it is acceptable for use in clinical applications or in motor performance evaluations (Chen Y. C. et al. 2015). Further studies proposed in their preliminary results that RGB-D sensors are suitable tools for tracking the kinematics of the upper limb. Furthermore, preliminary results indicate that they might also be used efficiently for patient evaluation by presenting data consistent with clinical scale evaluations (Scano A. et al. 2016). Similarly, encouraging results were found in a study in which motion analysis tests were conducted on a cohort of Parkinson patients, suggesting that these devices could be used to analyze the kinematics of impaired subjects (Rocha P. et al. 2015). A good correlation between parameters computed by both systems was found in another study having its focus on gait analysis evaluations (Eltoukhy M. et al. 2015). Another study (Ozturk et al. 2016) describes that the Kinect V2 was used to evaluate a small cohort of neurological patients. Other studies dealt with issues of repeatability of measurements using Kinect V2 and revealed promising results which can be further investigated (X. Chen et al. 2017).

1.3 Industrial applications

Human motion tracking has only recently acquired visibility in industrial contexts. Recent roadmaps (Terkaj W. et al. 2019), (Santos C. et al. 2017) suggested the need of human-centered approaches and solutions for improving workers' health, injury prevention and motion tracking applicability in working environments (Geiselhart F. et al. 2016). Thus, in recent years, there has been a growing interest in motion tracking technologies since they became widely available and strategically relevant outside of standard clinical environments. A first field of application was injury prevention: it has been suggested that, as most manual labor-intensive roles in industry require elaborate movements in unmonitored environments, this could lead to injuries and work-related injuries (Christy Du et al. 2007). Secondly, motion tracking systems could provide data on the stress and strain imposed on the human body, thus helping to improve workstation safety (Christy Du et al. 2007), avoid unnecessary work hazards and ensure safe and successful human-robot interactions (Ramey A. et al. 2011), (Basso F. et al. 2013). Moreover, tracking technologies have been used to properly provide designers with data to help them improve products, by increasing their ease of use (Colombo G. et al. 2013), (Myroslav Bachynskyi et al. 2014). An offline use of motion tracking is found in a recent work (Pellegrinelli S. et al. 2016) that presented a method by which changing the manipulator's behavior in volume sections has had a higher probability to find a human cooperator. Occupied volumes were computed based on pre-recorded data of the human motion.

Another important aspect of both industrial and rehabilitative motion capture deals with possible obtrusive settings, such as when interacting with a robot. In certain human-robot interactions, the machine is required to co-operate or mimic operators; motion tracking is essential to avoid harmful or unwanted interactions (Glasauer S. et al. 2010). Certain works have proposed methods of motion tracking integrated in the context of human-robot interaction, in order to achieve this goal (Field M. et al. 2009).

Lastly, it is noteworthy that many recent laboratory studies used bio-inspired approaches based on tracking systems to assess human-robot interaction, when testing devices for assisting manual works (Kim S. et al. 2018). These recent works aim to translate biomedical technologies to industrial settings.

1.4 Comparing gold standard systems and low-cost devices

Given the major application of human motion tracking in clinical settings and the growing interest in human-centered approaches even outside of the biomedical field, certain studies were performed in order to assess the usability of RGB-D devices and assess their accuracy and reliability with respect to gold standard systems (Bonnchere et al. 2014), (Scano A. et al. 2014), (Pfister A. et al. 2014), (Otte K. et al. 2016), (Cai L. et al. 2019). Comparing a marker-based system with Kinect (Bonnchere B. et al. 2014), (Scano A. et al. 2014), the authors showed good sensitivity of the RGB-D sensor, even though they focused on a small sample of subjects and only reaching movements. Another study (Pfister A. et al. 2014) has shown a high correlation between the gait parameters registered with a marker-based system and those registered by the Kinect device, confirming its effectiveness, although they suggest further improvements in its sensitivity for appropriate use in a clinical environment. The accuracy of the Kinect V2 in full body acquisitions, focused on walking and balance control, has been tested (Otte K. et al. 2016), concluding that Kinect V2 could achieve a good level of precision for motion analysis. Another work (Cai L. et al. 2019) concentrated only on specific degrees of freedom of the upper limb. They tested the accuracy of the sensor and found that the RGB-D sensor could approximate the

results of the marker-based system, even though the range of movements analyzed was quite limited. A thorough analysis (Galna B. et al. 2014) studied in detail the performance of Kinect in movement tracking with respect to the Vicon system. From the results of the study, one can conclude that the system is suitable for motion tracking with limited movements. Another study presented a detailed analysis aimed at verifying the suitability of the RGB-D devices as a tool in rehabilitation environments (Giancola S. et al. 2017). This study compared Microsoft's Kinect V2 and a marker-based acquisition system, indicating that there is no systematic bias between the two acquisition systems and that there was a high correlation between most of the parameters of interest.

In general, it has been found that there was a limited number of studies that focused on assessing the validity of RGB-D sensors in evaluating the upper-limb movement which related to tasks exploring the full extent of the workspace. Specifically, it was noted that previous studies in this field concentrated mainly on classic rehabilitation tasks, rather than mapping the variety of upper-limb gestures typical of working and real-life applications.

1.5 Aim

The aim of this study was to provide a comparison of the Kinect V2 device with the Vicon system regarding the tracking capabilities of the upper limbs and trunk of the human body during simulated daily life gestures. These data will be used for applications in rehabilitation and industrial scenarios in the context of a newly founded European project 'Mindbot' (https://cordis.europa.eu/project/id/847926). The tests were performed in the motion acquisition laboratory of the National Research Council of Italy (Consiglio Nazionale delle Ricerche - CNR) in Italy, Lecco.

Chapter 2 Materials and methods

2.1 Participants

The participants were recruited in order to create a homogeneous group of 15 people belonging to a similar age range with no evident musculoskeletal impairments. Table 2.1 presents a list of the participants to the study and their physical characteristics, such as age, height, weight and dominant limb.

Table 2.1. List of subjects and their physical attributes

Subject ID	Height [m]	Weight [kg]	Dominant limb	Sex	Age [years]
Subject 1	1.78	65	Right	M	24
Subject 2	1.66	54	Right	F	23
Subject 3	1.79	80	Right	M	35
Subject 4	1.77	57	Right	M	24
Subject 5	1.72	65	Right	F	20
Subject 6	1.71	62	Left	F	19
Subject 7	1.75	63	Right	M	19
Subject 8	1.75	85	Right	M	22
Subject 9	1.67	52	Right	F	23
Subject 10	1.62	53	Right	F	25
Subject 11	1.65	48	Right	F	24
Subject 12	1.88	75	Right	M	24
Subject 13	1.80	80	Right	M	24
Subject 14	1.58	49	Right	F	25

2.2 Equipment

For completing the proposed tasks, the motion acquisition laboratory was equipped with:

A Vicon Vero system composed of 10 infrared cameras; a set of reflective markers for motion tracking with the Vicon system. In this experimental condition, a total of 34 markers were used, 25 for subject preparation and 9 as references on the target;

One Kinect V2.0 device (Figure 2.1 left panel) for human body tracking in space using 2 cameras, one RGB, for frame acquisition with sampling frequency around 30Hz, and a time of flight infrared camera, for depth sensing;

Two general purpose computers: one connected to the Vicon system and containing the software for the acquisition and for the pre-processing of the data, and the other general-purpose device containing a custom-made software in C#, which communicated directly with the Kinect device and is able to return a file containing 25 points of interest composing the SDK Kinect Skeleton;

A circular target (Figure 2.1 right panel**)** of 60 cm of diameter with 9 points of interest named N, NE, E, SE, S, SW, W, NW and O. This target was used as a reference for the subject to execute the required movements (Scano A. et al. 2019).

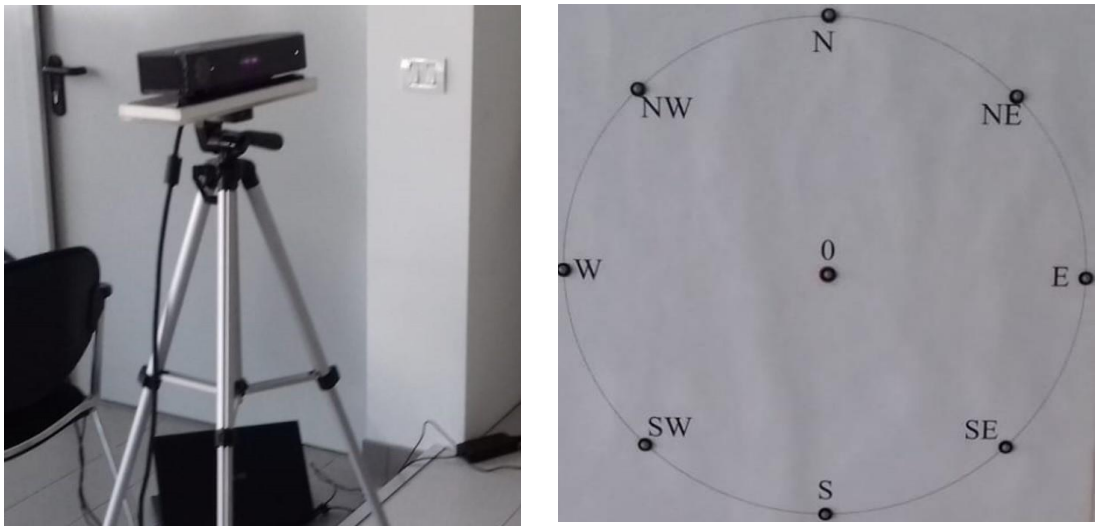

Figure 2.1. Kinect V2.0 device (left panel) and circular target (right panel).

2.3 Movement description

Each subject was asked to execute two types of movements with the right upper limb. The selected tasks were point-to-point and hand exploration movements (Scano A. et al. 2019), commonly adopted in the context of motor rehabilitation. These are gestures extrapolated from daily life activities, which allow exploring the upper limb's available workspace up to its limits.

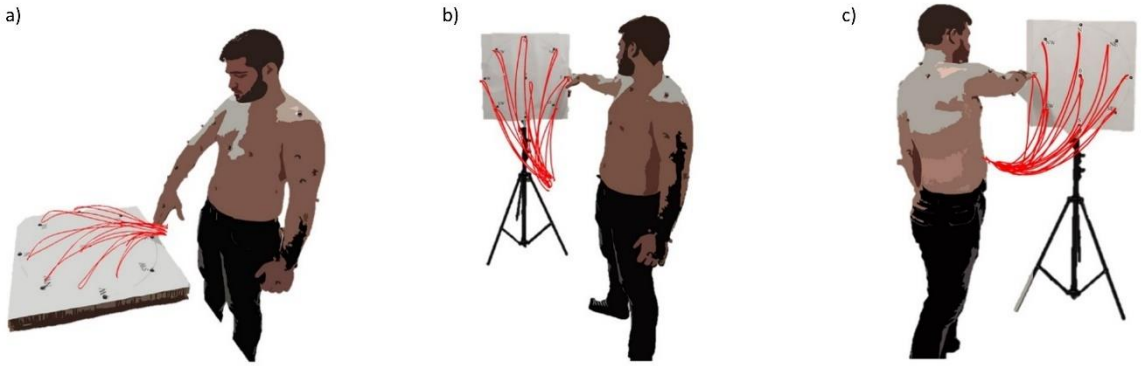

Figure 2.2. Full trajectory of the hand during the point-to-point movement in 3 different sectors of the upper limb workspace.

Point-to-point (Figure 2.2): is a paradigmatic movement used by clinicians to test motor capabilities of patients. It was chosen for its wide use in the rehabilitation contexts (Chen Y. C. et al. 2015). The movement involves multi-joint coordination and is used often in daily life activities. The subject started from a predefined resting position with the upper arm leaning along the body, then reached toward a specific point on the circular target and then returned to the starting position. The first movement, performed by each subject, was reaching towards the 'O' point, then back to resting position. Afterwards the subject pointed to 'NE', back to resting position, and then continued the motion pattern clockwise until reaching the 'N' point, and backwards.

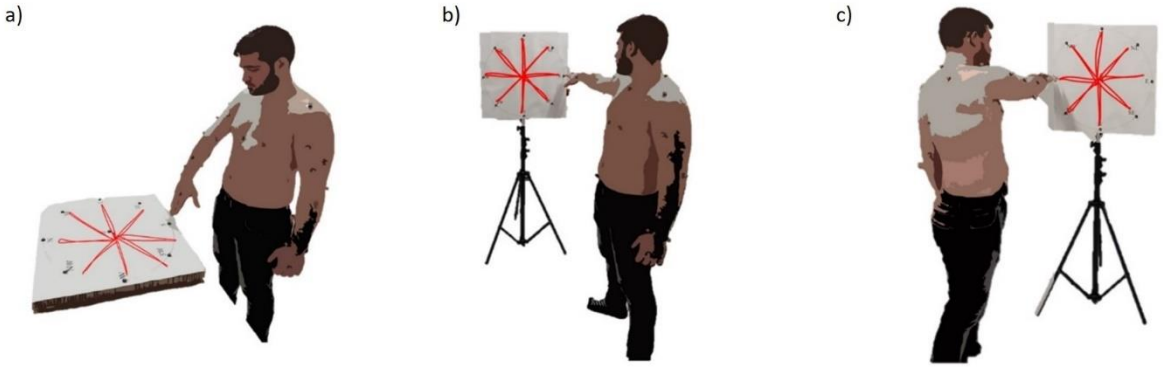

Figure 2.3. Full trajectory of the hand during the exploration movement in 3 different sectors of the upper limb workspace.

Workspace exploration (Figure 2.3): is another gesture conceived to simulate movements on a working surface and object displacement for distal limb coordination. For this movement, like the previous one, a circular target was used as reference to drive the subject's movement. The objective of each participant was to move the hand radially across the target, starting from the resting position and going to different points on the circumference. The resting position for this movement was upright with the hand pointing towards the 'O' point. The first movement was towards 'NE', then back to 'O', and the motion pattern proceeded clockwise until the subjects reached 'N', and finally back to 'O'.

2.4 Experimental Set-up

2.4.1 Motion acquisition laboratory set-up

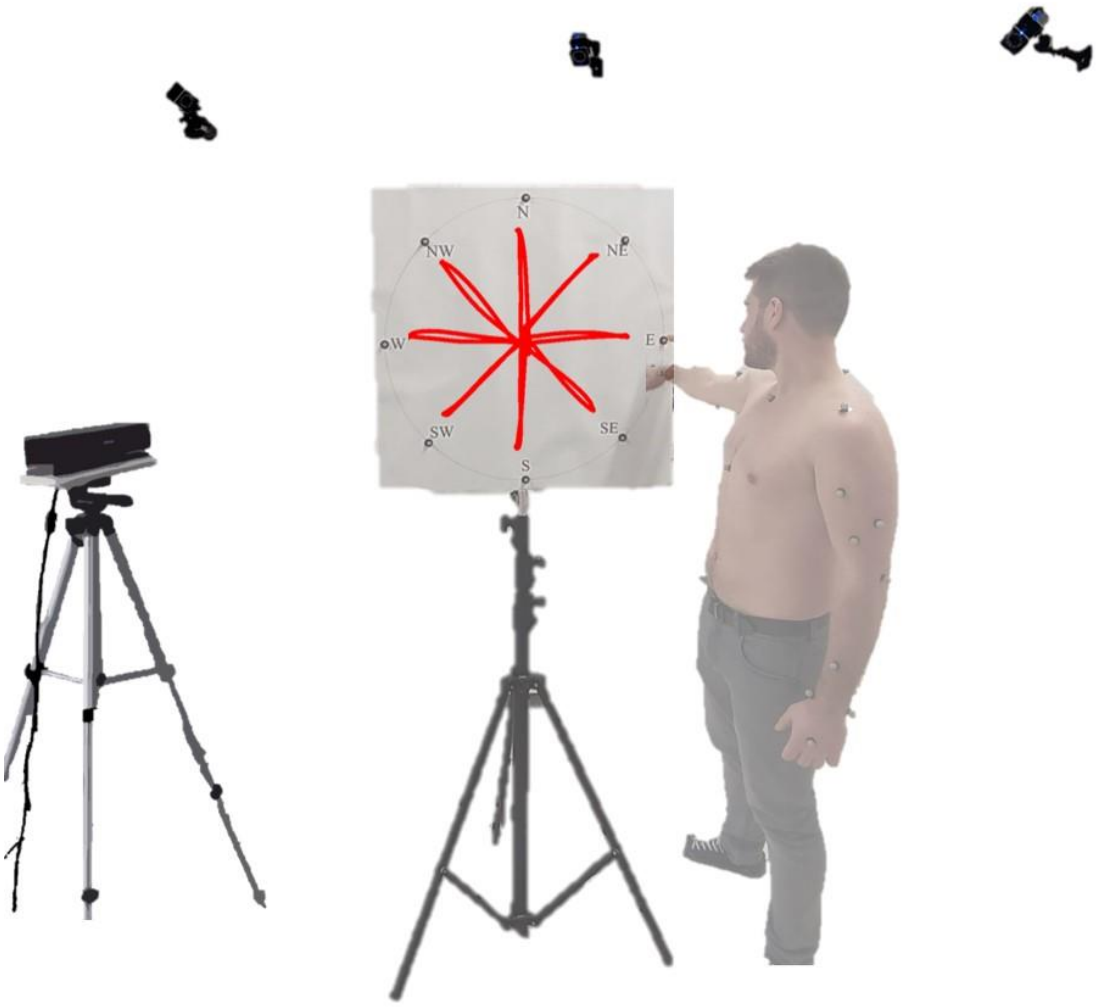

Figure 2.4. Experimental set-up.

The necessary equipment was placed in the acquisition volume of the Vicon system. The subject faced frontally with respect to the Kinect at 2.5m away from the device (Otte K. et al. 2016). Each type movement was performed in three different positions within the subject's workspace in order to test a bigger portion of the device's field of view. The three positions selected for the target were in front of the subject (Figure 2.2 and Figure 2.3 a),on the right side of the subject (Figure 2.2 and Figure 2.3 b) and on the left side of the subject (Figure 2.2 and Figure 2.3 c). Furthermore, each movement was performed twice by each subject. A typical acquisition condition is represented in Figure 2.4.

2.4.2 Subject Preparation

The subject was required to either wear a tight sleeveless T-shirt or to be shirtless in order to be able to attach the markers on the skin. The markers are placed according to the upper limb model designed for the Vicon system (Figure 2.5), 5 markers are placed on the trunk of the participant, one on each shoulder, 3 on each upper arm, 2 on each elbow, 3 on each forearm and one on each hand, for a total of 25 markers.

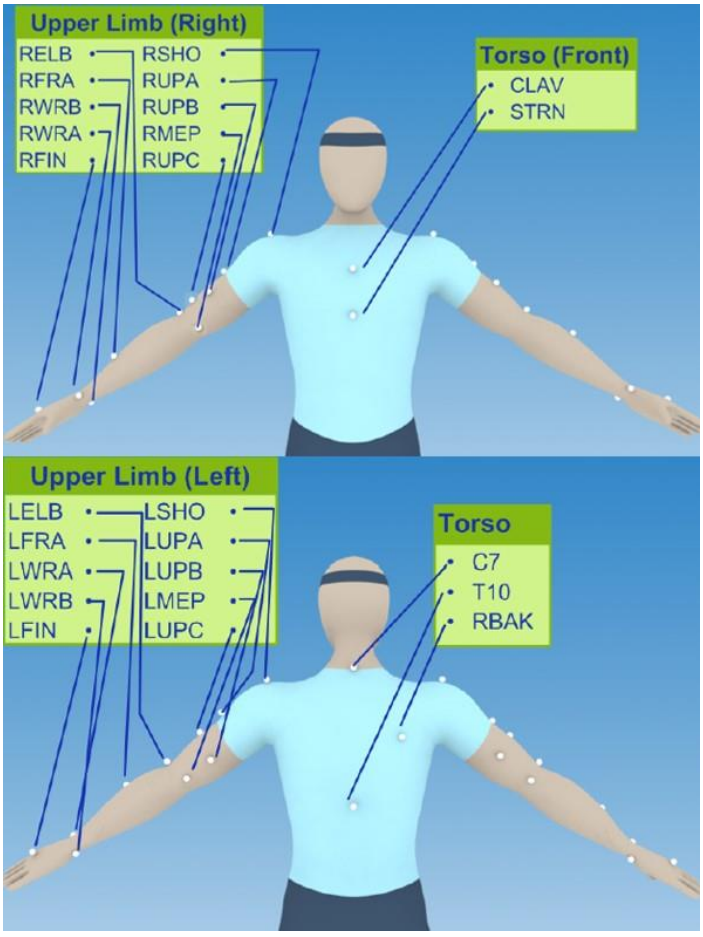

Figure 2.5. Position of markers according to the upper limb model. The upper chart represents the front view of the subject. The lower chart represents the back view of the subject.

2.5 Acquisition protocol

Before each recording session, the Vicon was calibrated in order to make corrections for the changes in the acquisition environment, such as different lighting conditions.

The datasets were acquired in the previously described environment concurrently with the chosen systems. Since the software guiding the Kinect and the Vicon system worked on different computers, the acquisition of the data could not start at the same time. For consistency, it was chosen to always start the recording with Vicon and only later with the Kinect. At the signal of the operator the subject had to start the movement. During the time periods when only one system was registering, it was paramount that the subject did not move.

The data registered with the Kinect were the positions of 25 anatomical points corresponding to the SDK skeleton (Figure 2.6), each associated to a point of interest of the body. In this study, the points of interest used were the ones regarding the right upper limb and the trunk.

On the other hand, the data acquired with the Vicon system were the positions of the 25 markers necessary to the use of the upper limb model. The upper limb model (Figure 2.7) requires a static acquisition for subject calibration, through which it reconstructs the joint centers of interest. The static calibration pose was upright with the arms straight along the trunk and the palms facing forward.

All files were named with the subject's ID, a sequence of 3 letters identifying the registered type of movement, a sequence of 2 letters identifying the orientation and lastly a number identifying in increasing order each acquisition (e.g. 'Subject_N_RCH_DX_1').

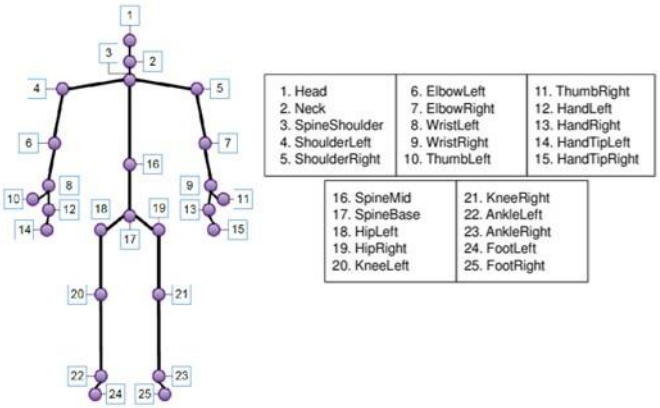

Figure 2.6. Front view of the Kinect V2 SDK Skeleton.

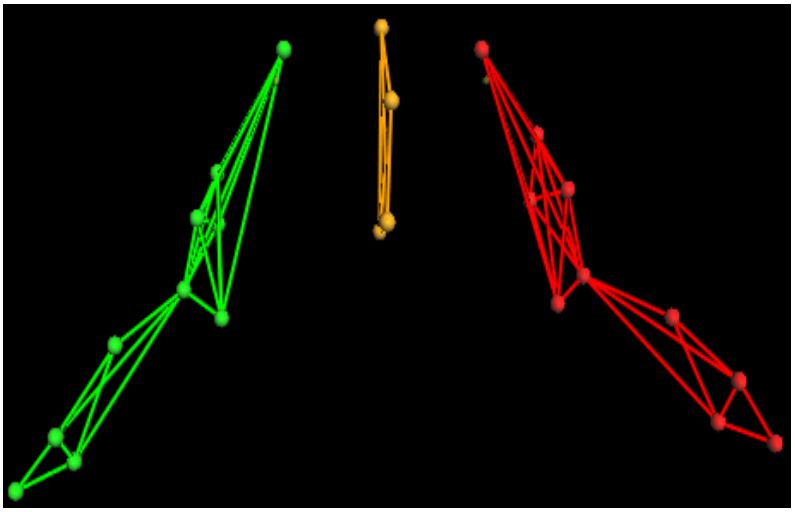

Figure 2.7. Front view of the Vicon upper limb model. The right upper limb is represented with green, the left upper limb with red and the trunk with yellow.

2.6 Data analysis

After the acquisition of the data, the software which communicated with the Kinect provided a file readable by Matlab (Matworks, Natich, MS). The file was structured as a matrix data type containing the time label of each frame and the coordinates of each point composing the SDK skeleton, with respect to the Kinect's reference system.

The dataset acquired with the Vicon system was pre-elaborated in the provided software. All the markers were labeled and tracked in the same virtual environment. Afterwards, using the upper limb model, the software was able to accurately reconstruct the position of the glenohumeral joint centers, humeroulnar joint centers and radiocarpal joint centers of both upper limbs. The data was then saved in a file which could be opened with Matlab.

After the data pre-elaboration, both datasets were analyzed using the same techniques. Both datasets were filtered with a low-pass filter at 5 Hz (Sinclair J. et al. 2013). Afterwards, all the needed degrees of freedom were extracted, 8 describing the right upper limb's movements and 3 describing the trunk's movements. Below, an exhaustive list of the degrees of freedom used in this study is presented:

- shoulder elevation
- shoulder rotation along the vertical axis
- shoulder internal-external rotation
- elbow extension
- hand flexion-extension
- hand pronation-supination
- hand deviation
- scapular elevation
- trunk torsion
- trunk anterior-posterior flexion
- trunk medial-lateral flexion

A subject specific reference system was created using two unit vectors, one aligned with the trunk of the subject ($\hat{t}$) and the other connecting the 2 glenohumeral joint centers ($\hat{s}$). The third vector $\hat{f}$ was computed as the cross product between $\hat{t}$ and $\hat{s}$. It represents the frontal direction with respect to the subject. Furthermore, to be sure that these 3 vectors were linearly independent, $\widehat{s''}$ was computed as the cross product between $\hat{f}$ and $\hat{t}$. And so, the tern $\{\hat{f}\ \hat{t}\ \widehat{s''}\}$ composes the subject specific reference system illustrated in Figure 2.8. All vectors were normalized in order to be unit vectors. This reference system was computed frame by frame and was used to compute the above-mentioned degrees of freedom.

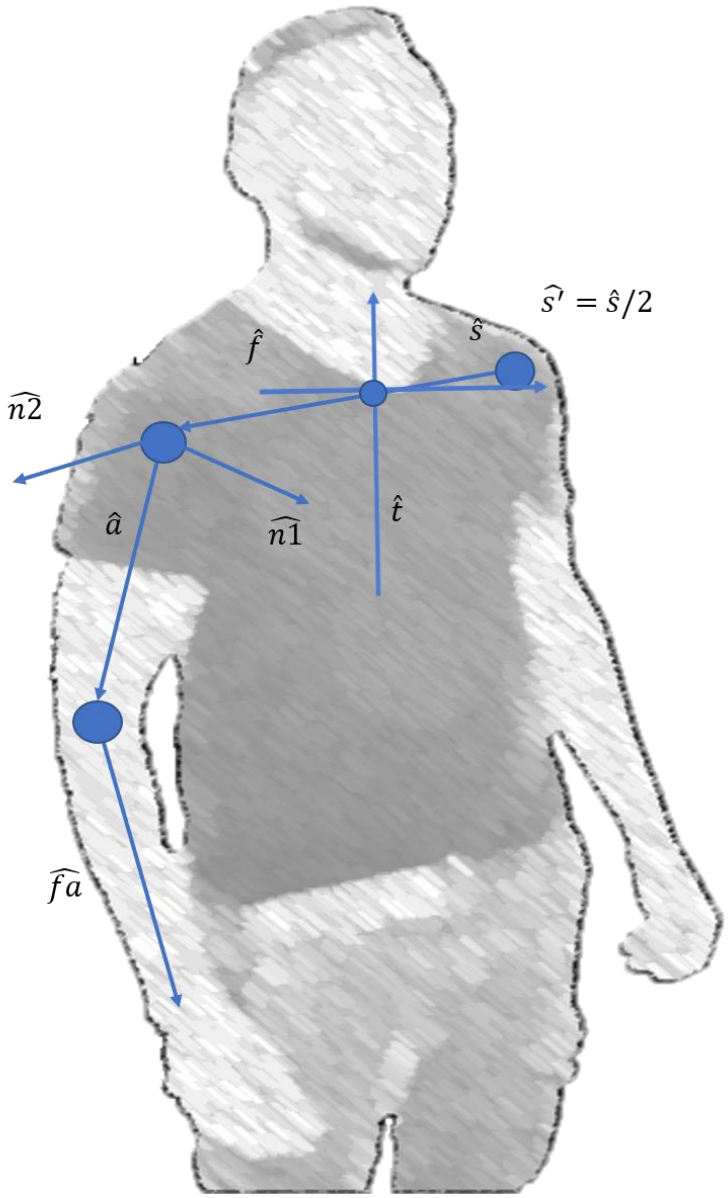

Figure 2.8. Subject specific reference system and local glenohumeral joint center reference system.

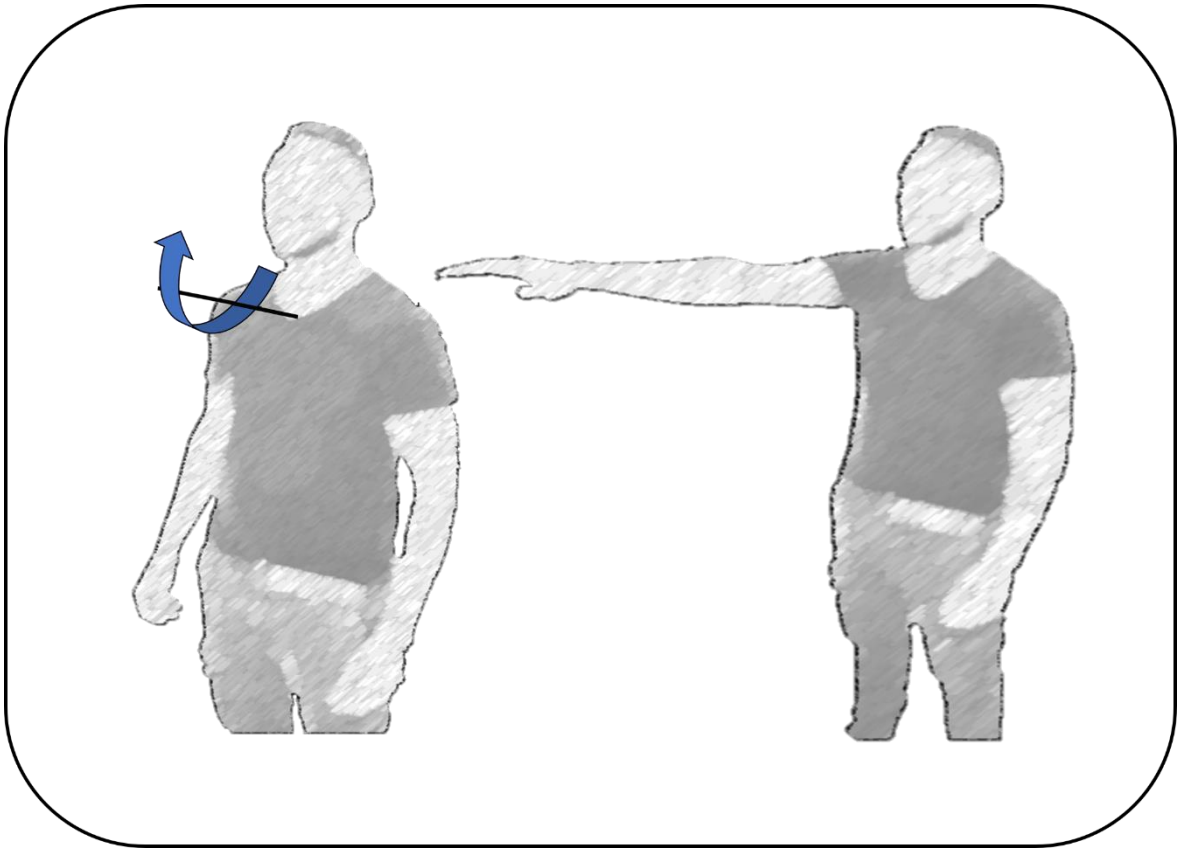

Figure 2.9. Shoulder elevation angle with rotation axis represented with black. The blue arrow indicates the direction of positive values.

Shoulder elevation (Figure 2.9) was the angle formed between the arm unit vector and the negative vertical unit vector of the subject's reference system ($-\hat{t}$). This variable assumed a null value if the upper limb was in the resting position, negative values if the shoulder was hyperextended and positive values if it was flexed. It was calculated as shown in (2.1):

$$Shoulder\ elevation = acos\ [\hat{a} \bullet (-\hat{t})] \quad (2.1)$$

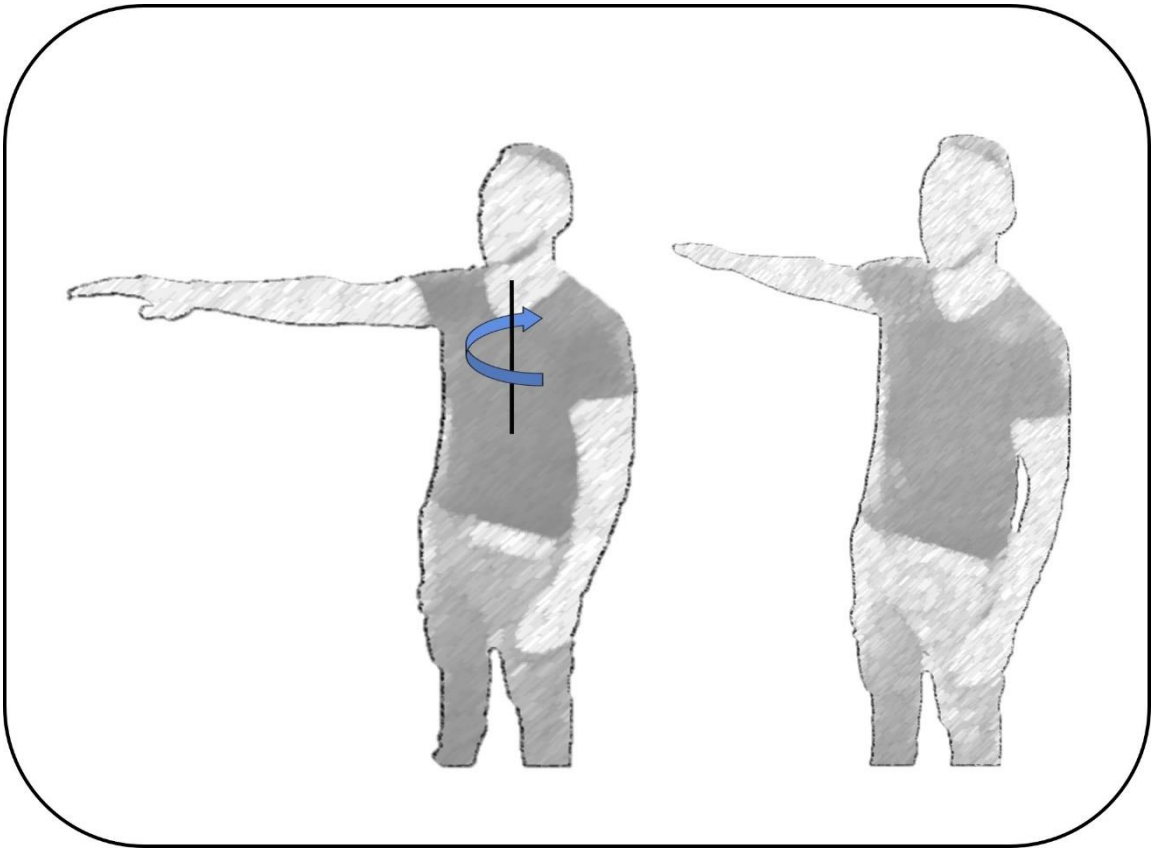

Figure 2.10. Shoulder rotation along the vertical axis with rotation axis represented with black. The blue arrow indicates the direction of positive values.

Shoulder rotation along the vertical axis (Figure 2.10) was chosen to be the angle of rotation of the upper arm vector in the plane Ψ defined by the vectors $\hat{f}$ and $\hat{s}$. To compute this angle the upper arm vector was projected on plane Ψ. The variable of interest was then computed as the angle formed between the projection of the upper arm and the unit vector $-\hat{f}$. The angle was computed as seen in (2.2). Afterwards, an offset was introduced in order to have a null value if the upper arm was aligned with the shoulder vector. This variable assumed positive values when the shoulder was in adduction and negative values when the shoulder was in abduction.

$$Shoulder\ rotation = acos\left[\widehat{ap} \bullet (-\hat{f})\right] - 90 \tag{2.2}$$

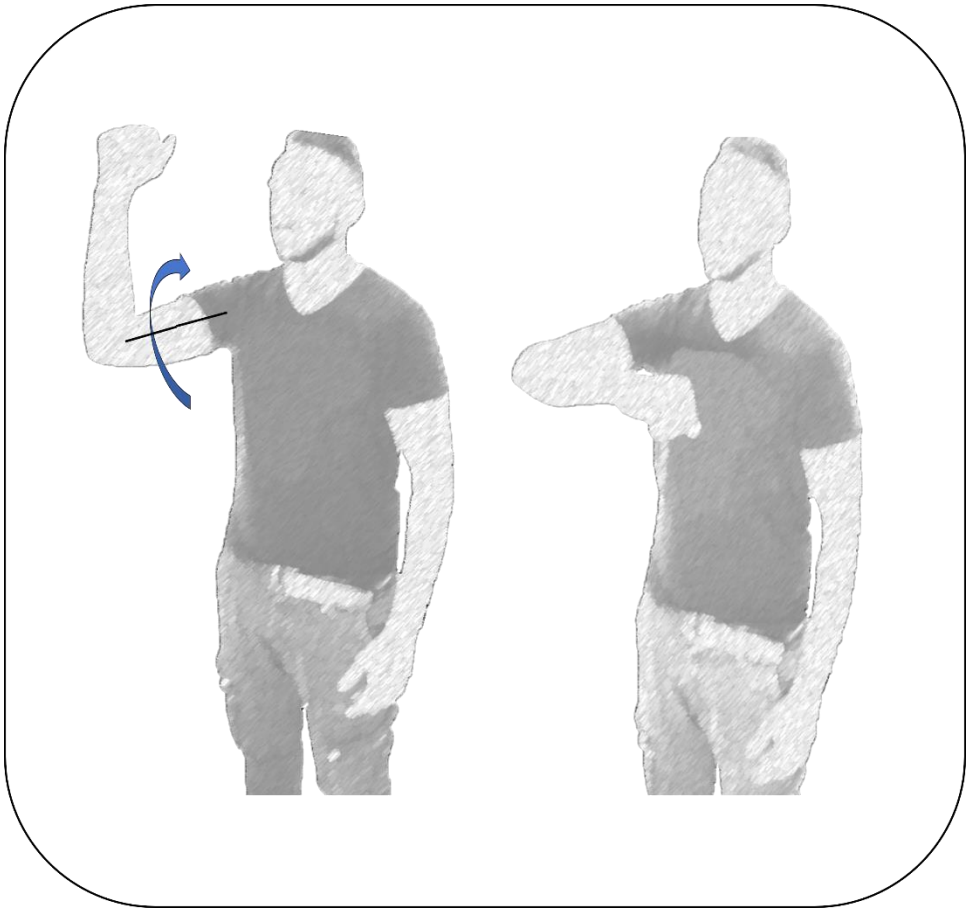

Figure 2.11. Shoulder internal-external rotation with rotation axis represented with black. The blue arrow indicates the direction of positive values.

Shoulder internal-external rotation (Figure 2.11) was considered to be the swiping angle of the arm on the transversal plane of the upper arm. The first step in extrapolating this variable was the computation of the leading vectors of the transversal plane of the upper arm. One of the leading vectors, labeled n1 in Figure 2.8, was computed as the cross product of the shoulder unit vector and the upper arm unit vector. The second leading vector, labeled n2 in Figure 2.8, was calculated as the cross product between the upper arm unit vector and n1. The internal-external rotation was computed as the angle between the projection of the forearm unit vector on the transversal plane and the unit vector n2, as shown in (2.3). Finally, an offset (-90°) was introduced in order to have a null value if the forearm vector was perpendicular to both arm vector and the shoulder vector. The variable computed in this way gave positive values in the case of counterclockwise rotations and negative values in case of the clockwise rotations. All auxiliary vectors described in this section can be visualized in Figure 2.8.

$$Shoulder\ internal - external\ rotation = acos\ (\widehat{af\_p} \bullet \widehat{n2}) - 90 \qquad (2.3)$$

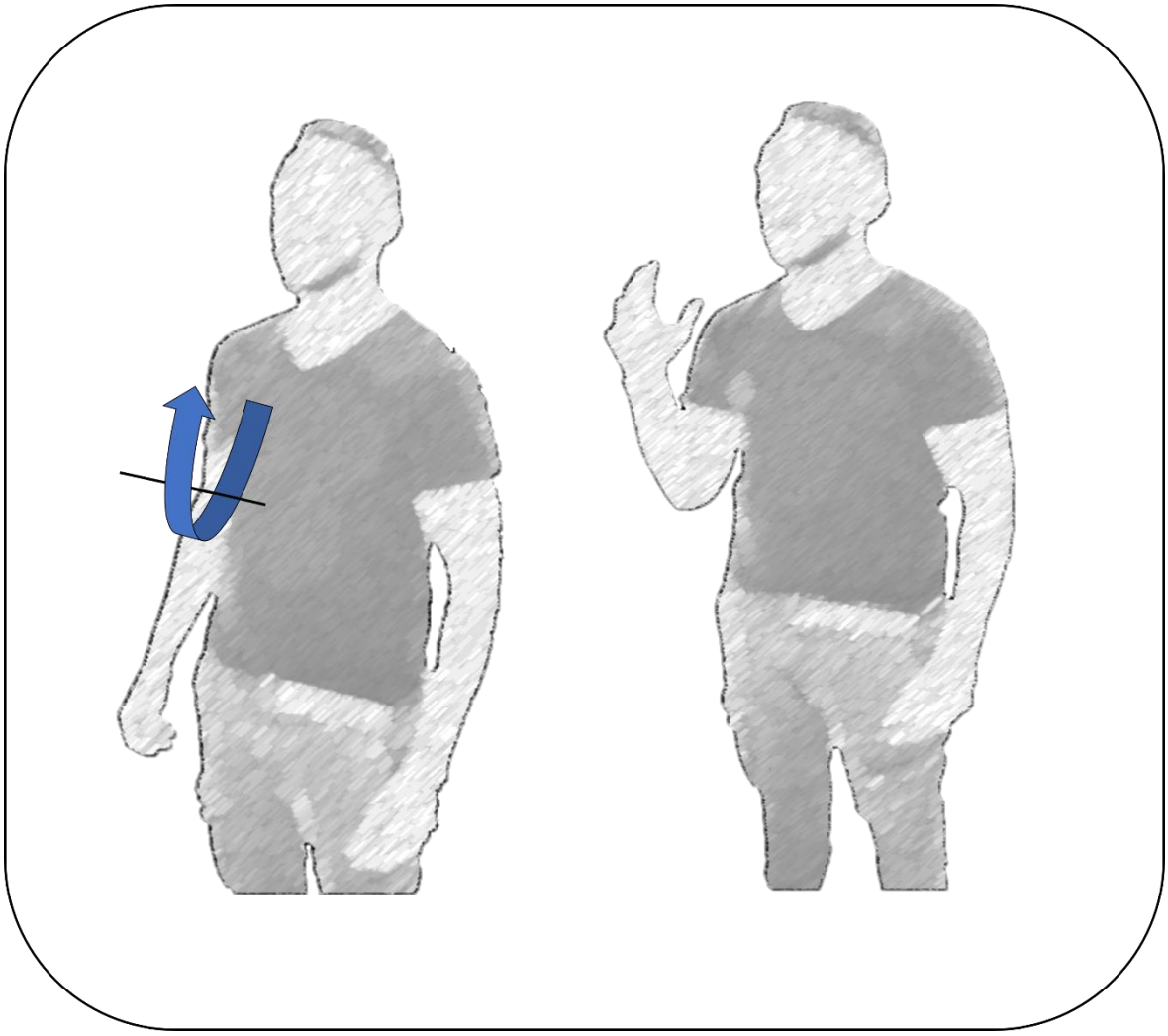

Figure 2.12. Elbow extension with rotation axis represented with black. The blue arrow indicates the direction of positive values.

Elbow extension (Figure 2.12) was the angle formed between the arm unit vector and the forearm unit vector. It was always positive and increased as the elbow was flexed. It was calculated as shown in (2.4).

$$Elbow\ extension = acos\ (\hat{a} \bullet \widehat{af}) \tag{2.4}$$

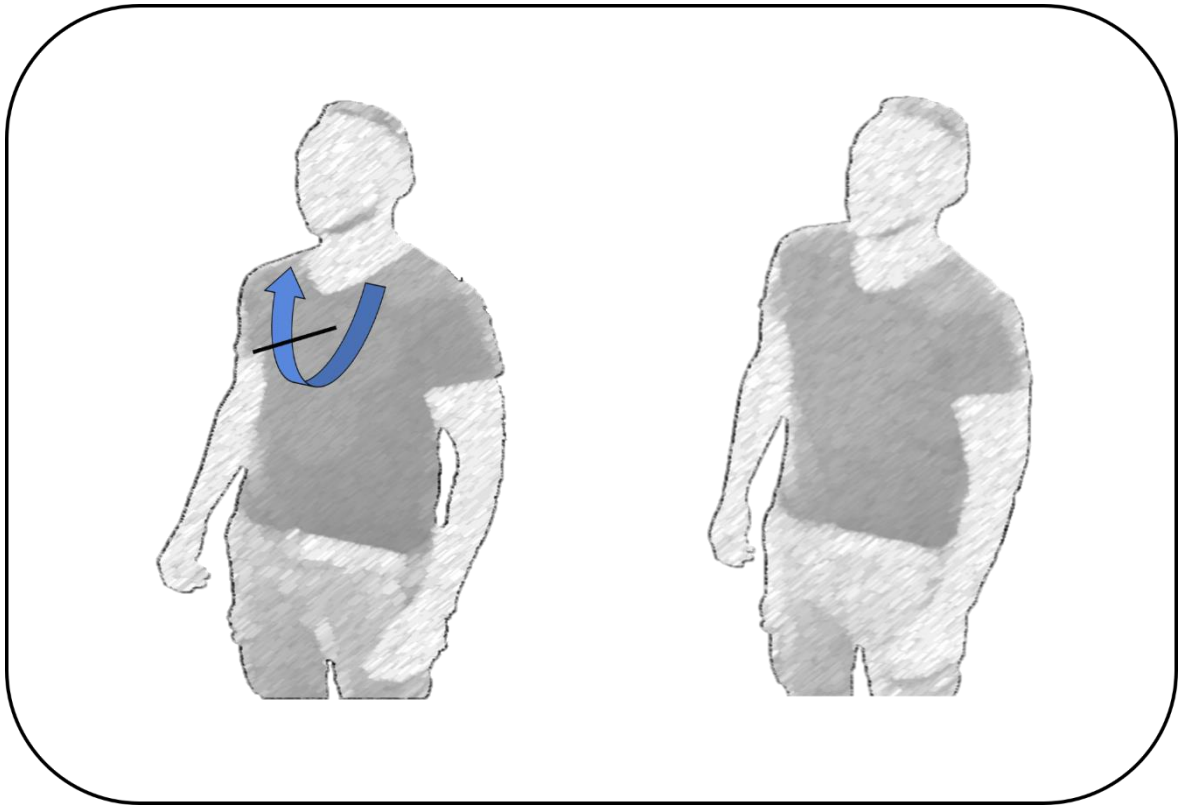

Figure 2.13. Scapular elevation angle with rotation axis represented with black. The blue arrow indicates the direction of positive values.

The scapular elevation (Figure 2.13) was computed as the angle formed between the shoulder unit vector in the initial frame and a vector $\widehat{s'}$. This second vector was a unit vector connecting the midpoint between the two glenohumeral joint centers and the right glenohumeral joint center. It was computed as seen in (2.5).

$$Scapular\ elevation = acos\ (\widehat{s'} \bullet (\hat{s})) \tag{2.5}$$

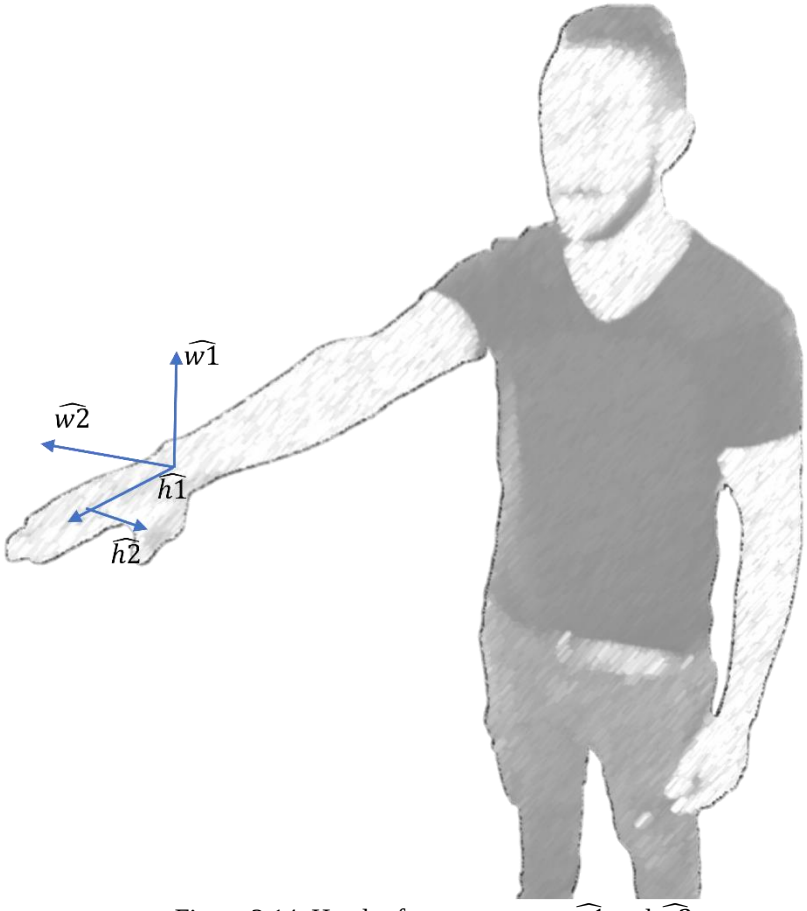

Figure 2.14. Hand reference vectors. $\widehat{w1}$ and $\widehat{w2}$ represent the local reference system. $\widehat{h1}$ approximates the longitudinal direction of the hand and $\widehat{h2}$ approximates the transversal direction of the hand.

The 3 variables used to describe the hand's motion are: hand flexion-extension, hand lateral deviation and hand pronation-supination. All these angles were difficult to compute using only the SDK skeleton of the Kinect for the scarcity of points denoting the width of the forearm. Only one point, associated with the thumb and whose position was not stable in complex movements, proved to be available.

In the process of computing the variables describing the hand's motion, 2 auxiliary vectors were employed. One was computed as the cross product between n2 and the forearm unit vector. This resulting vector was labeled $\widehat{w1}$. The second one, labeled $\widehat{w2}$, was computed as the cross product between the forearm unit vector and $\widehat{w1}$. Both $\widehat{w1}$ and $\widehat{w2}$ were designed to be perpendicular to the forearm and served as references for the movement. Next, the hand was approximated in length and width by 2 vectors $\widehat{h1}$ and $\widehat{h2}$. The first one going from the wrist to the tip of the hand and the second going from the tip of the hand to the thumb. To ease the reader, a visual representation of the above described vectors is presented in Figure 2.14.

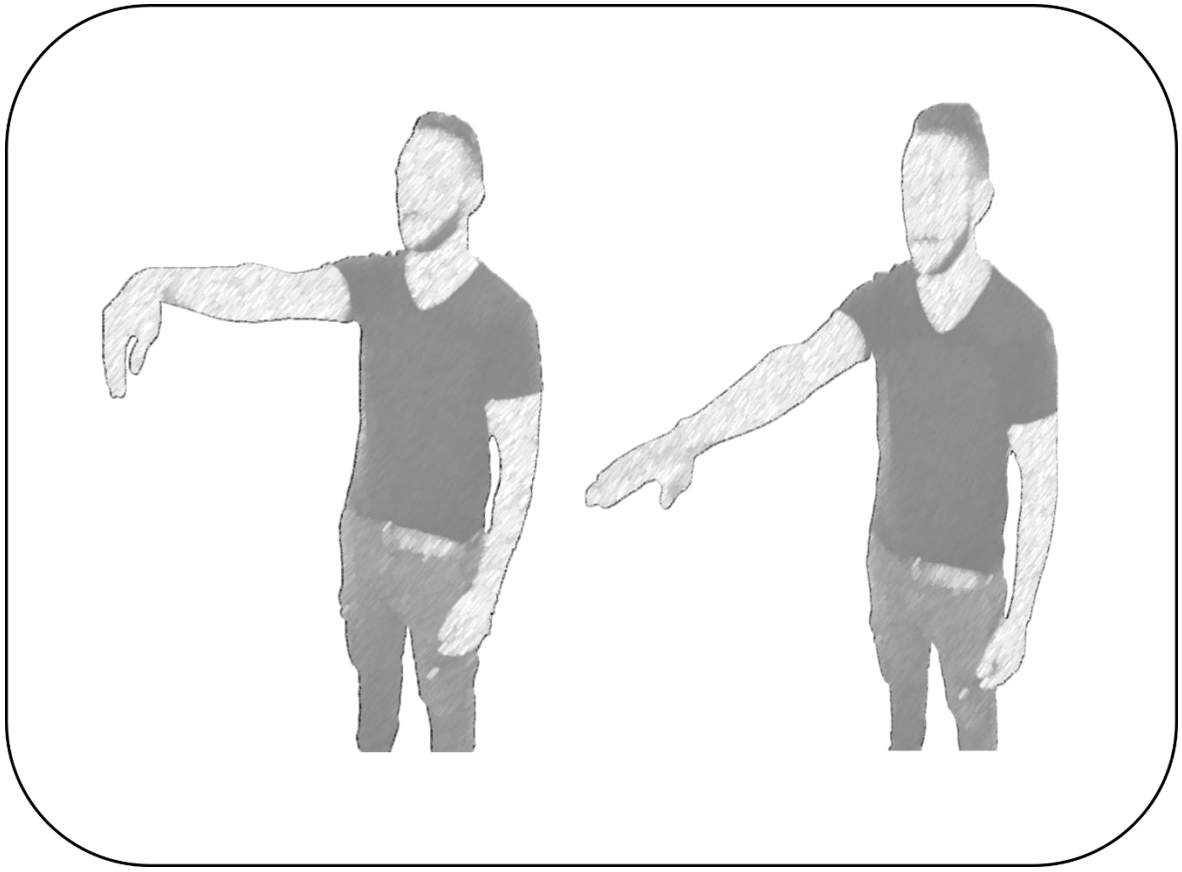

Figure 2.15. Hand flexion-extension with rotation axis represented with black. The blue arrow indicates the direction of positive values.

The hand flexion-extension angle (Figure 2.15) was computed by projecting $\widehat{h1}$ vector on plane Π , with leading vectors $\widehat{w1}$ and the forearm unit vector. The variable was defined as the angle formed between the projection of the hand vector on the plane Π and $\widehat{w1}$. It was computed as shown in (2.6). This variable was corrected with an offset in order to have a null value when the hand was aligned with the forearm. This variable was conceived to yield negative values if the hand was flexed and to be negative if the hand was extended.

$$Hand\ fexion - extension = acos\ (\widehat{u\_hand}\_\Pi \bullet \widehat{w1}) - 90 \tag{2.6}$$

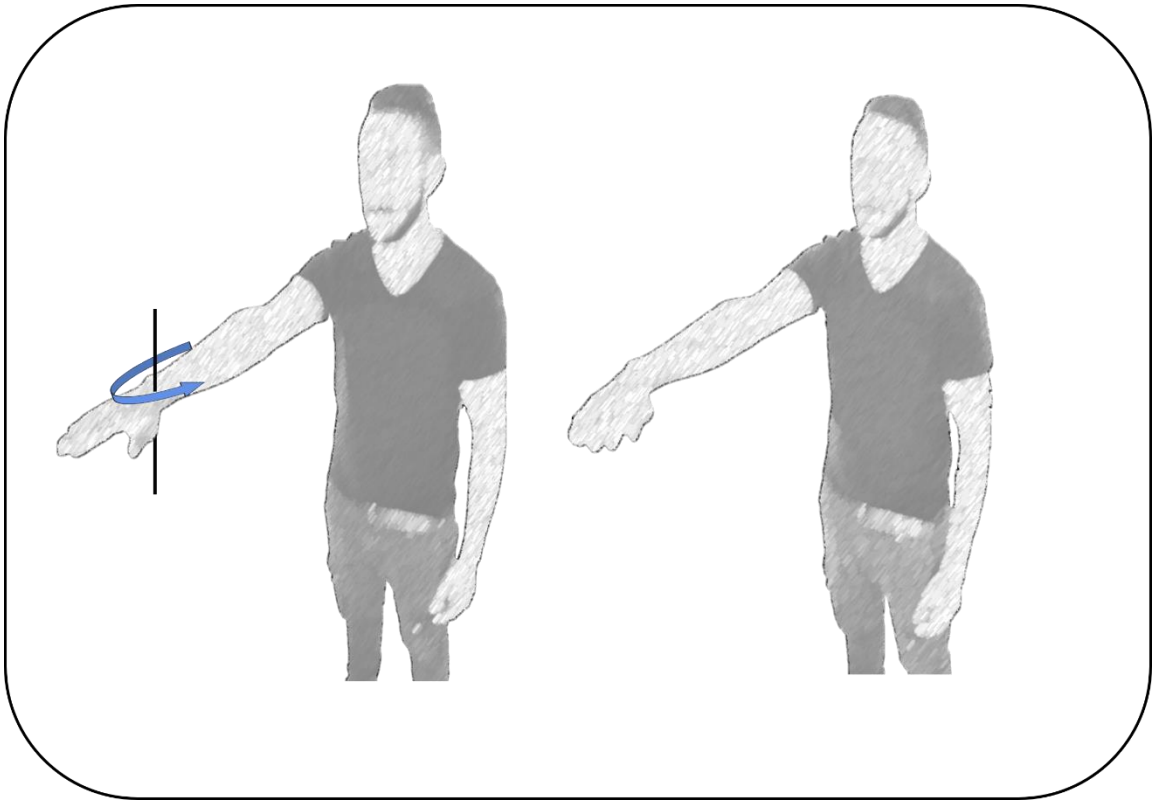

Figure 2.16. Hand deviation angle with rotation axis represented with black. The blue arrow indicates the direction of positive values.

The hand deviation angle (Figure 2.16) was computed by projecting $\widehat{h1}$ on plane Φ, which has vectors $\widehat{w2}$ and the forearm unit vector as leading vectors. The variable was defined as the angle formed between the projection of $\widehat{h1}$ on the plane Φ and $\widehat{w2}$. It was computed as shown in (2.7). To have a zero-deviation angle when the hand was aligned with the forearm, the variable was corrected with a constant. For medial deviations, the associated angle was positive, conversely for lateral deviations, the associated angle was negative.

$$Hand\ deviation = acos\ (\widehat{u\_hand}\_\Phi \bullet \widehat{w2}) - 90 \quad (2.7)$$

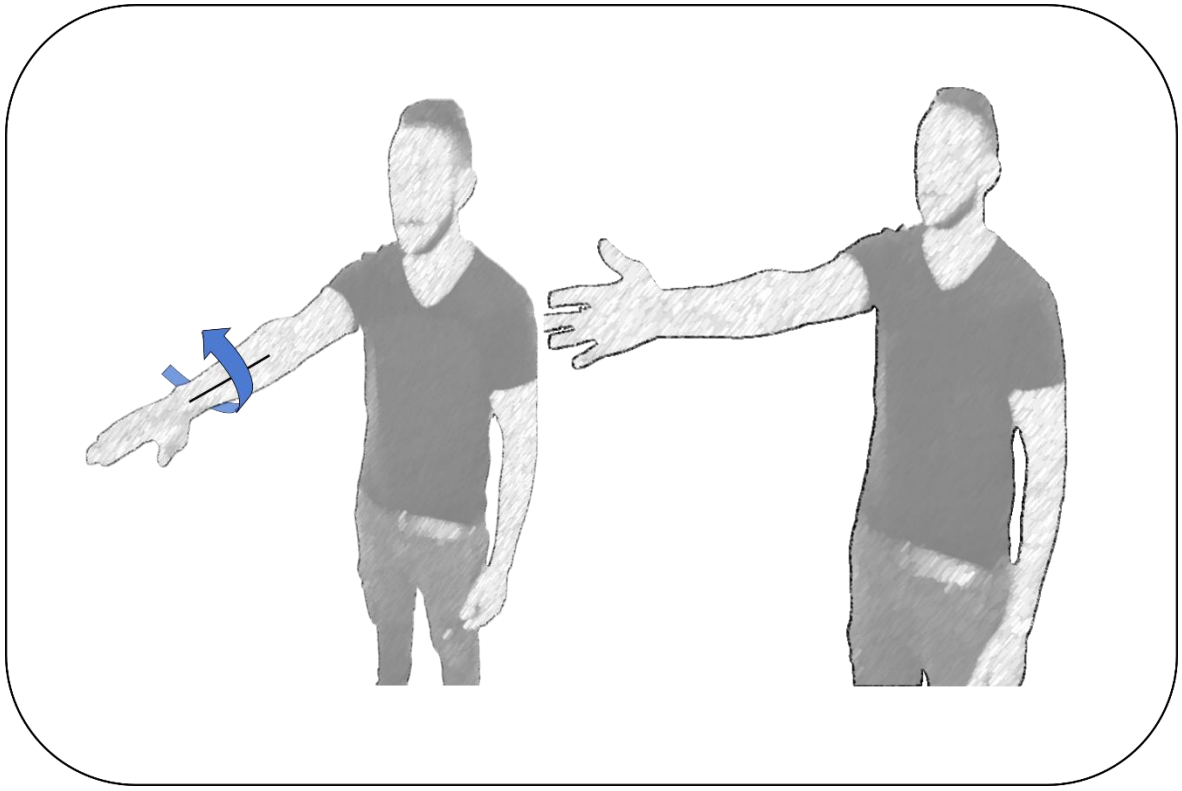

Figure 2.17. Hand pronation-supination with rotation axis represented with black. The blue arrow indicates the direction of positive values.

The hand pronation-supination angle (Figure 2.17) was computed by projecting $\widehat{h2}$ on plane Ω, with leading vectors $\widehat{w1}$ and $\widehat{w2}$. The variable was computed as the angle between $\widehat{h2}$ projected on the plane Ω and $\widehat{w1}$. The formula by which it was computed is shown in (2.8). In order to have a null value when $\widehat{h2}$ and $\widehat{w2}$ were aligned, it was corrected with a constant. It yielded positive values for clockwise rotations and negative angle values for counterclockwise rotations.

$$Hand\ pronation - supination = acos\ (\widehat{u\_hand2\_\Omega} \bullet \widehat{w1}) - 90 \quad (2.8)$$

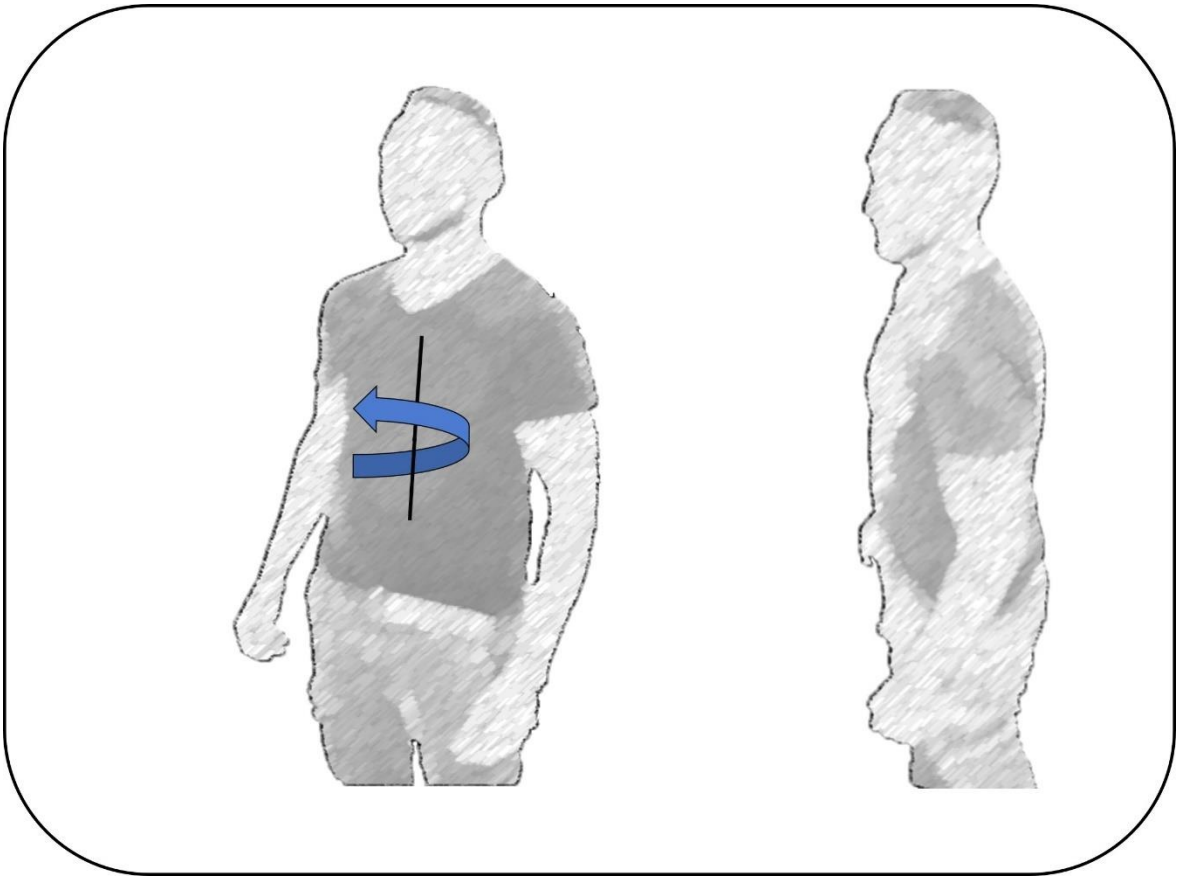

Figure 2.18. Trunk torsion along with rotation axis represented with black. The blue arrow indicates the direction of positive values.

Trunk torsion (Figure 2.18) was chosen as the angle of rotation of the trunk in the coronal plane, defined by vectors $\hat{f}$ and $\hat{s}$. It was computed as the angle between the projection of $\hat{s}$ on the coronal plane and a reference vector. The reference vector was taken as the first orientation of the frontal vector in the opposite direction ($-\hat{f}$), at the beginning of each acquisition. It was calculated as seen in (2.9) and was corrected with a constant in order to have a 0° rotation when the shoulder vector was aligned with its first position. The trunk torsion assumed positive values for counterclockwise rotations and negative for clockwise rotations.

$$Trunk\ torsion = acos\left[\hat{s} \bullet \left(-\hat{f}\right)\right] - 90 \tag{2.9}$$

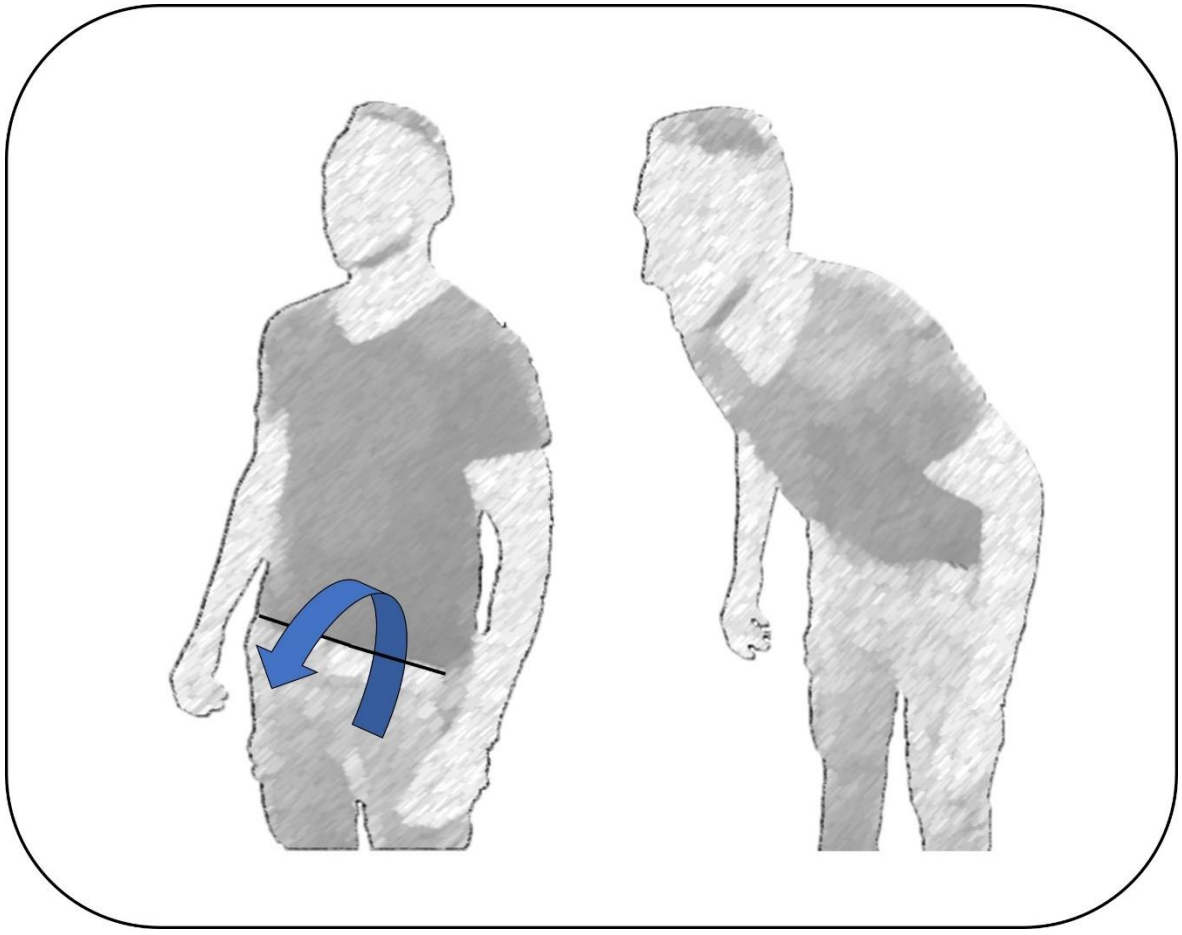

Figure 2.19. Trunk anterior-posterior flexion with rotation axis represented with black. The blue arrow indicates the direction of positive values.

Trunk anterior-posterior flexion (Figure 2.19) was the flexion of the trunk in the sagittal plane. The sagittal plane was defined as the plane with leading vectors $\hat{f}$ and $\hat{s}$ in their first iteration. The variable was taken as the angle formed between the trunk vector projected on the sagittal plane and the frontal axis vector ($\hat{f}$). This variable assumed positive values if the subject leaned forward and negative when leaning backward. It was computed as shown in (2.10).

$$Trunk\ anterior - poesterior\ flexion = acos\ (\widehat{t\_sag} \bullet \hat{f}) \tag{2.10}$$

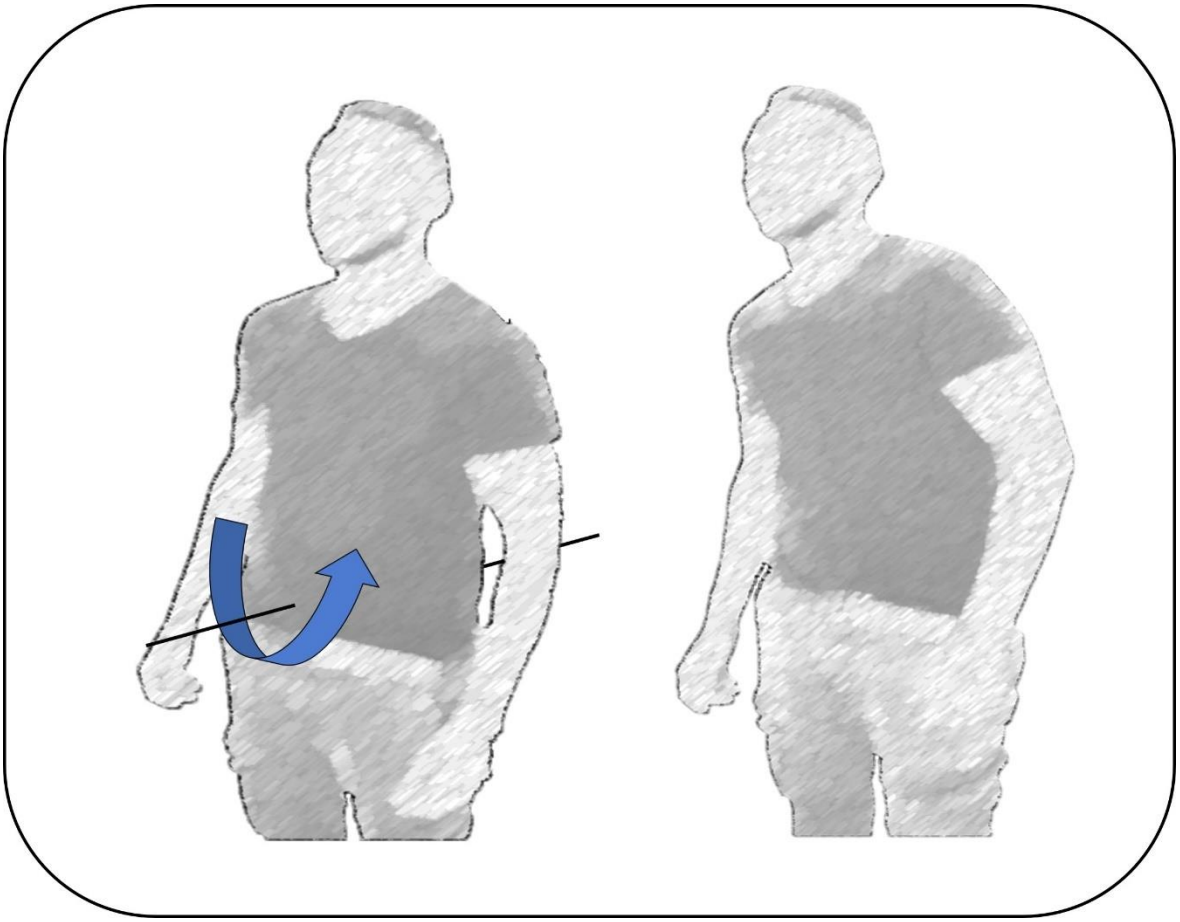

Figure 2.20. Trunk medial-lateral flexion with rotation axis represented with black. The blue arrow indicates the direction of positive values.

Trunk medial-lateral flexion (Figure 2.20) was the trunk flexion in the frontal plane, with leading vectors $\hat{t}$ and $\hat{s}$ in the first frame. The variable of interest was the angle formed between the projection of the trunk vector on the frontal plane and the negative shoulder unit vector. This angle was computed as shown in (2.11) and the it was corrected with a constant in order to yield a null value if the subject was upright. The variable was designed to give positive rotation angles when the subject leaned to the right and negative for leaning to the left.

$$Trunk\ medial-lateral\ flexion = acos\left[\widehat{t\_front} \bullet \left(-\hat{s}'\right)\right] - 90 \tag{2.11}$$

2.7 Pilot subject

In parallel to the theoretical definition of the degrees of freedom to be used, certain tests were conducted on a pilot subject to verify if all variables were identifiable with the RGB-D device. The tests consisted in making the subject reproduce specific movements designed to enhance or isolate each specific degree of freedom.
Figure 2.21 illustrates the collection of the degrees of freedom obtained each with a specific movement. As it was anticipated previously, the degrees of freedom regarding the hand are very noisy and unstable, but quite clearly identifiable in simple movements.

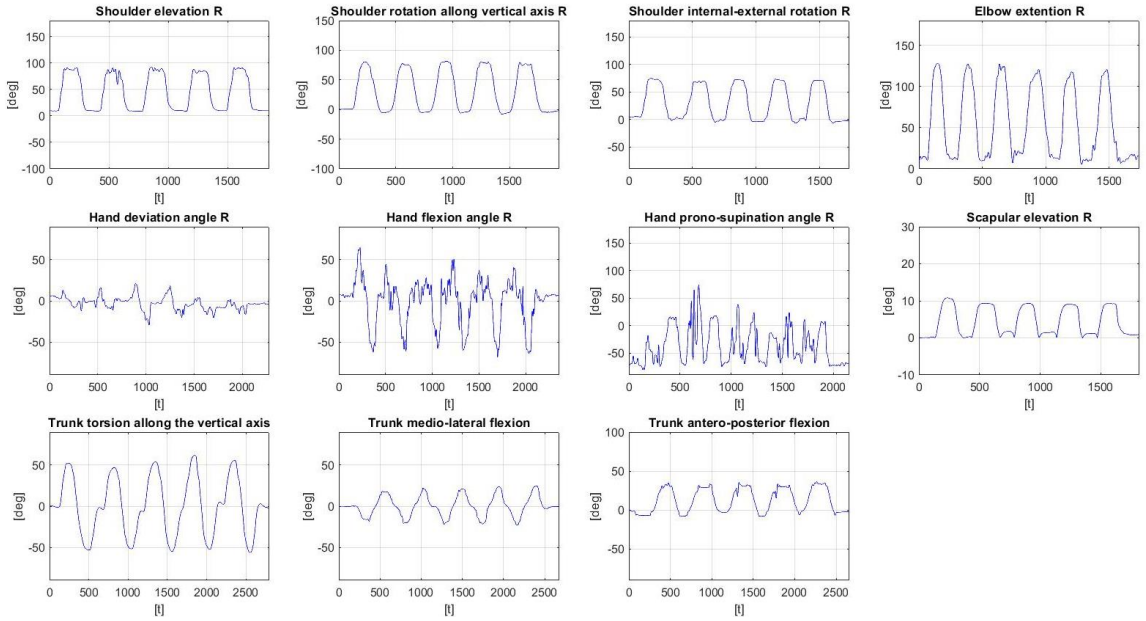

Figure 2.21 Degrees of freedom extrapolated separately through selective movements.

2.7.1 Selective movements description

The shoulder elevation was extracted through a simple rotation of the upper arm in the sagittal plane of the body. The movement had to be stopped when the upper limb was perfectly extended in front of the subject as parallel as possible to the floor. The pilot subject had to start in a vertical position with his arms along his body. This movement is visualized in Figure 2.9
To emphasize the variable of shoulder rotation along the vertical axis a shoulder adduction movement was chosen. The subject started upright with the right arm elevated up to 90°. The movement consisted in a rotation of the upper arm in the coronal plane of the body and had to be ended when the arm was aligned with the shoulders. This movement is represented in Figure 2.10.
The elbow extension variable was emphasized by the rotation of the arm around the axis of the humeroulnar joint. The subject started in the same pose as for the shoulder elevation movement. This movement is illustrated in Figure 2.11.
The shoulder internal-external rotation was identified by rotating the arm in the transversal plane of the upper arm. The subject started upright with the arm elevated at 90° and the elbow flexed at 90°. From this pose the

subject had to rotate the forearm counter-clockwise around the upper-arm's axis. This movement is represented in Figure 2.12.
The extraction of the scapular elevation was achieved by a simple vertical translation of the shoulder. The movement began from the starting position described for the shoulder elevation. This movement is represented in Figure 2.13.
For each of the 3 movements describing the hand's kinematics, the subject started from the same starting position, with the upper arm elevated at 90°, palms facing downwards, and the hand aligned with the forearm. For the extraction of the hand flexion-extension the hand had to be rotated in the sagittal plane, the identification of the hand deviation was achieved by rotating the hand in the coronal plane, lastly the hand pronation-supination was elicited by rotation the hand in the frontal plane of the body. These three movements can be visualized respectively in Figure 2.15, Figure 2.16 and Figure 2.17.
To emphasize the variables describing the trunk's kinematics, the subject had to start upright with arms along the body. For the trunk torsion, the participant had to rotate the trunk to the left and then to the right in the coronal plane. For the trunk anterior-posterior flexion, the movement that the subject had to reproduce was to lean forward and return. For the trunk medial-lateral flexion the movement asked of the subject was to lean to the right and then to the left. These three movements are visualized respectively in Figure 2.18, Figure 2.19 and Figure 2.20.

2.8 Algorithm description

The next step in the data processing workflow was the development of an algorithm which compared the two datasets, tackling the issues of different acquisition times and different frame acquisition frequencies.
To properly compare the acquired datasets, they had to be synchronized and normalized in time. Each movement was segmented into different repetitions and then each repetition was further segmented into 2 phases, a forward phase and a backward phase.
The synchronization for both movement types was achieved using an extrapolated signal which had a distinct and repeatable waveform. To segment both movements, the hand absolute distance from the initial position in each frame was chosen (Figure 2.22 and Figure 2.23). The point-to-point movement was composed of 9 repetitions, one for each point on the circular target including the 'O', and are respectively: 'O', 'NE', 'E', 'SE', 'S', 'SW', 'W', 'NW', 'N'. The phase segmentation was performed in such a way to have the forward phase going from the start of the movement to the moment in which the arm reached the target, meanwhile the backward phase started from where the first one ended and continued until the subject returned to the initial position. For this type of movement, the most relevant phase was the forward phase, hence it was the phase that was used for the dataset comparison.
The workspace exploration movement was composed by 8 repetitions due to the nature of the movement and they are respectively: 'O>NE>O', 'O>E>O', 'O>SE>O', 'O>S>O', 'O>SW>O', 'O>W>O', 'O>NW>O', 'O>N>O'. The phase distinction was the same as for the point-to-point movement.

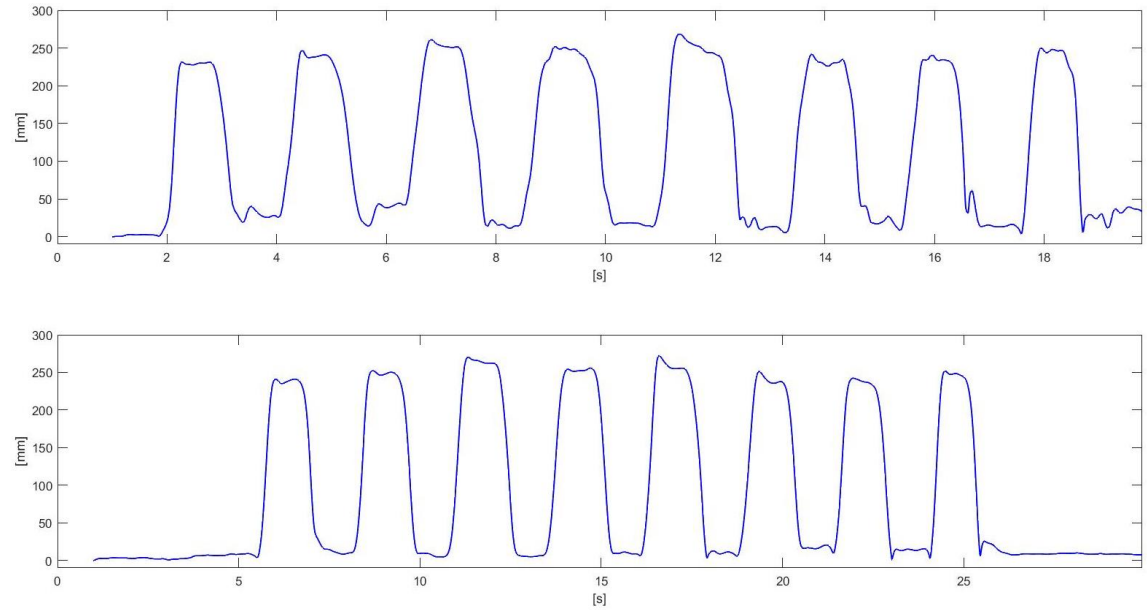

Figure 2.22. Segmentation of a typical workspace exploration movement. The upper plot represents the signal computed with the Kinect; the lower chart represents the same variable computed with the Vicon system.

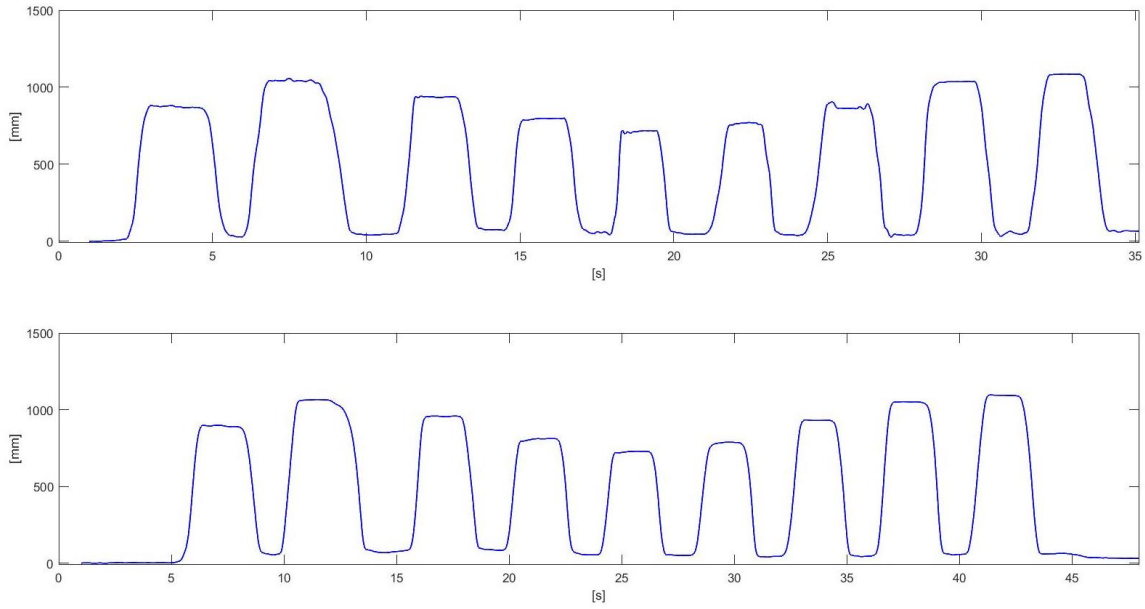

Figure 2.23. Segmentation of a typical point-to-point movement. The upper plot represents the signal obtained with the Kinect; the lower chart represents the same variable computed with the Vicon system.

2.8.1 Movement segmentation

The process of segmentation started with a thresholding of the chosen variable. This process was necessary to identify all the repetitions of a movement. The threshold was chosen empirically in order to ensure the identification of each repetition. The chosen threshold was of 150 mm. Figure 2.24 and Figure 2.25 illustrate the effects of the thresholding for each movement type.

Each repetition was identified by a red wave in Figure 2.24 and Figure 2.25. This preliminary step was not enough to define the full pattern of each repetition, since the wave pattern should start and end when the subject is in the resting position. In order to complete the segmentation of each repetition, 2 characteristic points of wave patterns were used, the onset and offset of each curve. The onset was identified by the zero-crossing point of the signal's first derivative before the movement started. The offset was identified by zero-crossing point of the signal's first derivative after the subject returned to the initial pose.

From a practical point of view, the implemented algorithm started from the first sample in each red wave and searched for the onset on the left of the red wave. The offset was searched on the right of the last sample of red wave. Each execution of a point-to-point movement yielded 9 onsets and 9 offsets, meanwhile each workspace exploration yielded 8 onsets and 8 offsets.

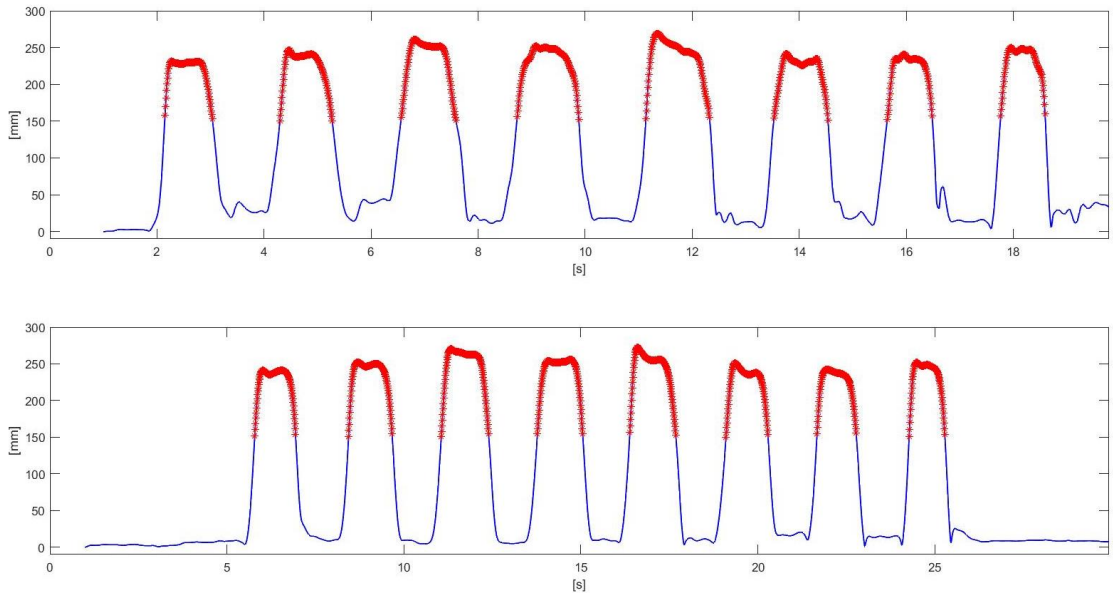

Figure 2.24. Thresholding effects on the workspace exploration movement. The upper plot represents the signal computed with the Kinect; the lower chart is the same variable computed with the Vicon system.

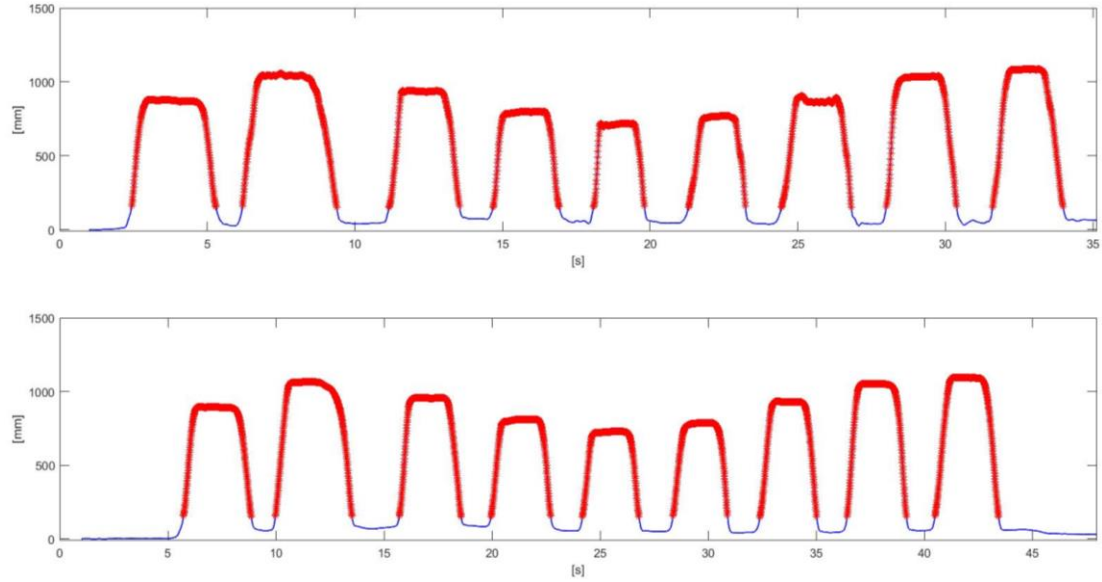

Figure 2.25. Thresholding effects for the point-to-point movement. The upper plot represents the signal computed with the Kinect; the lower chart is the same variable computed with the Vicon system.

Figure 2.26 and Figure 2.27 illustrate the effects of the phase segmentation algorithm. For each repetition 3 points were identified: the onset, the offset and the midpoint. The midpoint was selected as the end of the forward phase and the start of the backward phase and was computed as the midpoint of each repetition. Doing so, a complete movement phase was identified, and the time normalization procedure could be performed.
The segmentation algorithm saved the coordinates of the onsets, offsets and midpoint of each phase (red dots shown in Figure 2.26 and Figure 2.27) for both datasets. This is then used by successive scripts to synchronize, normalize and confront the datasets.

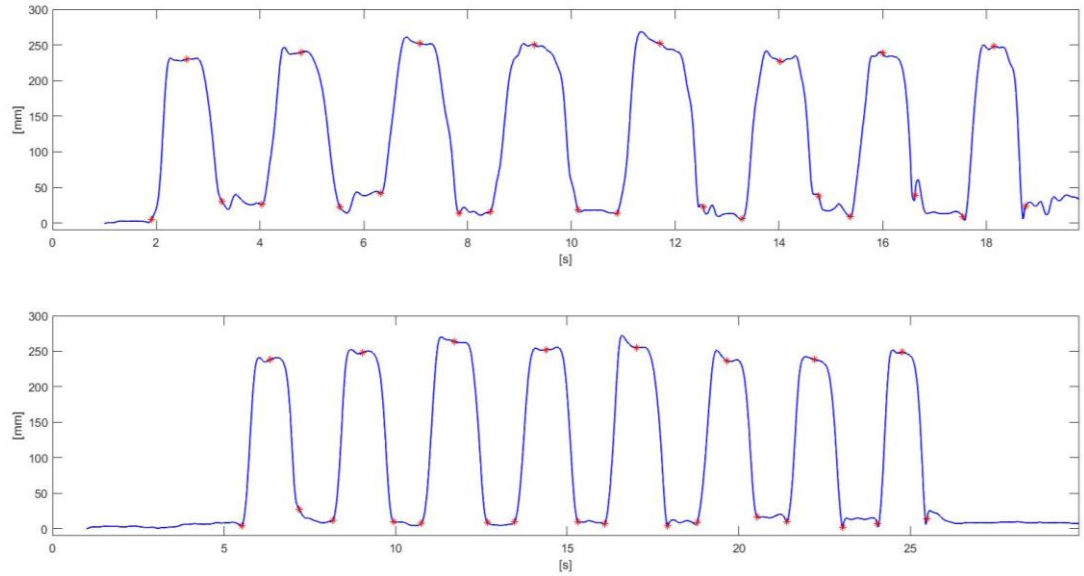

Figure 2.26. Phase separation end goal of workspace exploration movement. The upper plot represents the signal computed with the Kinect; the lower chart shows the same variable computed with the Vicon system.

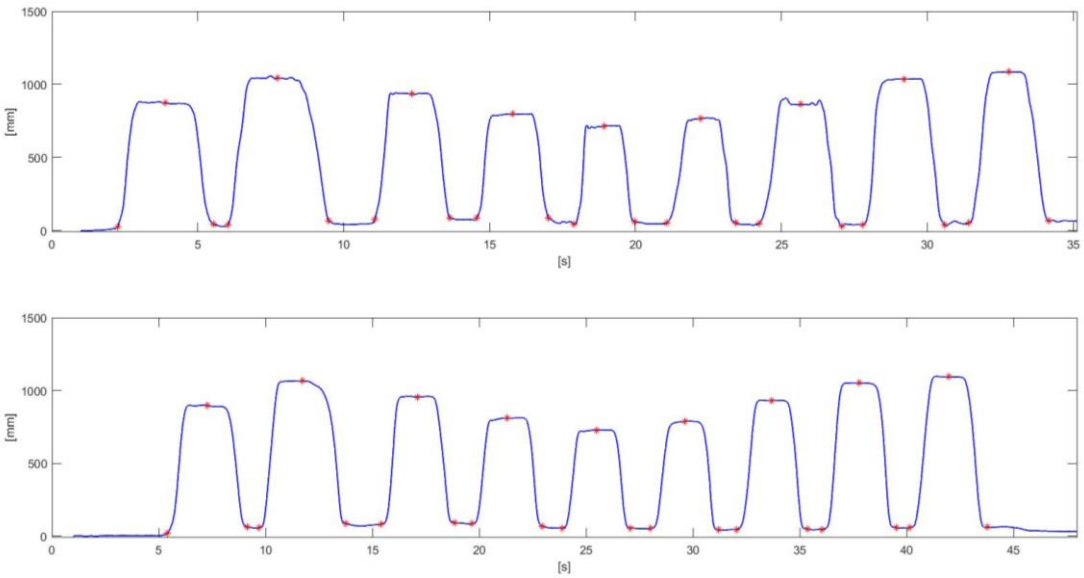

Figure 2.27 Phase separation end goal of a point-to-point movement. The upper plot represents the signal computed with the Kinect; the lower chart shows the same variable computed with the Vicon system.

2.8.2 Dataset Synchronization

Synchronization consisted in coupling each phase of one dataset to the corresponding one of the other dataset. Afterwards, time normalization was achieved by resampling each phase at 100 samples per phase. Figure 2.28 and Figure 2.29 show the shoulder elevation variable synchronized and normalized in time respectively for workspace exploration and point-to-point movement.

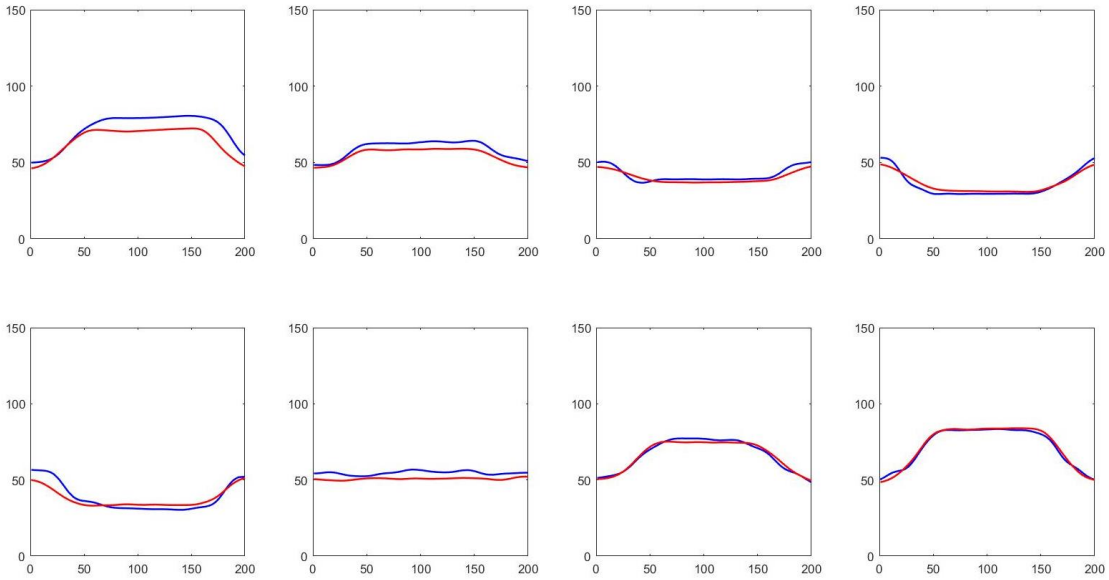

Figure 2.28. Synchronization and time normalization of the shoulder elevation for the workspace exploration movement. The variable obtained with the Kinect is represented with blue and with red the same variable acquired with the Vicon system is shown.

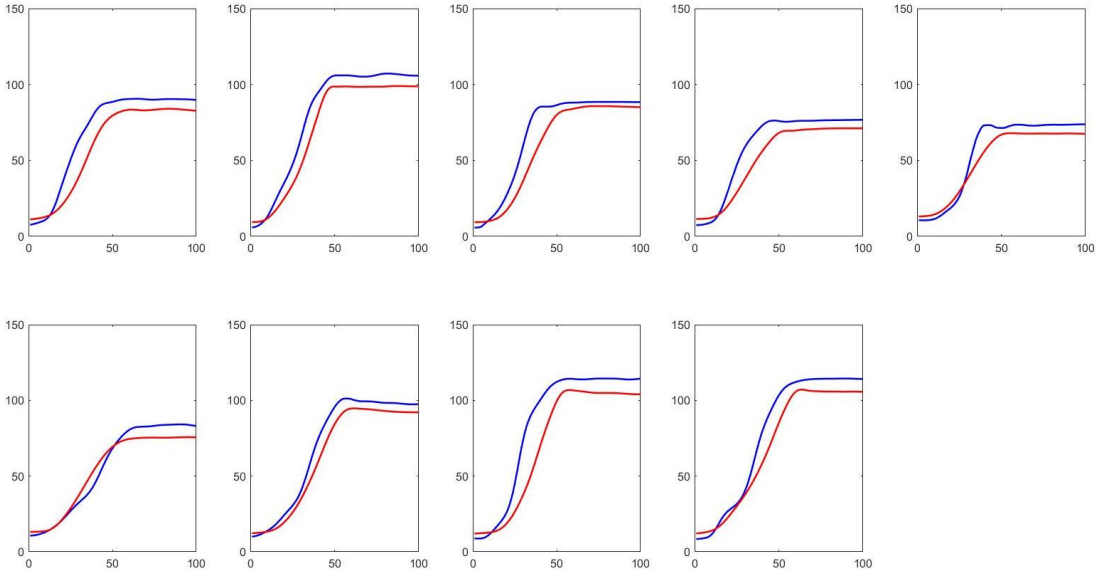

Figure 2.29 Synchronization and time normalization of the shoulder elevation for the point-to-point movement. The variable obtained with the Kinect is represented with blue and with red the same variable acquired with the Vicon system is shown.

The last step before the statistical analysis was the comparison between the two datasets and the choice of the comparison metric. In this study, the Euclidean angular distance (Ead) was used since it provided both information for the morphology related to the phase and the absolute mean difference. This metric was applied to each phase separately, obtaining the mean angular error for each phase. The scripts described so far saved the elaborated data for each subject in a data struct designed as illustrated in Figure 2.30.
Subsequently, the elaborated data was subdivided into two different datasets, a test dataset and a retest dataset.

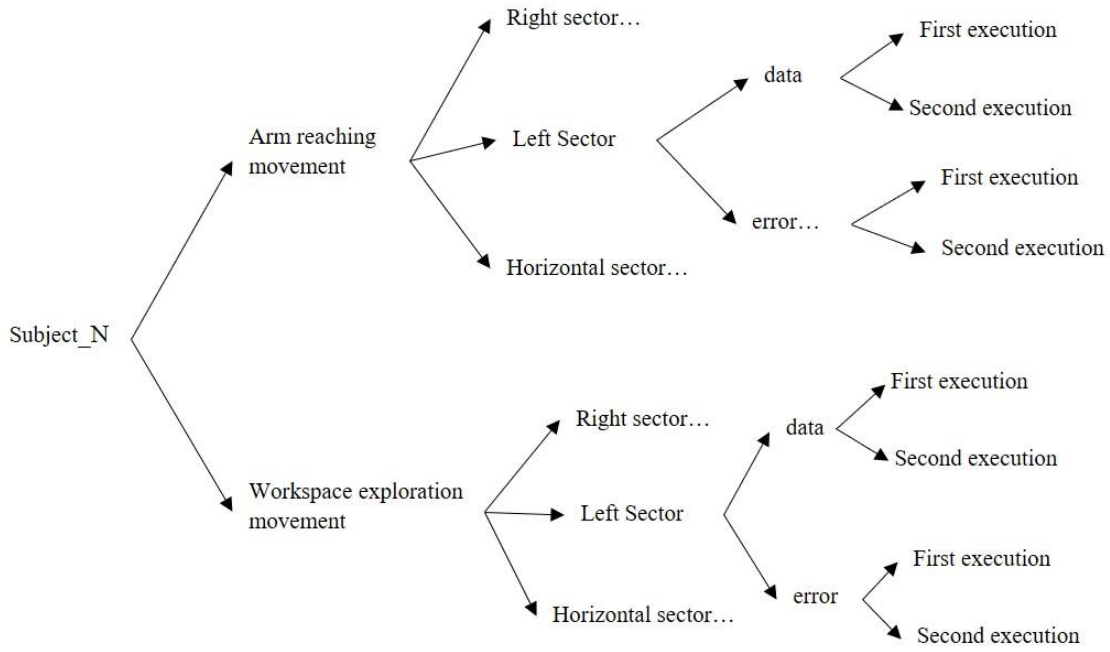

Figure 2.30. Structure of the output data for each Subject.

2.9 Statistical analysis

The final step in the data analysis was the statistical evaluation of the dataset and the analysis on the reliability of the device. The statistical evaluation was performed with a 2-way ANOVA test with degrees of freedom and sectors as factors. The test was structured in this way to investigate differences between the registered variables and the variation of the device's performance within the available workspace of the upper limb. Moreover, a multiple comparison test was implemented to evaluate the significance of the results obtained through the 2-way ANOVA test. Further in this document the results of the statistical analysis will be illustrated both for a specific subject and for the whole population of subjects. While analyzing the statistics on whole population of subjects, each subject was interpreted as a repetition of the observed data. The reliability was evaluated through the interclass correlation coefficient (ICC) between the test and retest dataset. In this evaluation each sector was treated separately to provide more detailed result on the device's reliability.

Chapter 3 Results

3.1 RGB-D system error

In this section of the document the results obtained through the protocol described so far will be presented. They will be presented both for one sample subject and for the whole population of subjects. Each degree of freedom was computed with respect to a subject specific reference system presented in section 2.6, Figure 2.8.

3.1.1 Sample subject results

The obtained results are summarized in three graphs: in the first chart a direct visual comparison between the two datasets is proposed. The time evolution of each phase computed by the Vicon system is represented in red. The same phase sequence computed by the Kinect is represented in blue; a second graph illustrates the error distribution phase by phase for each degree of freedom; lastly the third presented graph offers visualization of the error on a map of the target. The map used the following color code: dark green indicates Ead≤5°; light green 5°<Ead≤10°; yellow 10°<Ead≤20°; red Ead>20°. For the single subject analysis, it was chosen to show only one execution of the movement in order to provide a more concise analysis.
The analysis of result will start from the workspace exploration movement.

Figure 3.1. Workspace exploration movement in the right sector.

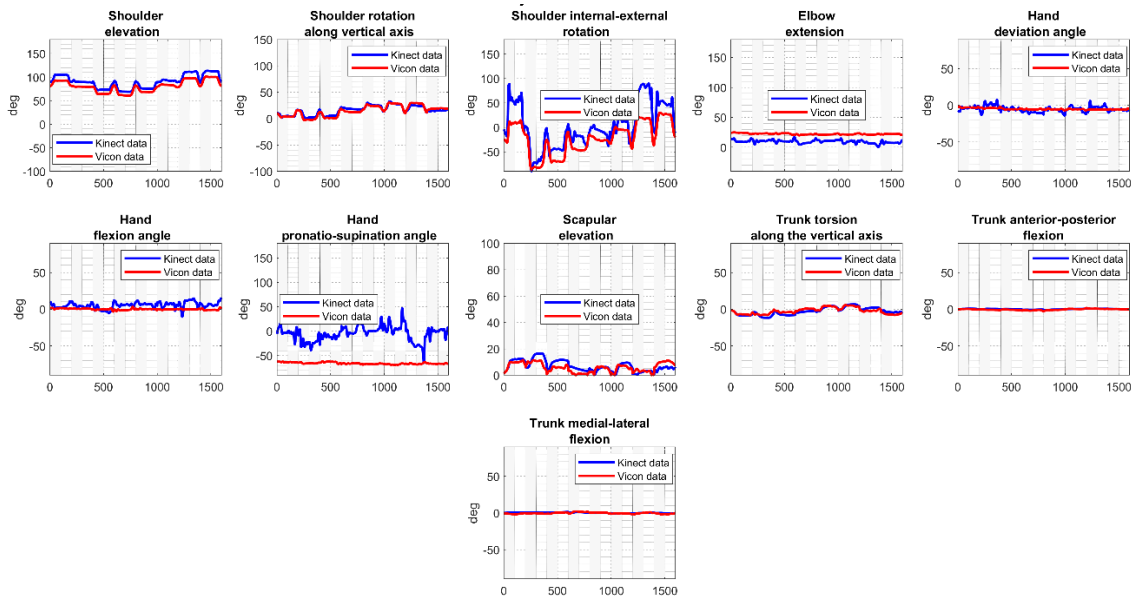

Figure 3.2. Subject 1 Workspace exploration, right sector: temporal sequence of phases. The Kinect dataset is represented with blue and the Vicon dataset with red.

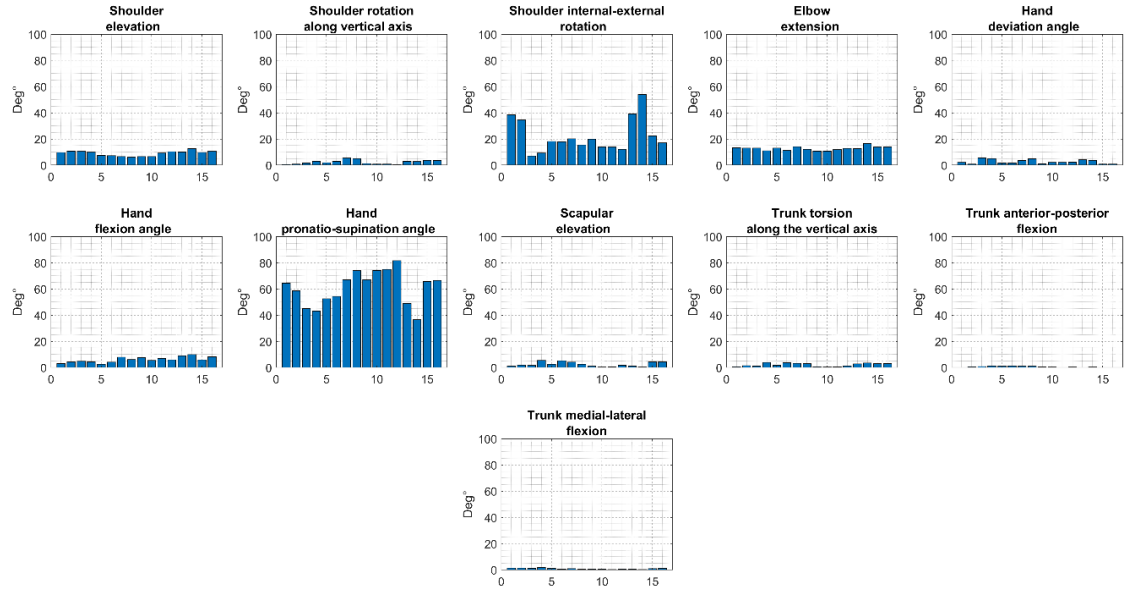

Figure 3.3. Subject 1: Workspace exploration, right sector error distribution.

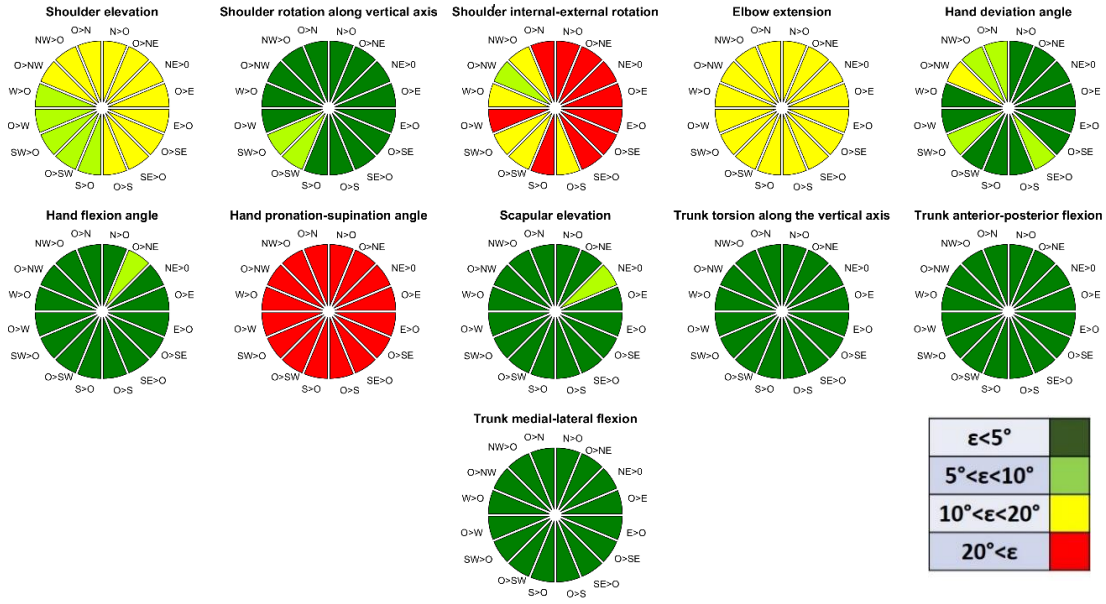

Figure 3.4. Subject 1: Error map of workspace exploration, right sector.

The first movement of Subject 1 is the workspace exploration in the right sector (Figure 3.1). In Figure 3.2 the difference between the two datasets is visually represented by overlapping the 2 signals phase by phase. The Vicon dataset is represented with red, the Kinect dataset with blue. Figure 3.3 is a representation of the error distribution for each degree of freedom phase by phase. Figure 3.4 illustrates a map of the performance of the RGB-D device on the circular target; each slice represents a phase of the movement. For workspace exploration movements, both forward and backward phases were both evaluated. The color code represents the error in each phase. It is dark green if the error is below 5°, light green if the error is between 5° and 10°, yellow if the error is between 10° and 20°. As one can note for most of the DoF, the tracking error is below 5°. The more critical variables for this specific movement were shoulder internal-external rotation and hand pronation-supination, which both present a poor tracking quality with an error mostly above 20°.

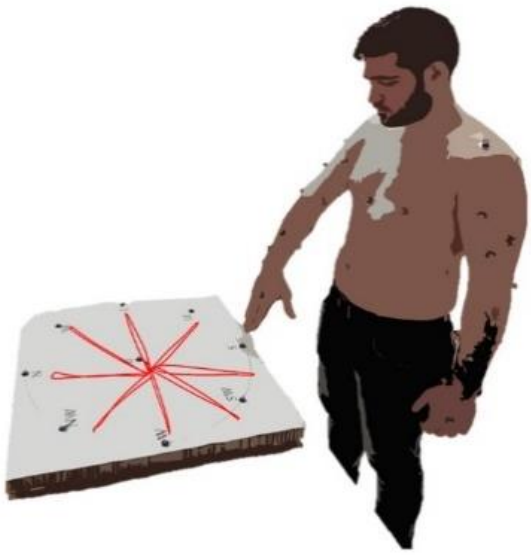

Figure 3.5. Workspace exploration movement in the central sector.

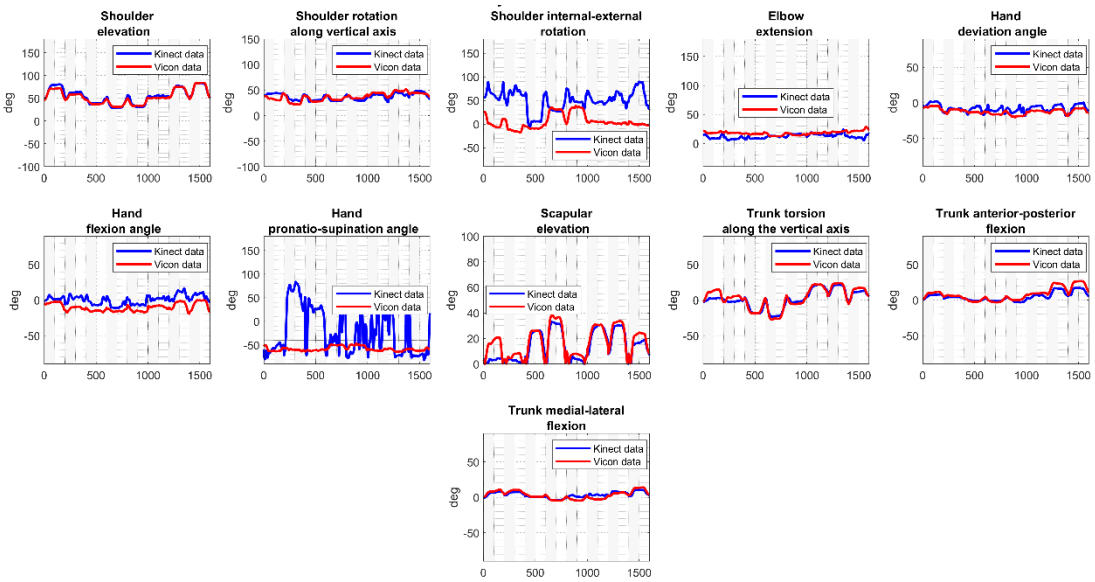

Figure 3.6. Subject 1: Workspace exploration, central sector: temporal sequence of phases. The Kinect dataset is represented with blue and the Vicon dataset with red.

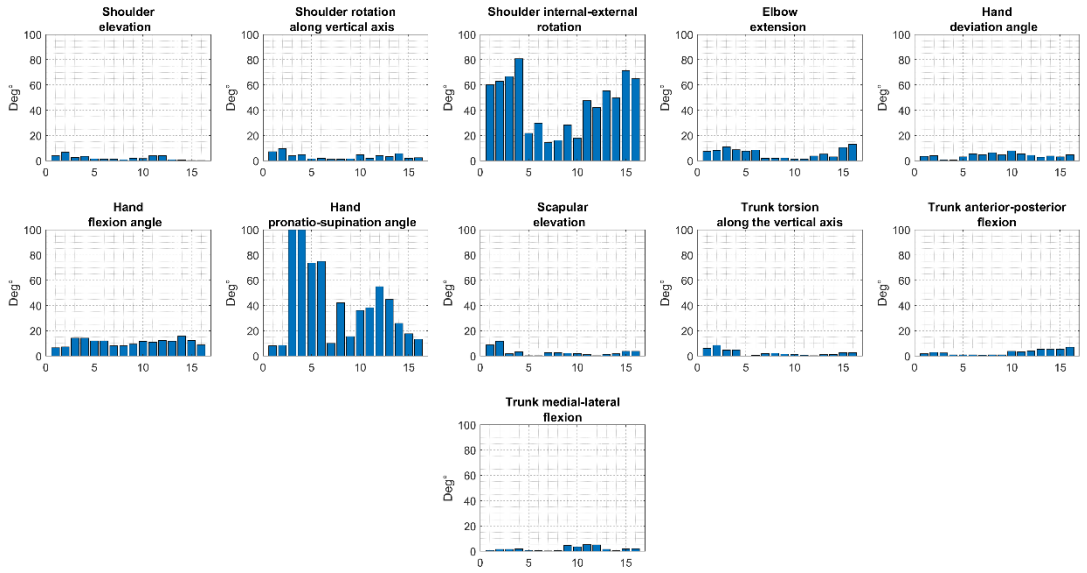

Figure 3.7. Subject 1: Workspace exploration, central sector error distribution.

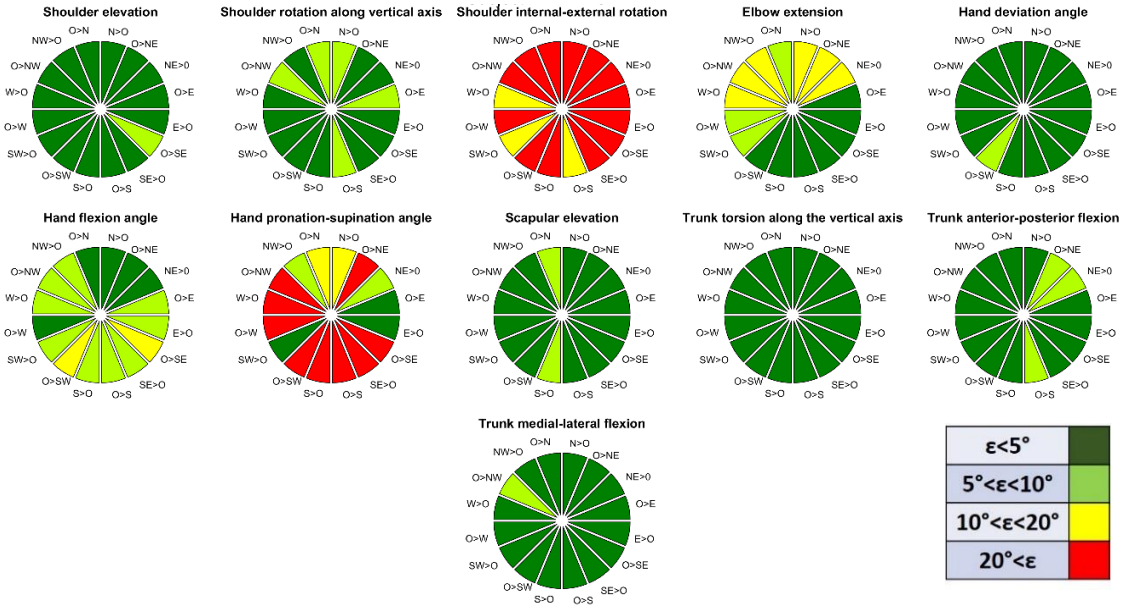

Figure 3.8. Subject 1: Error map of workspace exploration, central sector.

The second analyzed movement is workspace exploration movement performed in the central sector (Figure 3.5). Figure 3.6 shows the temporal sequence of phases for the workspace exploration movement in the central sector, the Vicon dataset is represented with red and the Kinect dataset with blue ; Figure 3.7 shows the error distribution for the same movement and Figure 3.8 shows the performance map of the device on the circular target. As per the previous movement, the performance quality of the RGB-D device in tracking most of the selected degrees of freedom is with an error below 10°. The elbow extension presents for specific phases a tracking error between 10° and 20°. Shoulder internal-external rotation and hand pronation-supination present an error mostly above 20°.

Figure 3.9. Workspace exploration movement in the left sector.

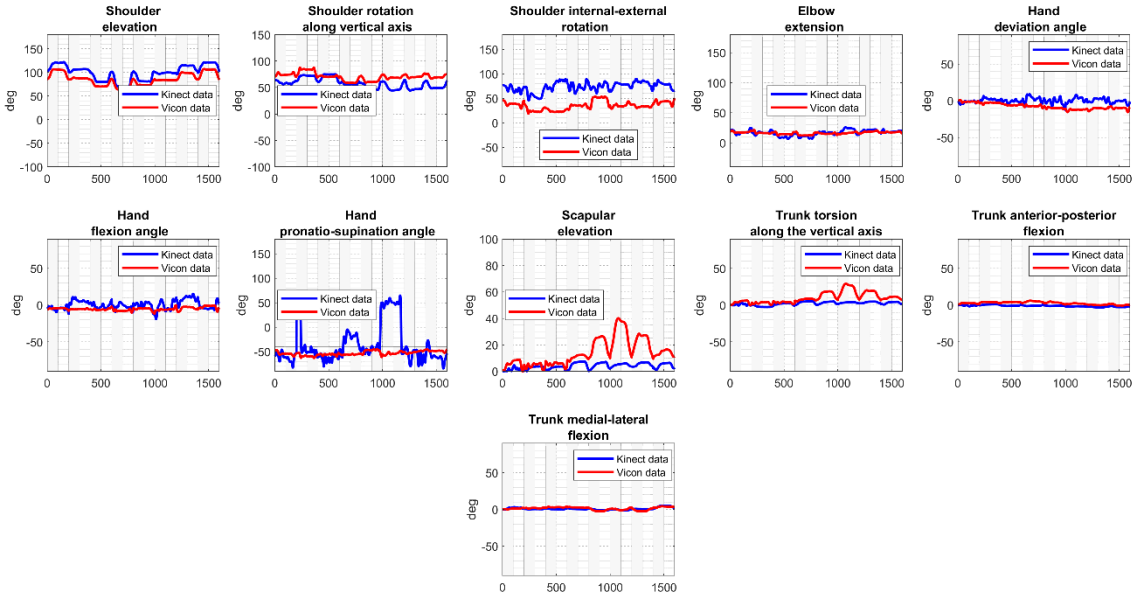

Figure 3.10. Subject 1: Workspace exploration, left sector: temporal sequence of phases. The Kinect dataset is represented with blue and the Vicon dataset with red.

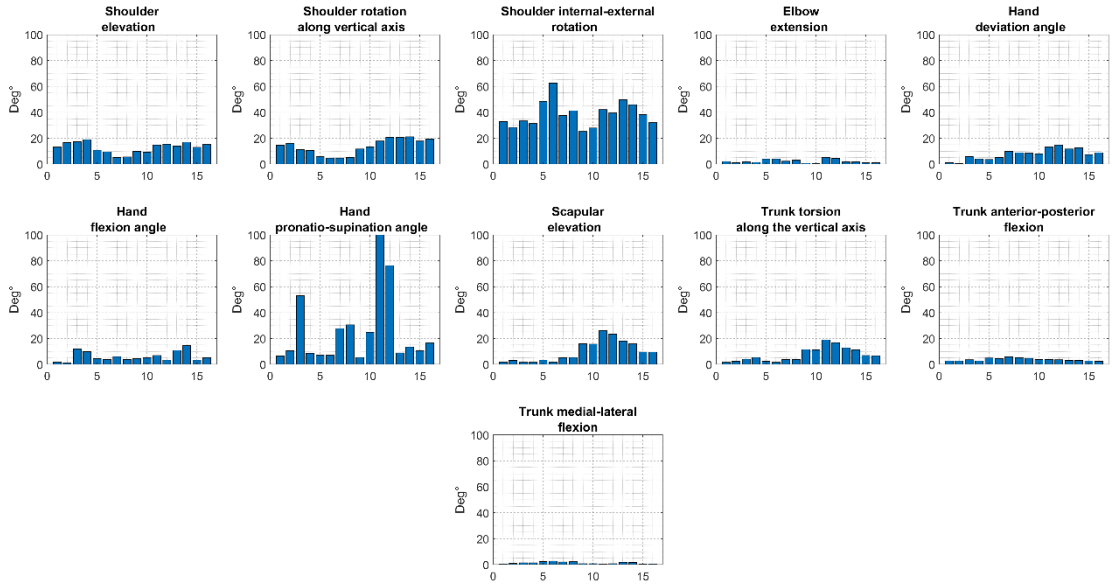

Figure 3.11. Subject 1: Workspace exploration, left sector error distribution.

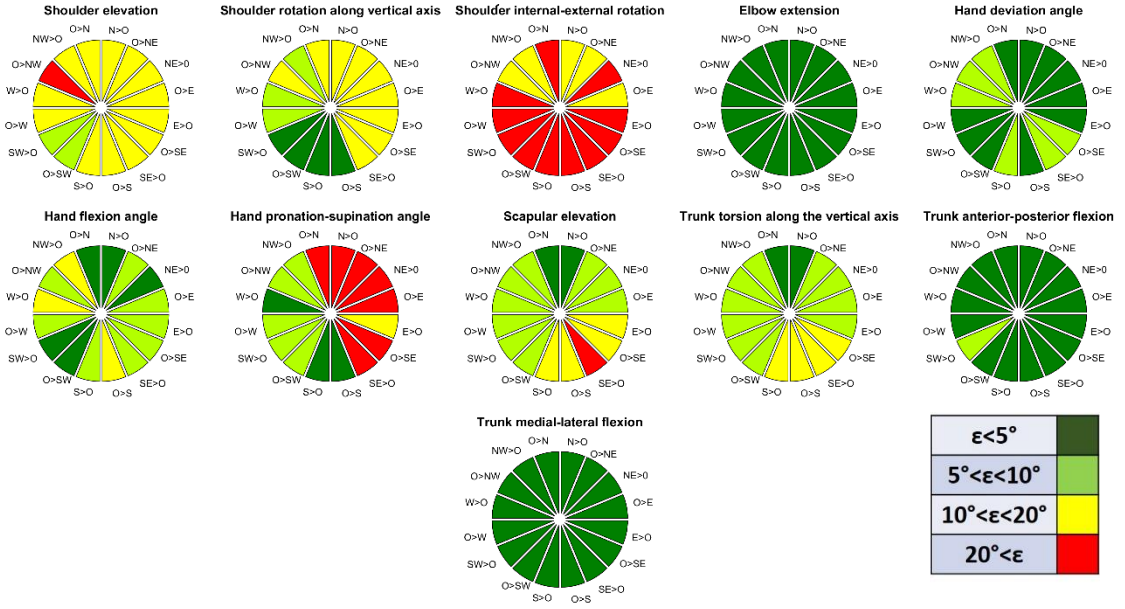

Figure 3.12. Subject 1: Error map of workspace exploration, left sector.

Next the results for the workspace exploration movement performed in the left sector will be presented (Figure 3.9). Figure 3.10 portrays the temporal sequence of phases for the workspace exploration movement in the left sector. The Vicon dataset is represented with red and the Kinect dataset is represented with blue. Figure 3.11 depicts the error distribution for the same movement, and Figure 3.12 shows the performance map of the device on the circular target. The performance quality of the RGB-D device in this sector has decreased with respect to the other two analyzed sectors. In this case, the degrees of freedom with the smallest error were elbow extension, hand deviation angle, trunk anterior-posterior flexion and trunk medial-lateral flexion. All these

variables were tracked for the most par with an error below 10°. The variables tracked with an error between 10° and 20° were shoulder elevation, shoulder rotation along the vertical axis, hand flexion-extension, scapular elevation and trunk torsion. As in the previous two movements, the two critical angles were shoulder internal-external rotation and hand pronation-supination, both tracked an error mostly above 20°.
Next, the result obtained by comparing the two systems for the point-to-point movement will be analyzed.

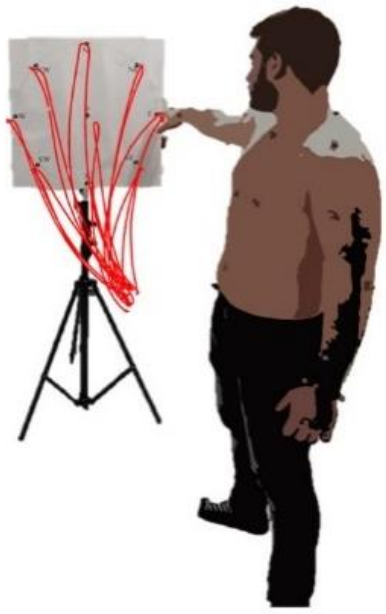

Figure 3.13. Point-to-point movement in the right sector.

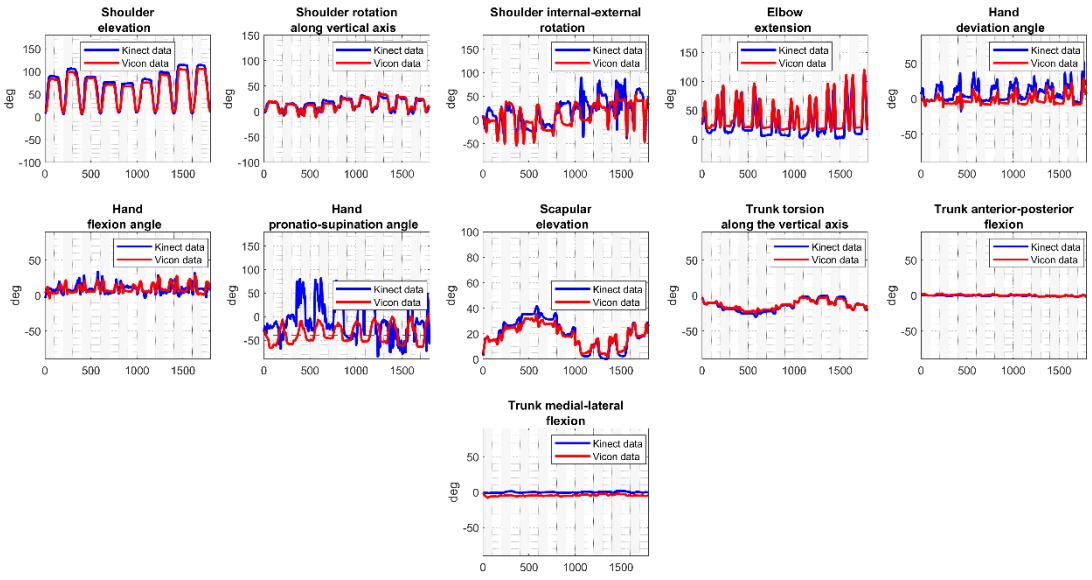

Figure 3.14. Subject 1: Point-to-point, right sector: temporal sequence of phases. The Kinect dataset is represented with blue and the Vicon dataset with red.

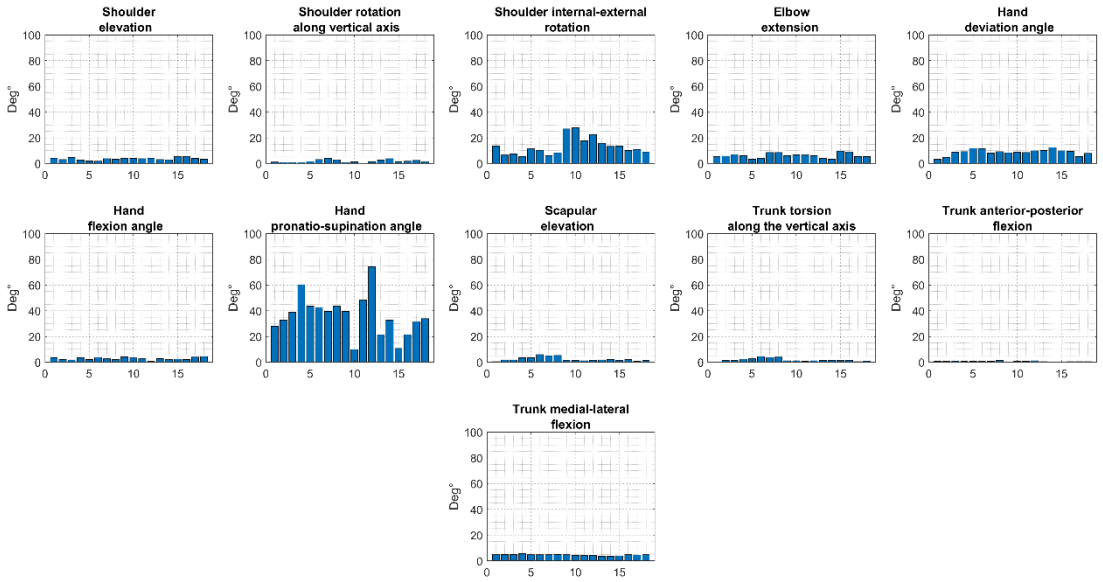

Figure 3.15. Subject 1: Point-to-point, right sector error distribution.

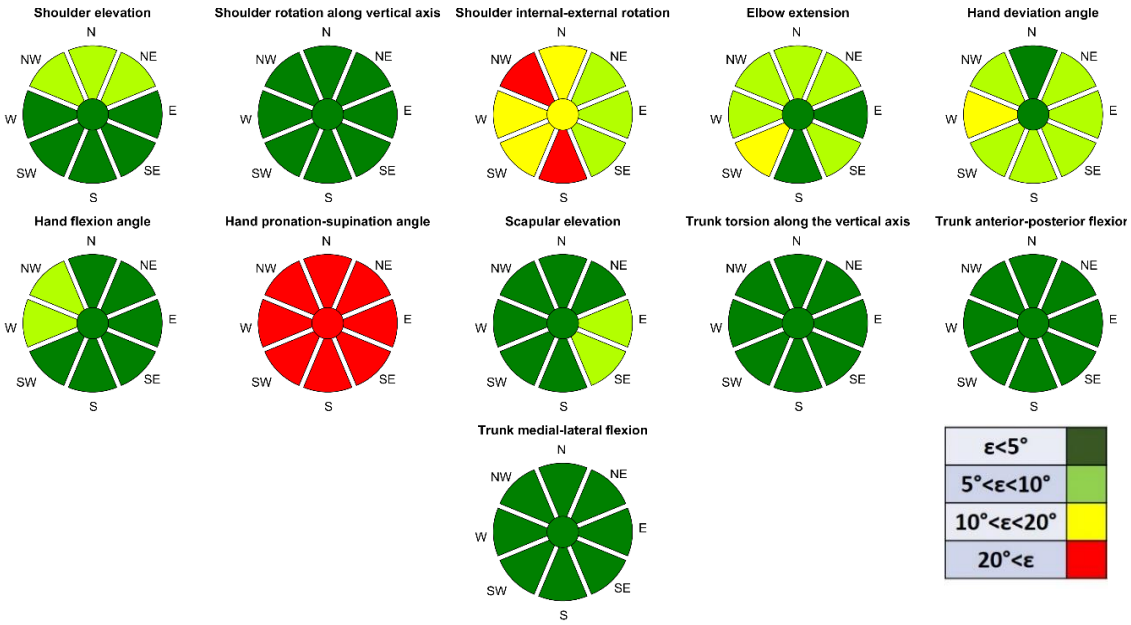

Figure 3.16. Subject 1: Error map of point-to-point, right sector.

The next movement to be analyzed is the point-to-point movement in the right sector (Figure 3.13). The Vicon dataset is represented with red and the Kinect dataset with blue. Figure 3.14 illustrates the time sequence comparison between the two datasets. Figure 3.15 shows the error distribution for this movement and Figure 3.16 portrays the error map on the target. For the point-to-point movement, it was decided to analyze the forward phase only. In this experimental condition, the variables tracked with an error below 10° were: shoulder elevation, shoulder rotation along the vertical axis, elbow extension, hand deviation angle, hand flexion angle, scapular elevation, trunk torsion, trunk anterior-posterior flexion and trunk medial-lateral

flexion. Meanwhile the variables tracked with an error mostly above 10° were shoulder internal-external rotation and hand pronation-supination.

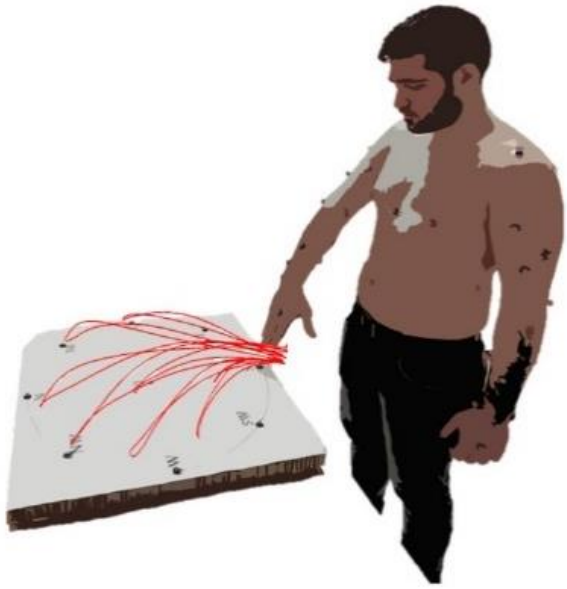

Figure 3.17. Point-to-point movement in the central sector.

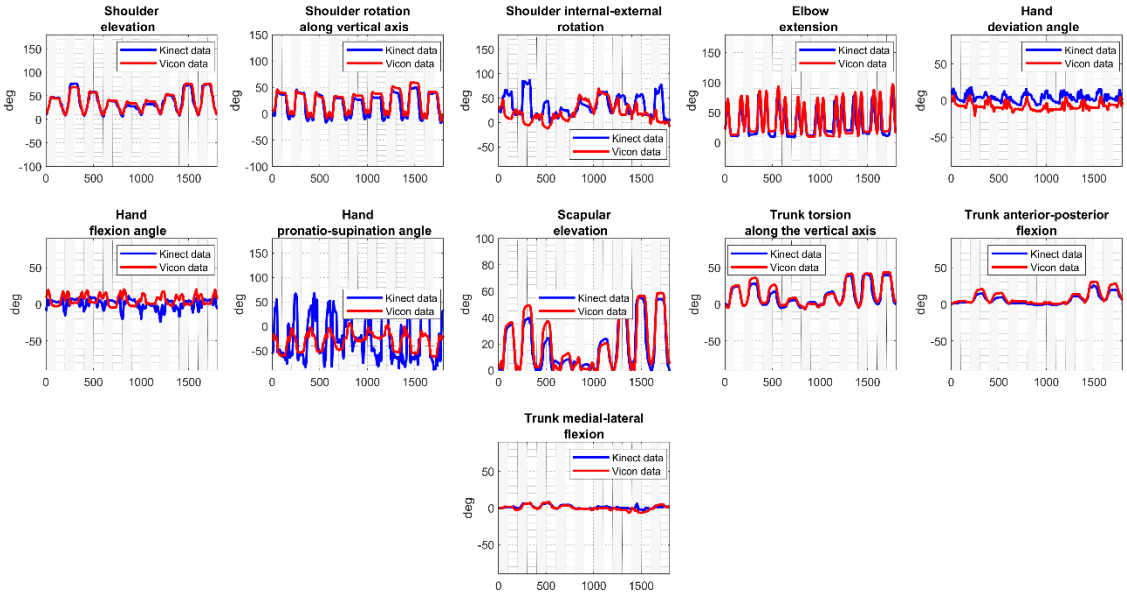

Figure 3.18. Subject 1: Point-to-point, central sector: temporal sequence of phases. The Kinect dataset is represented with blue and the Vicon dataset with red.

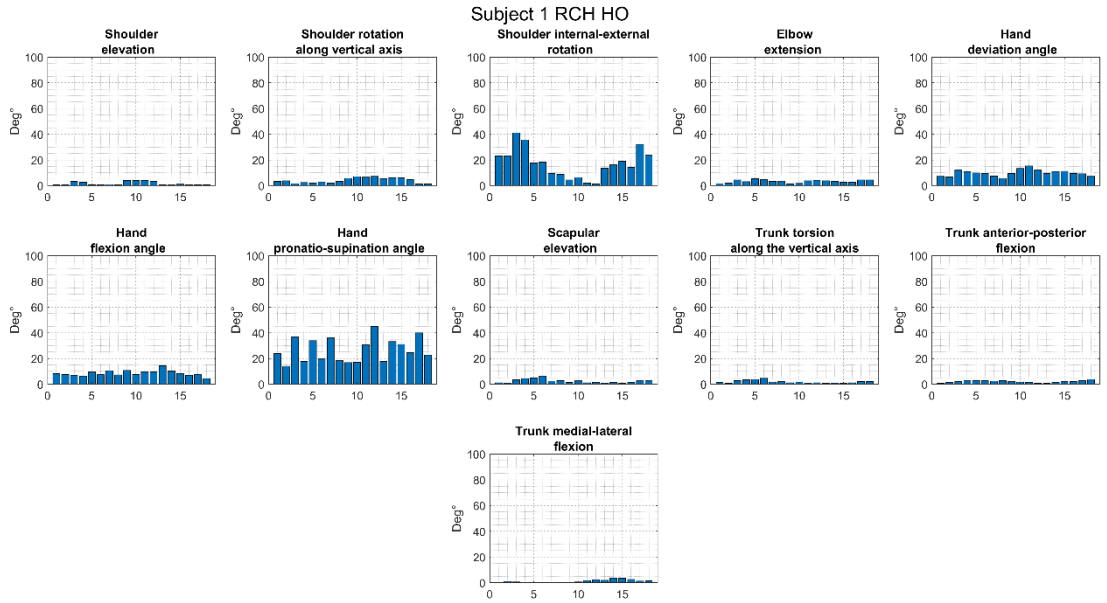

Figure 3.19. Subject 1: Point-to-point, central sector error distribution.

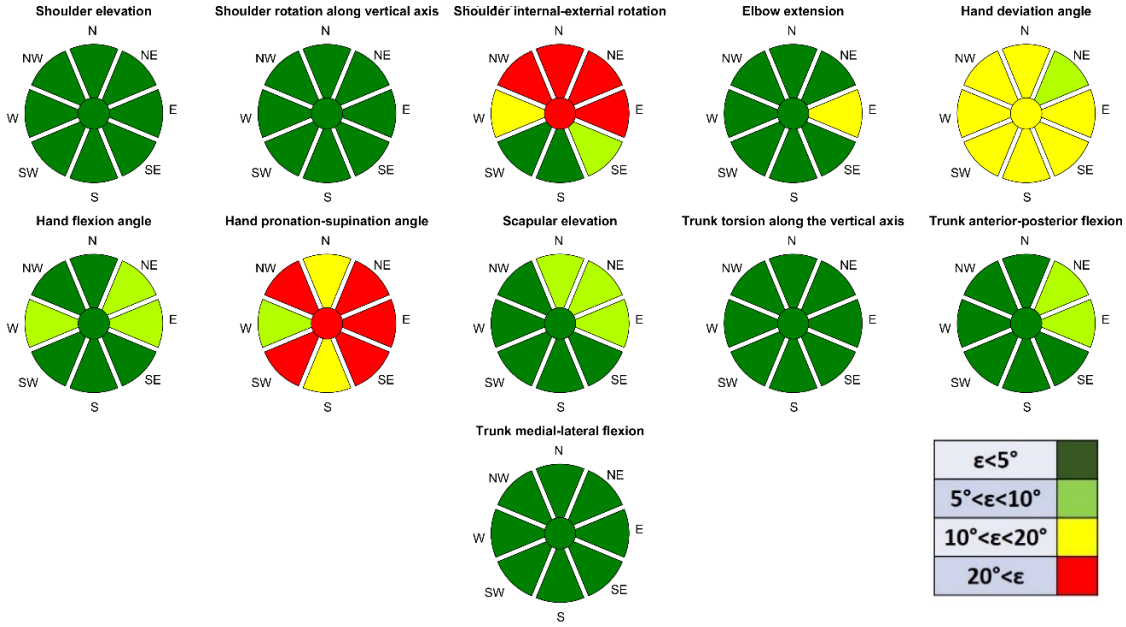

Figure 3.20. Subject 1: Error map of point-to-point, central sector.

Next the results extrapolated from the point-to-point movement performed in the central sector will be presented (Figure 3.17). In Figure 3.18, one can see the overlap between the two datasets for the point-to-point movement in the central sector. The datasets were represented with red for the Vicon system and the Kinect dataset with blue. In Figure 3.19, the error distribution for the same movement and in Figure 3.20 the error map. The variables tracked with an error below 10° e: shoulder elevation, shoulder rotation along the vertical axis, elbow extension, hand flexion angle, scapular elevation, trunk torsion, trunk anterior-posterior flexion

and trunk medial-lateral flexion. Meanwhile the variables tracked with an error mostly above 10° were shoulder internal-external rotation, hand pronation-supination and hand deviation angle.

Figure 3.21. Point-to-point movement in the left sector.

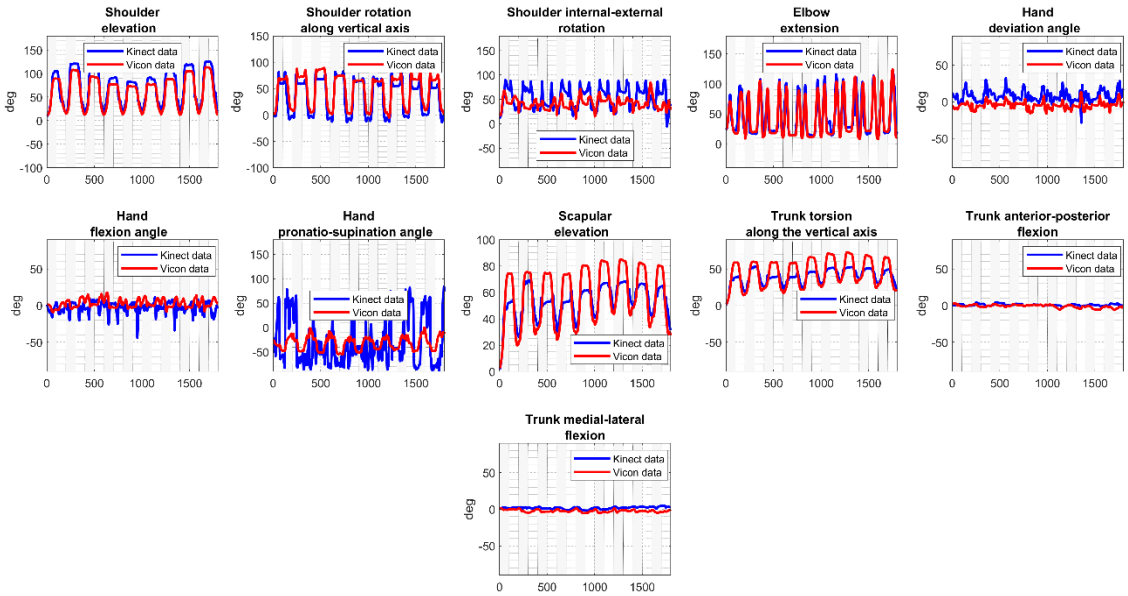

Figure 3.22. Subject 1: Point-to-point, left sector: temporal sequence of phases. The Kinect dataset is represented with blue and the Vicon dataset with red.

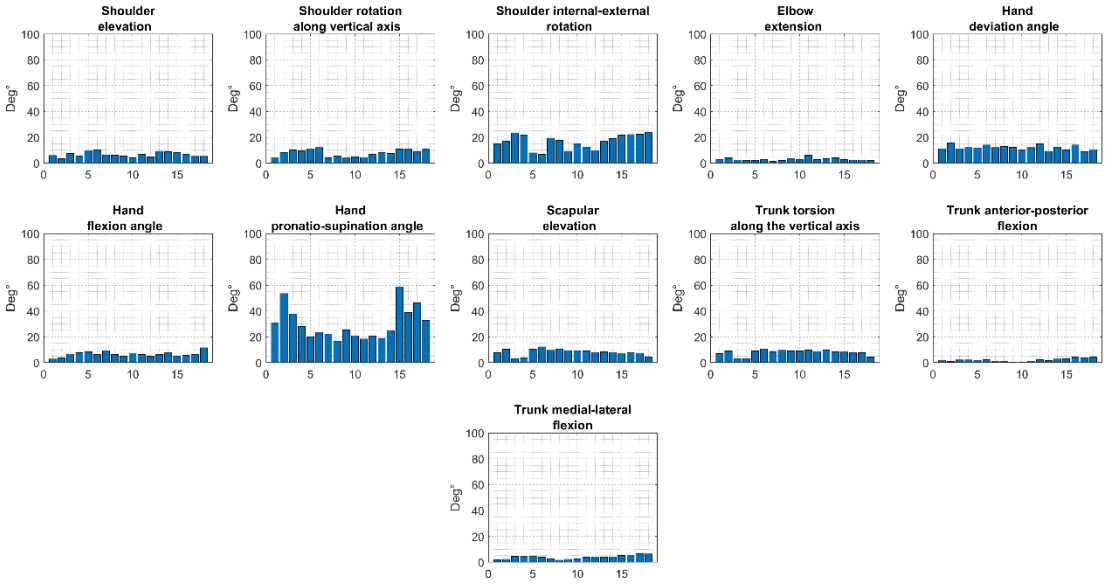

Figure 3.23. Subject 1: Point-to-point, left sector error distribution.

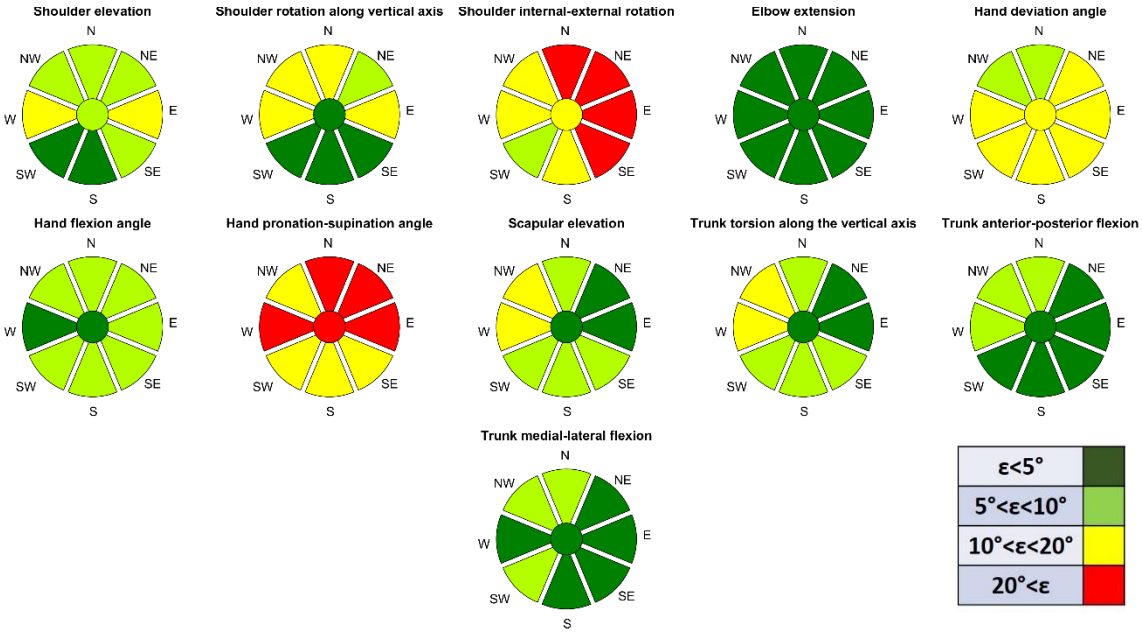

Figure 3.24. Subject 1: Error map of point-to-point, left sector.

Lastly the point-to-point movement in the left sector will be analyzed (Figure 3.21). Figure 3.22 illustrates the visual comparison between the two datasets. Figure 3.23 shows the error distribution for this movement and Figure 3.24 the error map. The error in this section of the workspace was higher with respect to the other two. The variables tracked with an error below 10° were: elbow extension, hand flexion-extension, trunk anterior-posterior flexion and trunk medial-lateral flexion. The variables tracked with an error mostly between 10° and 20° were: shoulder elevation, shoulder rotation along the vertical axis, hand deviation angle, scapular elevation and trunk torsion. Finally, the angles tracked with an error mostly above 20° were: shoulder internal-external rotation and hand pronation-supination.

3.1.2 Sample subject statistical analysis

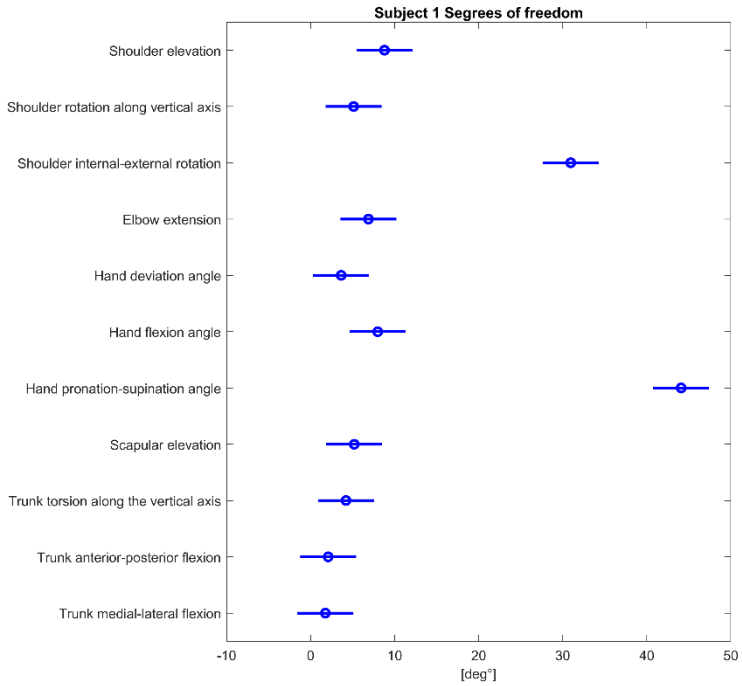

Figure 3.25. Subject 1: workspace exploration movement: 2-way ANOVA, DoFs comparison.

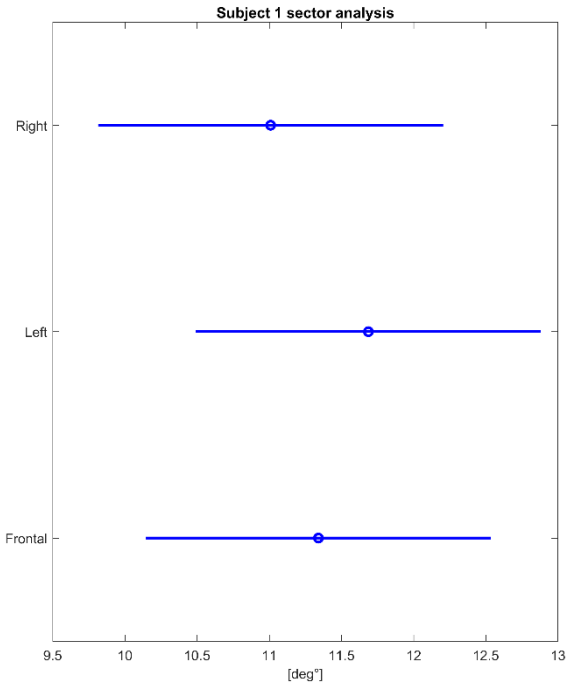

Figure 3.26. Subject 1: workspace exploration movement: 2-way ANOVA, sector comparison.

For the sake of a more concise analysis, only the results obtained through the test dataset will be presented. The reliability of the RGB-D sensors will be studied in section 3.2. The results of the 2-way ANOVA test performed on the first subject for the workspace exploration movement are represented in Figure 3.25 and Figure 3.26. Looking at Figure 3.25, a clustering between the degrees of freedom can be identified. The shoulder elevation angle resulted having a mean of 8.80° and the test failed to capture the statistical difference between it and shoulder rotation along the vertical axis (p=0.79), elbow extension (p=0.99), hand deviation angle (p=0.31), hand flexion-extension (p=1), scapular elevation (p=0.81) and trunk torsion (p=0.49). Meanwhile, it resulted different from: shoulder internal-external rotation (p<0.05), hand pronation-supination (p<0.05), trunk medial-lateral flexion (p=0.047) and trunk anterior-posterior flexion (0.028). Shoulder rotation along the vertical axis results having a mean of 5.12°, elbow extension presented a mean of 6.88°, hand deviation angle presented a mean of 3.63°, hand flexion-extension resulted having a mean of 7.99°, scapular elevation angle presented a mean of 5.19°, trunk torsion resulted having a mean of 4.21°, trunk anterior-posterior flexion of 2.09° and trunk medial-lateral flexion of 1.76°. Shoulder internal-external rotation presented a mean of 30.94 and was different from all other degrees of freedom (p<0.05). Hand pronation-supination presented a mean of 44.09 and was different from all the other degree of freedom (p<0.05).
Figure 3.26 illustrates the comparison between the three sectors. The right, left and central sectors presented respectively a mean of 11.01, 10.58 and 11.34. All three sectors' differences were statistically insignificant presenting a p-value between right and left sectors of 0.78, between right and central sectors of 0.94 and between central and left sectors of 0.94.

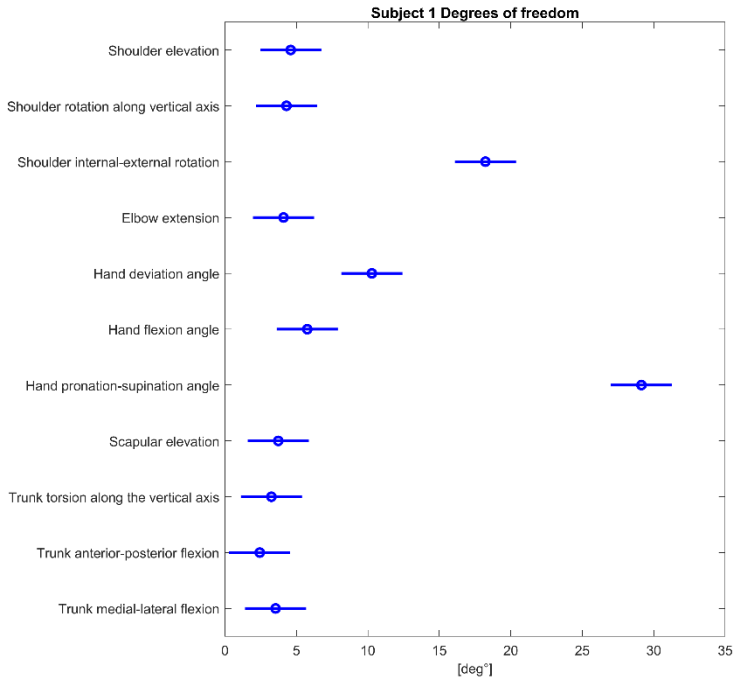

Figure 3.27. Subject 1: point-to-point movement 2-way ANOVA, DoFs comparison.

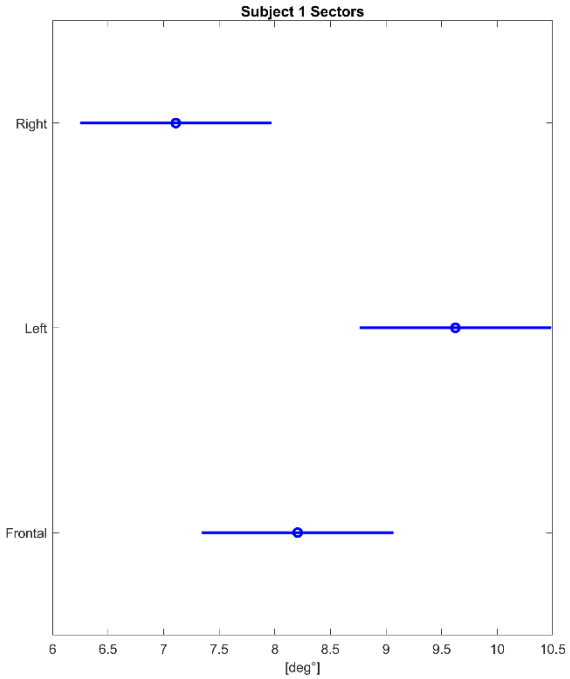

Figure 3.28. Subject 1: point-to-point movement: 2-way ANOVA, sector comparison.

From the results illustrated in Figure 3.27 and Figure 3.28 it is clear that the point-to-point movement yields a different clustering between the data with respect to workspace exploration. As portrayed in Figure 3.27, 4 clusters of variables can be identified. The shoulder elevation presented a mean of 4.61° and was grouped with shoulder rotation along the vertical axis with a mean of 4.31° (p=1), elbow extension with a mean of 4.11° (p=1), hand flexion angle with a mean of 5.77° (p=0.99), scapular elevation with a mean of 3.74° (p=0.99), trunk torsion with a mean of 3.26° (0.99), trunk anterior-posterior flexion with a mean of 2.44° (p=0.87) and trunk medial-lateral flexion with a mean of 3.55° (p=0.99). The second group composed only by hand deviation angle with a mean of 10.28° ($p<0.05$ with respect to all other). The third composed only by shoulder internal-external rotation with a mean of 18.23° ($p<0.05$ with respect to all other) and lastly the third group composed solely by hand pronation-supination angle with a mean of 29.14° ($p<0.05$ with respect to all other).

Figure 3.28 presents the differences between the three sectors. In this case the right, left and central sectors had respectively a mean of 7.11°, 9.08 and 8.21°. The right and left sectors were distinct one from the other with a p-value of 0.018. On the other hand, the central sector presented a weak statistical similarity with both right (0.3) and left (0.13).

3.1.3 All subjects' results

In this next section the mean performance of the RGB-D sensor will be presented by mapping the error of the device on the circular target as seen in section 3.1.1. The averaged data error (all subjects) for workspace exploration in the right sector was reported (Figure 3.29). The same result for the central (Figure 3.30) and left (Figure 3.31) sectors were reported. The same results were also reported for point-to-point for the right sector (Figure 3.32) central sector (Figure 3.33), and left sector (Figure 3.34).

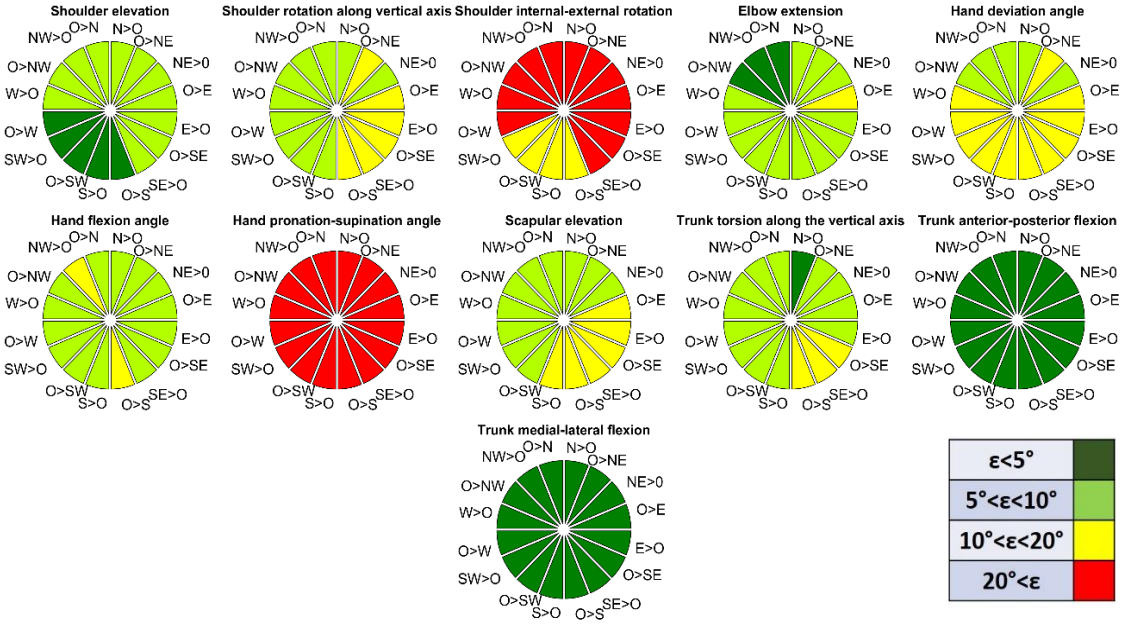

Figure 3.29. Mean error map: workspace exploration movement right sector

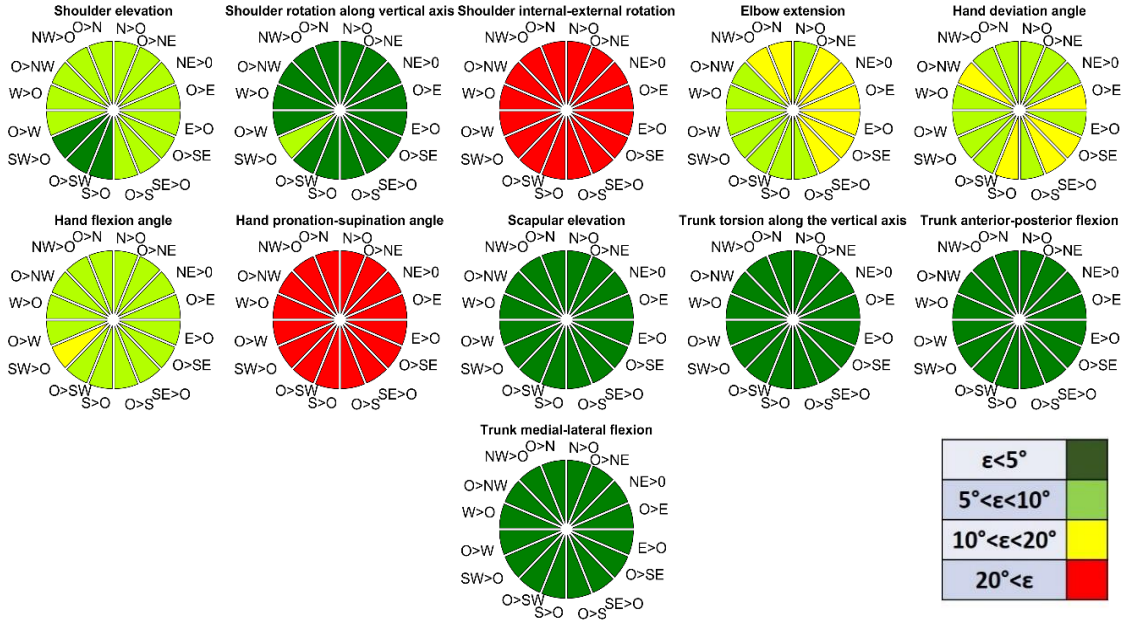

Figure 3.30. Mean error map: workspace exploration central movement sector

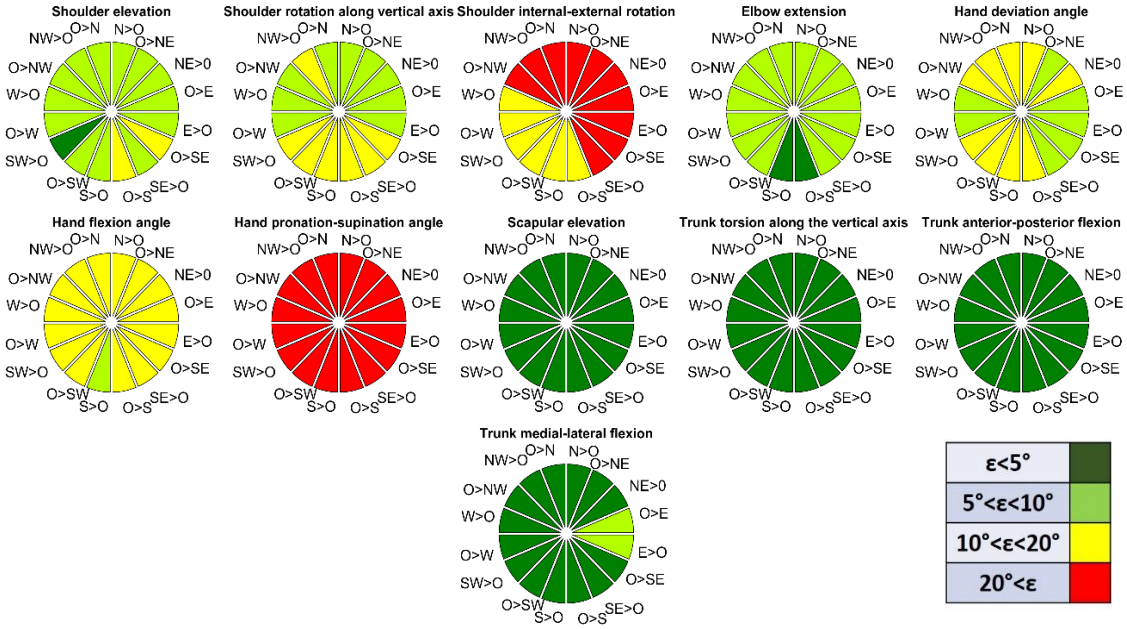

Figure 3.31. Mean error map: workspace exploration movement left sector

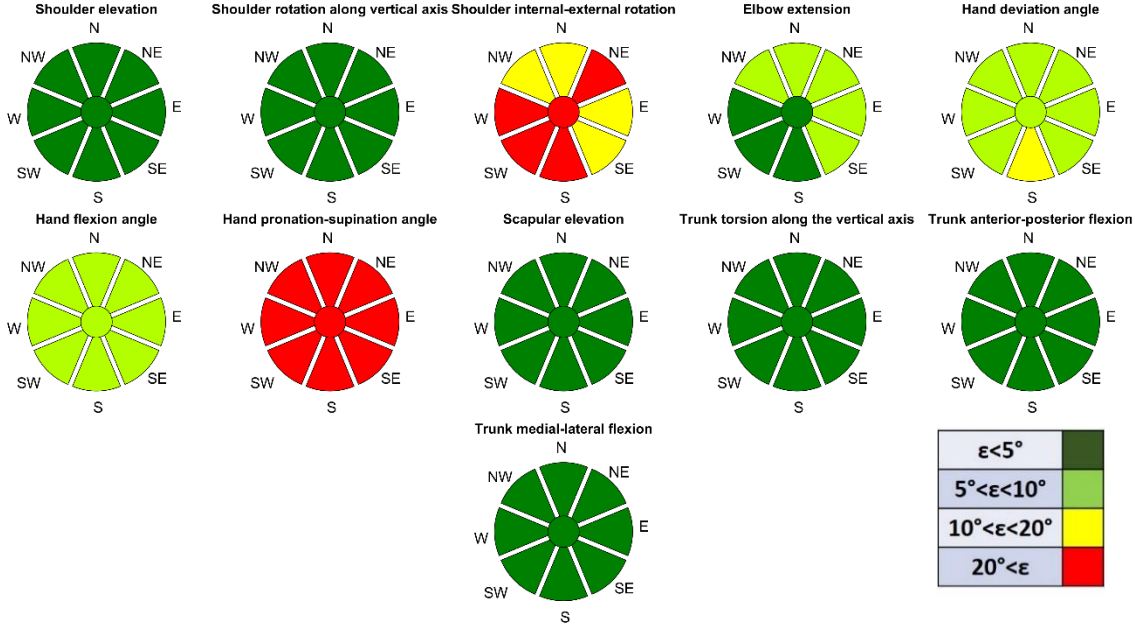

Figure 3.32. Mean error map: point-to-point movement right sector

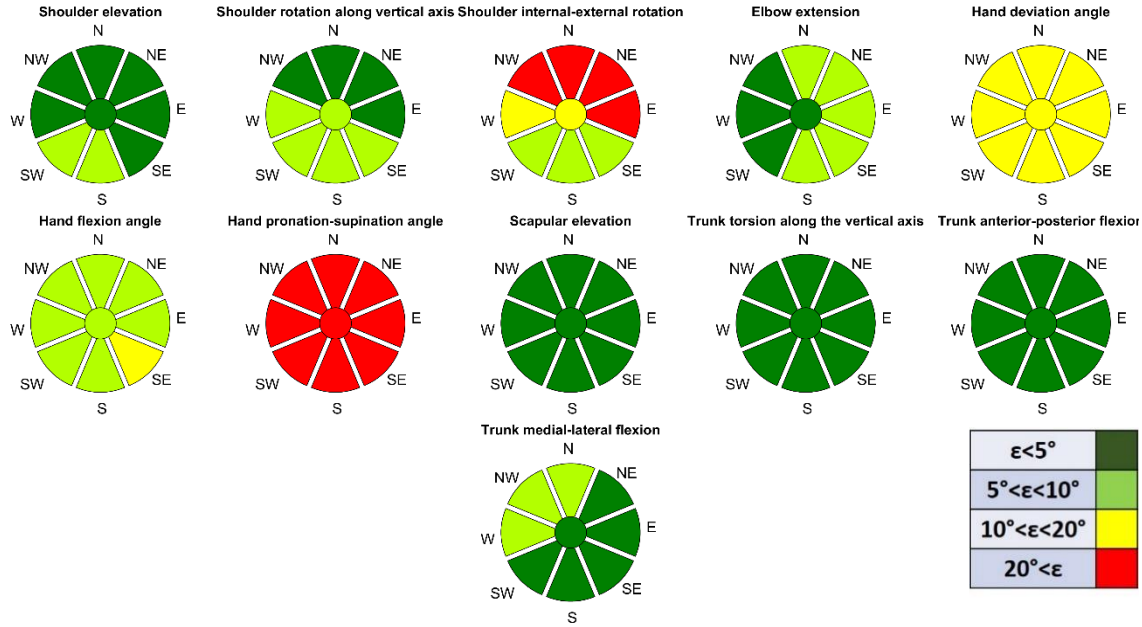

Figure 3.33. Mean error map: point-to-point movement central sector

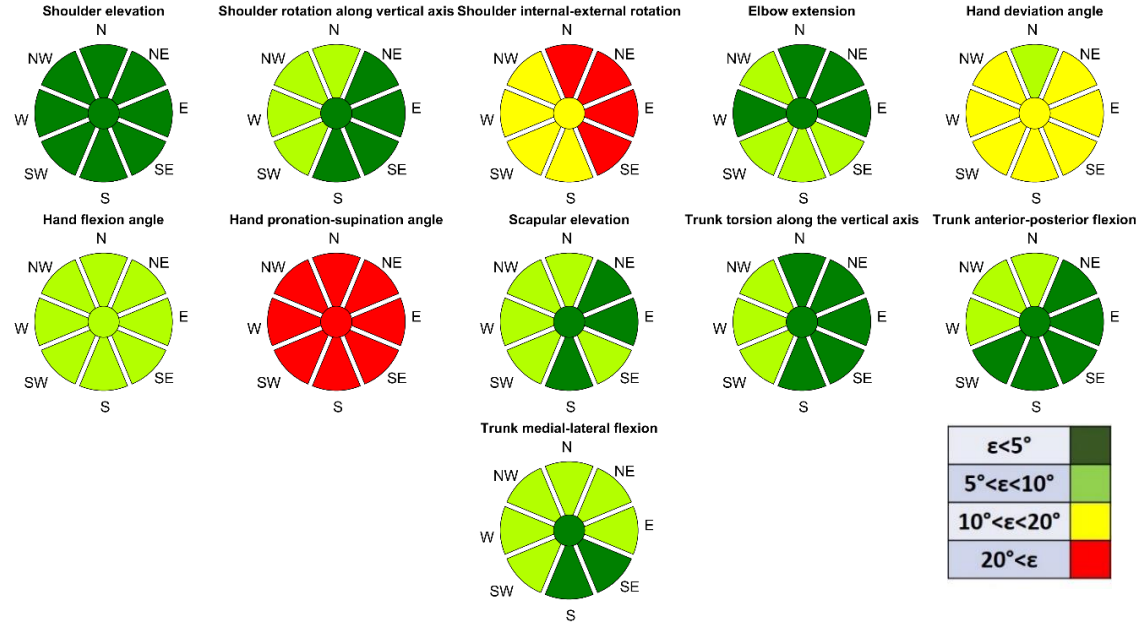

Figure 3.34. Mean error map: point-to-point movement left sector

The directional pie-charts had 16 cardinal directions for the workspace exploration meanwhile only 9 for the point-to-point movement. The graphical representation adopted the following thresholds: dark green indicated Ead≤5°; light green 5°<Ead≤10°; yellow 10°<Ead≤20°; red Ead>20°.

3.1.4 All subjects' statistical analysis

The presented results were related to the test dataset. The comparison between test and retest is presented in section 3.2. The two-way ANOVA analysis outlined that, on average, seven DoF presented a mean error lower than 10°. Two DoF presented an average error in the 10°- 20° range and one greater than 20° for both executed movements (point-to-point and exploration). Furthermore, one had error greater than 20° and different mean between point-to-point and exploration movements.

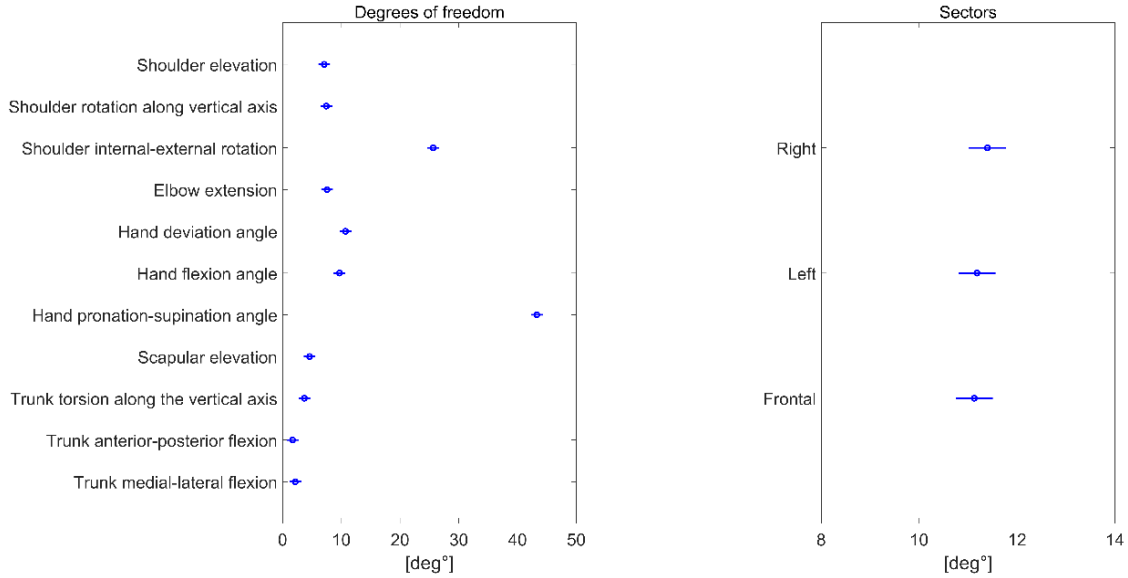

Figure 3.35. Workspace exploration movement: 2-way ANOVA test dataset. The left chart presents the results of the multiple comparison test performed between the degrees of freedom. The right chart depicts the multiple comparison test performed between the sectors.

The tests performed on the workspace exploration movement provided a clustering between the degrees of freedom and outlined that there is significant difference between the three sectors. Six groups of variables could be identified: shoulder elevation, shoulder rotation along the vertical axis and elbow extension grouped together by having similar mean with respect to shoulder elevation respectively ($p=1$ and $p=0.99$) and very different from the rest of the variables with $p<0.01$ for all three. Hand pronation-supination and hand flexion-extension had high similarity between each other ($p=0.87$) and different from all the others ($p<0.01$). Then, scapular elevation, trunk torsion and trunk medio-lateral have had similar means, respectively compwered to trunk torsion ($p=0.94$), meanwhile trunk antero-posterior flexion had a statistically similar mean only to trunk medio-later flexion ($p=0.99$) but different from trunk torsion ($p=0.05$) and different from scapular elevation ($p<0.01$), lastly shoulder internal-external rotation and hand pronation-supination had means statistically different from each other and from the rest ($p<0.001$). In the case of exploration, the inter-sector error was differently distributed: all the sectors had no statistical differences (central, 11.13°), right (11.39°) and left (11.18°).

Comparing right and left sectors, they resulted to be similar (p=0.79). The same can said for right and central (p=0.68) and for central and left (p=0.98). A clear visual representation is provided in Figure 3.35, where we show the distinction of the statistical analysis between test-retest.

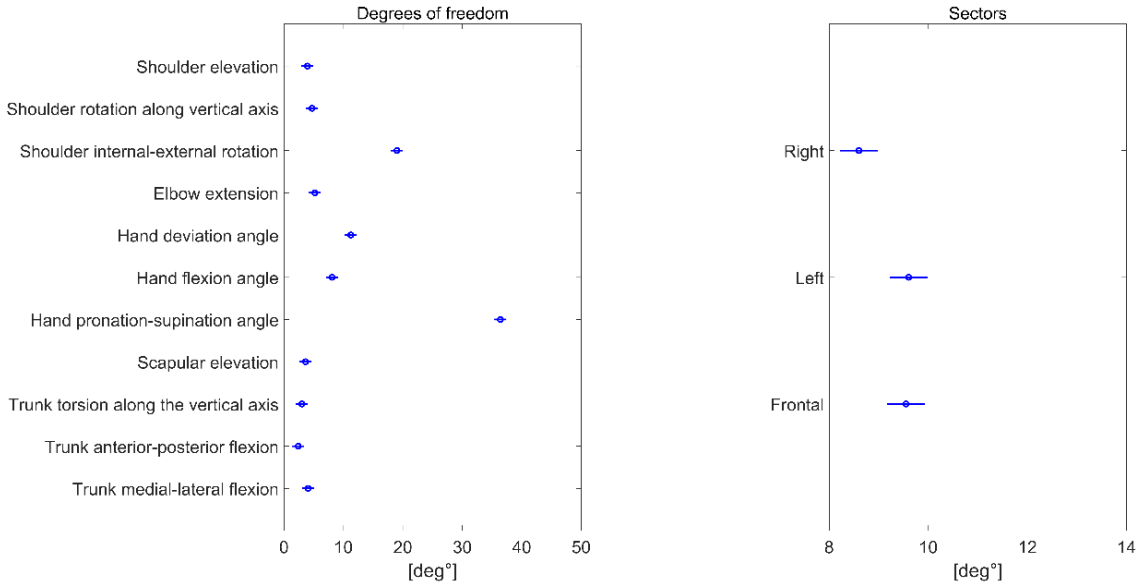

Figure 3.36. Point-to-point movements: 2-way ANOVA test dataset. The left chart presents the results of the multiple comparison test performed between the degrees of freedom. The right chart depicts the multiple comparison test performed between the sectors.

A more in-depth analysis of the point-to-point movement revealed that trunk torsion, trunk antero-posterior flexion, trunk medio-lateral flexion, shoulder elevation, shoulder rotation along the vertical axis, elbow extension and scapular elevation were tracked with an error lower or equal to 5°. The hand deviation angle and hand flexion-extension were tracked with an error range between 5° and 15°. The shoulder internal-external rotation was reconstructed with a mean error of about 20°. Lastly, the hand pronation-supination angle had a mean error greater than 20°. Furthermore, the mean of shoulder elevation had statistical similarity (same angular error) with the means of shoulder rotation along the vertical axis (p=0.96), scapular elevation (p=0.99), trunk torsion (p=0.78), trunk medio-lateral flexion (p=1), elbow extension (p=0.59) and trunk antero-posterior flexion (p=0.61). While shoulder internal-external rotation, hand pronation-supination, hand flexion-extension and hand deviation had means statistically different from each other and from the other angles ($p<0.001$). Meanwhile, from the comparison between the sectors, it was found that the average error in right sector was smaller than in the other two sectors, ranging between 8° and 9°, and was statistically different from the left and central sectors (respectively, p=0.012 and p=0.0053). Left and central sectors had similar means and were statically similar (p=0.96); the mean error varied between 9° and 10°. A clear visual representation is provided in Figure 3.36.

3.2 RGB-D system repeatability

In this section, the reliability was investigated through test-retest dataset comparison. For a general view of the reproducibility, the interclass correlation coefficient (ICC) between the datasets separately for each sector and for each movement was also computed. The point-to-point movement presented an interclass correlation coefficient of 0.81 ($p = 0$) for the right sector, the ICC of 0.82 ($p = 0$) for the central sector and the same index equal to 0.73 ($p<0.001$) for the left sector. Meanwhile, the exploration movement presented an ICC of 0.84 ($p = 0$) for the right sector, ICC of 0.75 ($p = 0$) for the central sector and of 0.62 ($p<0.001$) for the left sector.
Furthermore, a series of visual representations of the circular target illustrate through a colormap the repeatability of the Kinect for each specific DoF in each sector with respect to the directionality of the target. The repeatability was computed as a difference between test and retest datasets. First, the repeatability for workspace exploration movement in the right sector was reported (Figure 3.37). Then, the same result was reported for the central (Figure 3.38) and left (Figure 3.39) sectors. The same results were also reported for point-to-point movement for the right sector (Figure 3.40), central sector (Figure 3.41) and left sector (Figure 3.42). The graphical representation used the following thresholds: dark blue indicated $\Delta Ead \leq 2°$; light blue $2° < \Delta Ead \leq 5°$; yellow $5° < \Delta Ead \leq 10°$; red $\Delta Ead > 10°$ An overview of the results is available in Table 3.1 and Table 3.2.

Table 3.1. Euclidean angular distance, ordered by degrees of freedom and sectors (test and retest), and ICC: Point-to-point movements

Degree of freedom	Test mean [deg°]	Retest mean [deg°]
Shoulder elevation	3.96	3.82
Shoulder rotation along the vertical axis	4.73	4.88
Shoulder internal-external rotation	19.00	18.18
Elbow extension	5.20	5.36
Hand deviation angle	11.25	11.60
Hand flexion-extension angle	8.10	7.89
Hand pronation angle	36.40	38.59
Scapular elevation	3.64	3.70
Trunk torsion	3.02	3.01
Trunk anterior-posterior flexion	2.41	2.61
Trunk medial-lateral flexion	4.06	4.22

Sectors	Test mean [deg°]	Retest mean [deg°]	ICC
Right	8.59	8.77	0.81
Central	9.55	9.73	0.82
Left	9.60	9.82	0.73

Table 3.2. Euclidean angular distance, ordered by degrees of freedom and sectors (test and retest), and ICC: Workspace exploration movements

Degree of freedom	Test mean [deg°]	Retest mean [deg°]
Shoulder elevation	7.09	6.92
Shoulder rotation along the vertical axis	7.44	8.67
Shoulder internal-external rotation	25.63	26.93
Elbow extension	7.56	7.43
Hand deviation angle	10.70	10.47
Hand flexion-extension angle	9.69	9.70
Hand pronation angle	43.28	44.06
Scapular elevation	4.60	4.67
Trunk torsion	3.70	4.16
Trunk anterior-posterior flexion	1.71	1.67
Trunk medial-lateral flexion	2.16	2.17

Sectors	Test mean [deg°]	Retest mean [deg°]	ICC
Right	11.39	11.81	0.84
Central	11.13	11.45	0.75
Left	11.18	11.34	0.62

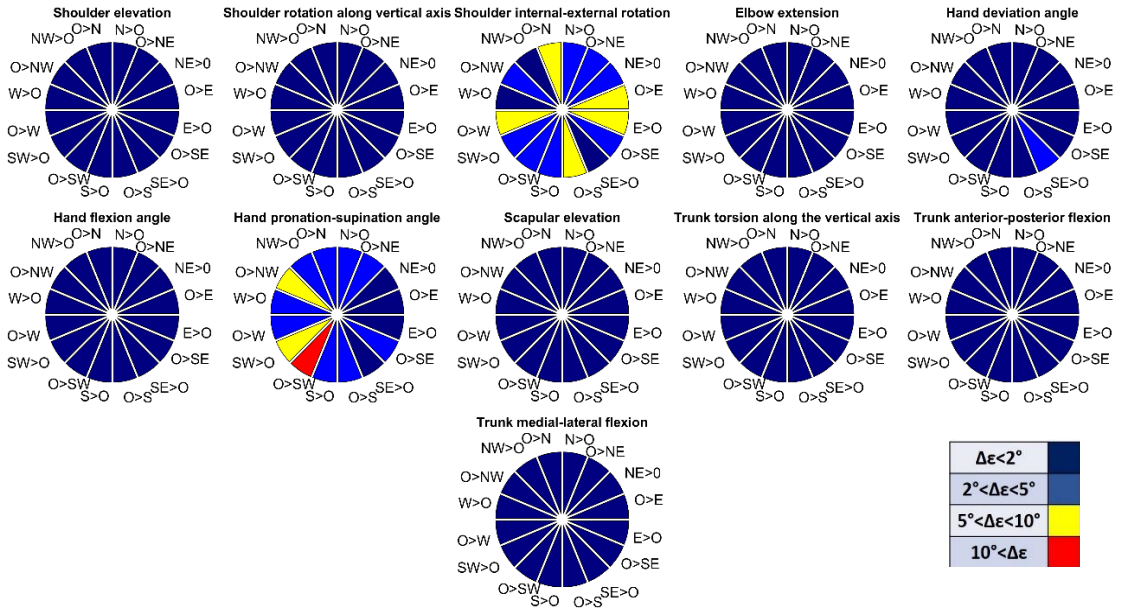

Figure 3.37. Reliability map: Workspace exploration movement right sector

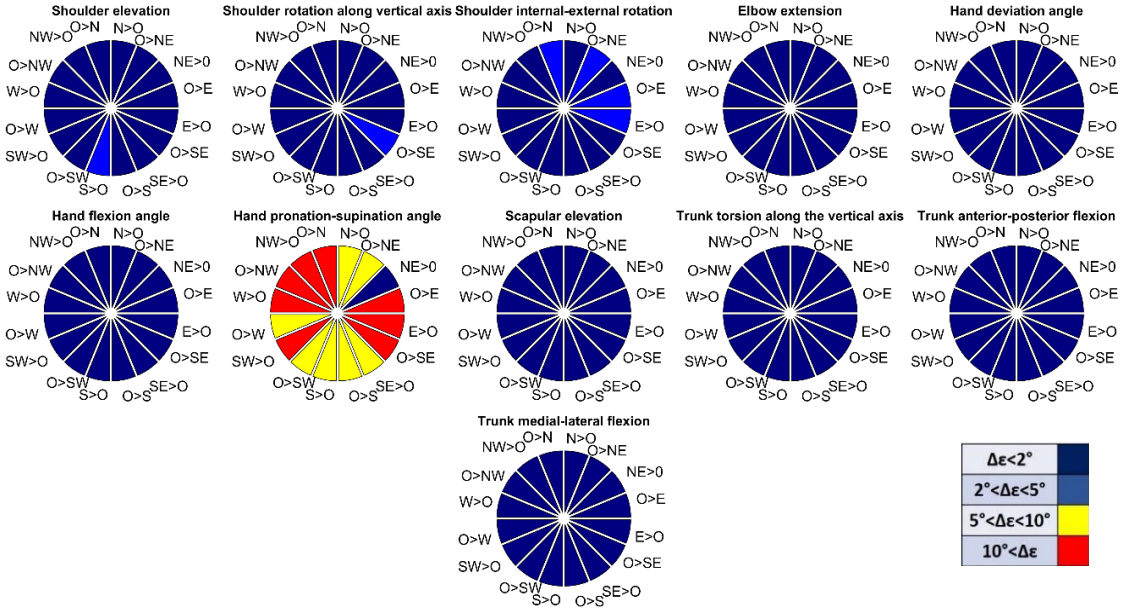

Figure 3.38. Reliability map: Workspace exploration movement central sector

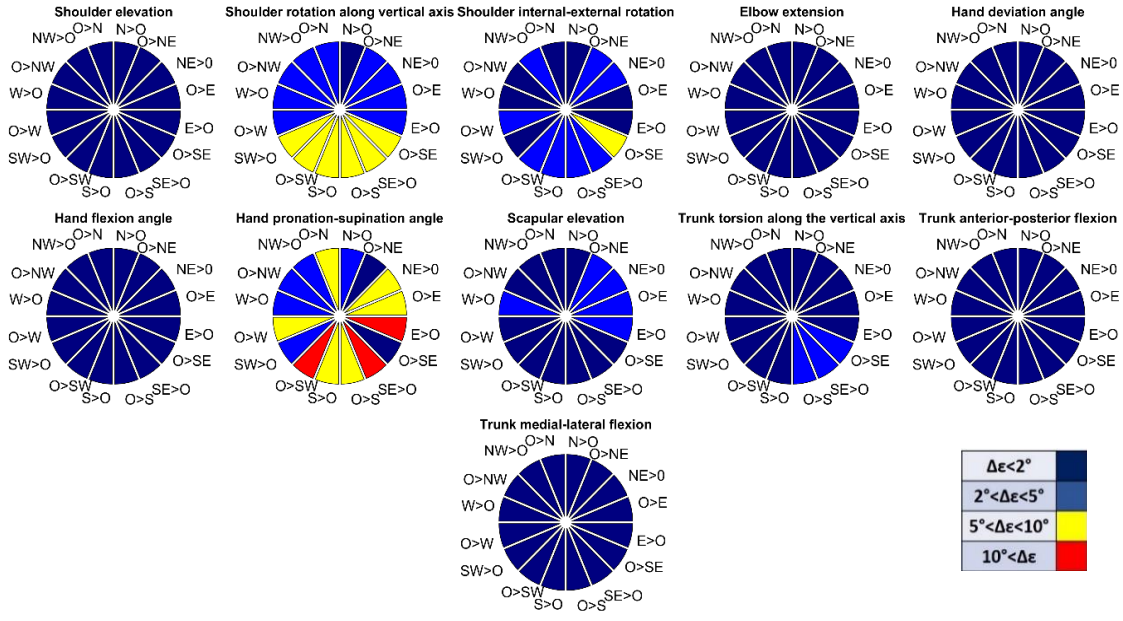

Figure 3.39. Reliability map: Workspace exploration movement left sector

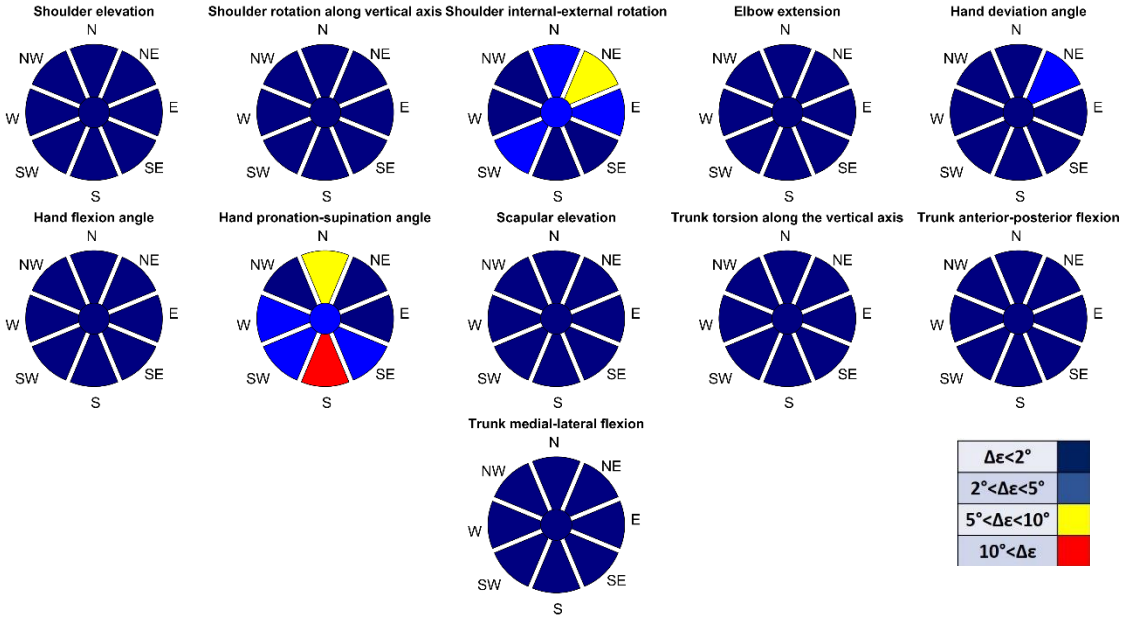

Figure 3.40. Reliability map: Point-to-point movement right sector

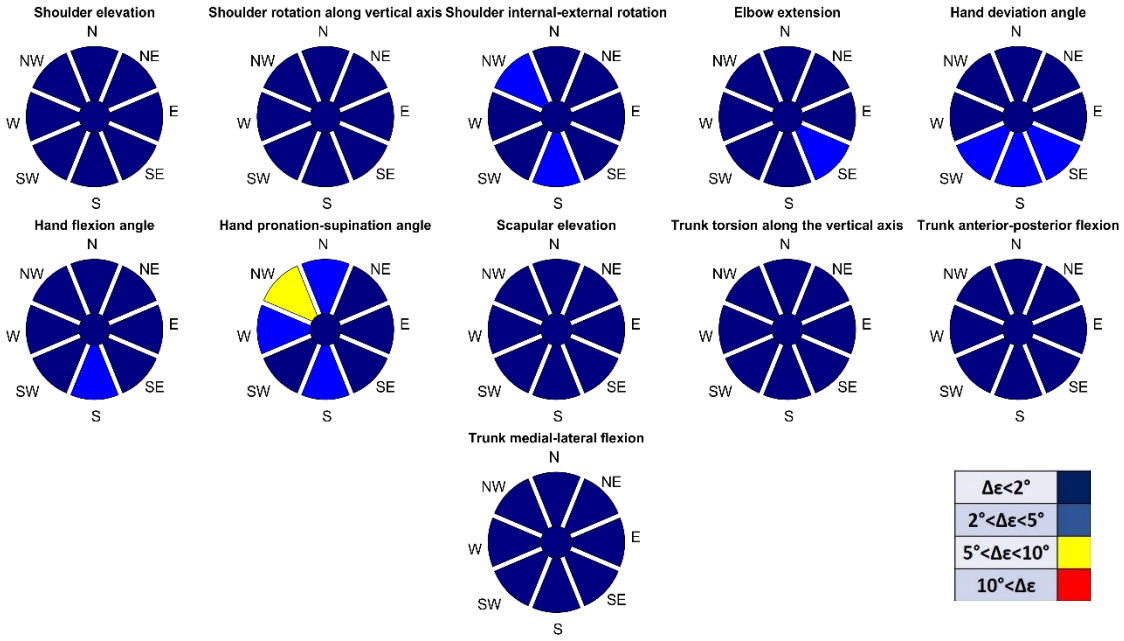

Figure 3.41. Reliability map: Point-to-point movement central sector

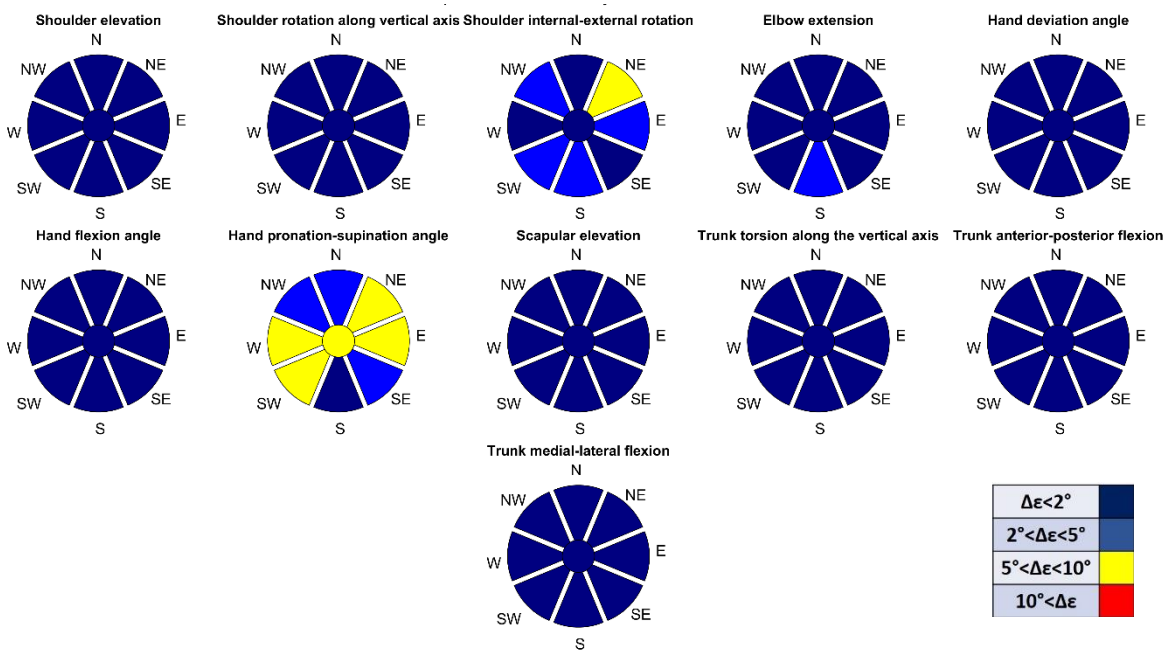

Figure 3.42. Reliability map: Point-to-point movement left sector

As can be noted, most degrees of freedom were tracked with intra-session error below 2 degrees of angular difference across all sectors and types of movements. One degree in particular, presented a poor inter-session error thus resulting less reliably approximated by the RGB-D device. Furthermore, in general it was found that the left sector presented a worst inter-session error providing a less reliable approximation of the movement.

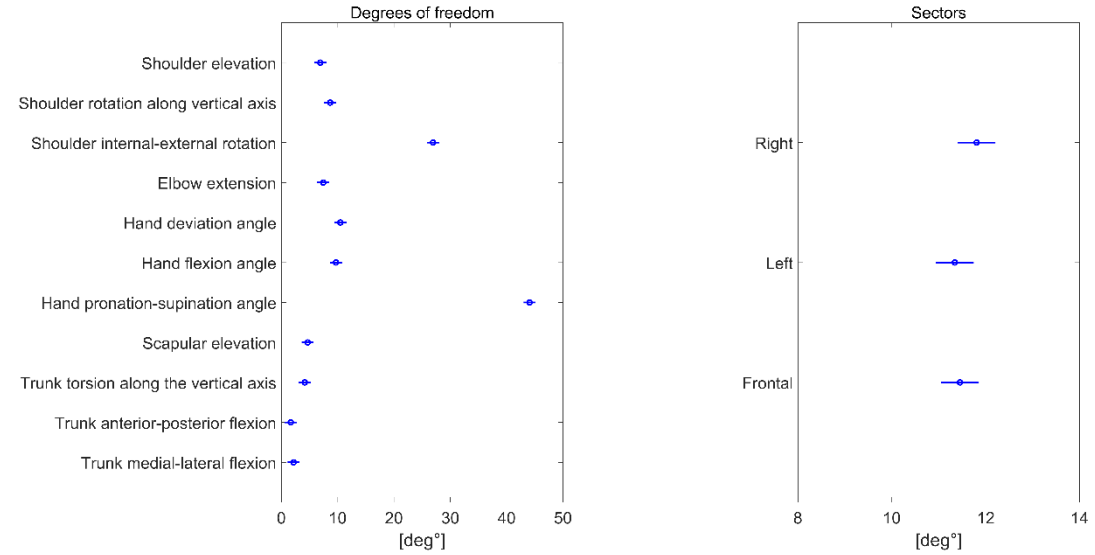

Figure 3.43. Workspace exploration movements: 2-way ANOVA retest dataset

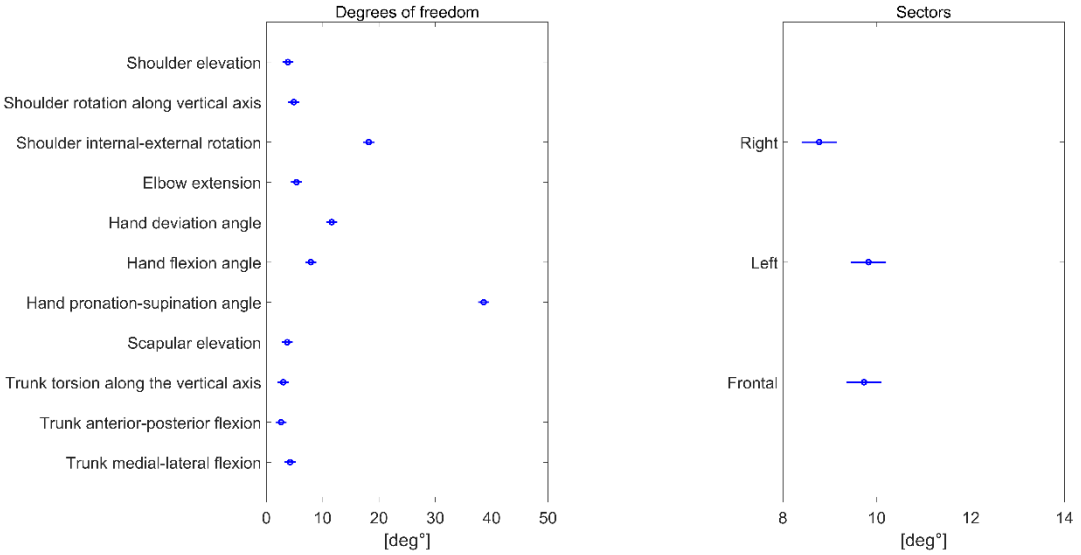

Figure 3.44. Point-to-point movements: 2-way ANOVA retest dataset

Figure 3.41 and Figure 3.42 show the results of the statistical analysis performed on the retest dataset used for the reliability assessment.

Chapter 4 Discussions

4.1 Overview

The RGB-D sensor tracked most of the degrees of freedom considered, resulting in errors sensibly smaller than the range of motion registered. It is necessary though, to highlight that two of the chosen variables presented a non-negligible tracking error with respect to the gold standard measuring systems. These critical variables were the 'shoulder internal-external rotation' and the 'hand pronation-supination' as already stated in the results, thus one should be mindful of relying on data related to these two particular variables. These limitations aside, the device offers reliable data in tracking point-to-point movements in the central and right sectors. It is also worth noting that examining hand movements and/or movements performed in the left sector has proven to be less reliable in the test-retest comparison.

4.2 Degrees of freedom

Most degrees of freedom were tracked with an error below 10°. This result is consistent with previous studies (Scano A. et al. 2014), in which the variables describing shoulder elevation and elbow extension were tracked with an error around 5°, but in a more constrained scenario (mono-directional reaching movements). The test of accuracy on healthy individuals, on indexes related to rehabilitation, revealed that most clinical parameters presented a high absolute agreement and no systematic bias between RGB-D and marker-based systems (Otte K. et al. 2016). Other similar investigations (Cai L. et al. 2019) found that most of the parameters extrapolated were tracked with an RMSE below 10°, which is comparable to the results obtained in the current document. Other studies reported even more precise results for shoulder tracking but focused on a restricted range of postures (Lee S. H. et al. 2015). The only degrees of freedom presenting a worse error were the ones related to hand movements. This finding suggests that one should be careful when registering hand-related kinematics with RGB-D cameras in a context of high variability. In fact, in the current study, two angles presented a large error: 'the shoulder internal-external rotation' and 'the hand pronation-supination'.

The first one is critical since it is based on the projection of the forearm on the transversal plane of the upper arm. This projection highly depends on the angle of elbow extension, which means that when the angle between the arm and upper arm approaches 0°, the shoulder internal-external rotation cannot be computed with high reliability since the arm is approaching kinematic singularity. Moreover, in similar configurations, small displacements in joint center reconstruction can produce unpredictable variations in the angle extrapolation. In this study, this condition is stressed since the limb is often in a fully extended posture of singularity (especially in exploration movements). This is most likely the reason for generally finding worse results in respect to previous works (Galna B. et al. 2014), (Lee S. H. et al. 2015). It is highly probable that, in a wide exploration of the workspace, the tracking is inferior to more constrained scenarios.

Since the two systems presented different virtual skeletons (Galna B. et al. 2014), angles such as pronation-supination of the forearm was roughly approximated. Using the Kinect SDK skeleton, this variable was computed using the angular variation of a unitary vector starting from wrist and pointing towards the thumb. The angular variation of this vector around the axis of the forearm could be assumed to be the hand pronation-supination if the subject did not open or close the hand. Meanwhile, the Vicon upper-limb skeleton provided markers which could accurately describe this rotation. A critical observation that made difficult the extrapolation of this angle was the difficulty of the Kinect device to identify the thumb. The results obtained are partially in line with the findings of a comprehensive previous study (Galna B. et al. 2014), revealing that fine movements related to the hand could benefit from ad-hoc hand-models, which were not implemented in this study. Moreover, in the assessment of body extremities (hands and feet), even previous works found lower signal-to-noise ratio (Otte K. et al. 2016) leading to poorly accurate tracking. Furthermore, the movements analyzed in this document were very demanding for reliable hand pronation and supination computation.
More broadly, an interesting finding is that the tracking performance appears to be better for movements with wide range of motions, such as point-to-point movements, which have been better tracked than hand exploration movements. Arguably, Microsoft's built-in algorithms have made it possible to better reconstruct wider movements with a broader articular range. These results should be taken into account when tracking individuals in environments where high tracking precision is required.

4.3 Sectors

So far, RGB-D sensors such as Kinect V2 were tested considering mainly the performance of the sensor for tracking gestures designed to emphasize specific degrees of freedom (Galna B. et al. 2014), or during rehabilitative-oriented tasks (Scano A. et al. 2014), (Scano A. et al. 2015), (Cameirão M. S. et al. 2016), (Pifster A. et al. 2014). The contribution of this study was to strongly characterize the performance of the RGB-D sensor in upper-limb movements in the context of continuous variability which is naturally found in daily-life tasks and working activities (Scano A. et al. 2019).
The accuracy in tracking workspace sectors differed amongst the two analyzed movements. For the point-to-point movement, it should be noted that there is a statistically significant difference for the left and central sectors, where tracking performance of the Kinect is poor with respect to the right sector. The latter's performance is likely due to the fact that even if the target was positioned to the left or in front of the subject, the movement was performed with the right arm. Consequently, during the execution of the tasks in these conditions, part of the subject's body was partially hidden by the arm for significant periods of time, causing the device to estimate the position of the covered points, probably introducing further errors. This experimental condition is common to RGB-D devices and should be considered as one of the main limitations to the adoption of such solutions in relation to marker-based systems. However, depending on the context, the use of ad-hoc algorithms might be considered to solve this issue. Self-occlusion problems are known to introduce tracking errors, as possible solutions have been studied and implemented with the use of more RGB-D sensors (Wu C. et al. 2017)
For the workspace exploration movement, it was found that the performance of the left and central sectors respectively were comparable, while for the right sectors it was slightly worse. However, the ICC for the right and central sectors proved to be higher and thus these two sectors provided more consistent and reliable data.

This suggests that in order to have the highest reliability and lowest error of measurement, the central sector might be the most appropriate for registering this type of movements. These results show that the use of RGB-D devices can be more critical in the presence of obstruction. However, it should be noted that the overall difference is limited to less than 3°, even when performances were not statistically repeatable.
The results might be of interest to the scientific community for estimating more reliable configurations for accurate gesture recognition in several domains (Cicirelli G. et al. 2015), particularly for the use of the upper-limb in ambient of assisted living, clinics and working environments (Mosca N. et al. 2017).

4.4 Repeatability

The test-retest allowed to characterize the reliability of the RGB-D sensor. It was found that repeatability was relatively high in both point-to-point and exploration movements, except for hand pronation and supination degree of freedom. These results are generally in line with previous findings. In fact, preliminary studies on healthy individuals acknowledged that RGB-D sensors offer the same repeatability of marker-based systems (Bonnchere B. et al. 2014). Similar results were found in a comprehensive rehabilitation-oriented study analyzing whole body movement, especially walking. The authors concluded that repeatability analysis yielded rather similar results for both Kinect V2 and Vicon (Otte K. et al. 2016). The results of the current study align with past studies which show acceptable reliability and sensitivity across sessions for many parameters measured by Kinect for both healthy subjects as well as for stroke patients (Mobini A. et al. 2015). Additionally, a high reliability for assessing the kinematics of the trunk and hips, and a low to moderate reliability for the lower limbs were found (Mentiplay B. et al. 2018). All these studies considered gestures strongly linked to degrees of freedom: the slightly more cautious results achieved in this study are possibly related to the choice of a more demanding protocol (choice of gestures, variability and configurations) that stressed the tracking capability of the sensor on generic movements. No significant differences were found in repeatability across sectors, even though, as expected, the left sector showed slightly worse repeatability, probably due to obstruction. A general overview of the results is presented in Table 4.1, Table 4.2, Table 4.3 and Table 4.4.

Table 4.1. Overview of the three sectors for the workspace exploration movement

Workspace exploration movement	Right sector	Central sector	Left sector
Accuracy	Moderate	Moderate	Moderate
Repeatability	High	High	Moderate

Table 4.2. Overview of the three sectors for the point-to-point movement

Point-to-point movement	Right sector	Central sector	Left sector
Accuracy	High	High	High
Repeatability	High	High	Moderate

Table 4.3. Overview of the degrees of freedom for workspace exploration movement

Degree of freedom	Error	Repeatability
Shoulder elevation	High	High
Shoulder rotation along the vertical axis	High	High
Shoulder internal-external rotation	Low	Low
Elbow extension	High	High
Hand deviation angle	Moderate	Moderate
Hand flexion-extension angle	High	High
Hand pronation angle	Low	Low
Scapular elevation	High	High
Trunk torsion	High	High
Trunk anterior-posterior flexion	High	High
Trunk medial-lateral flexion	High	High

Table 4.4. Overview of the degrees of freedom for the point-to-point movement

Degree of freedom	Error	Repeatability
Shoulder elevation	High	High
Shoulder rotation along the vertical axis	High	High
Shoulder internal-external rotation	Low	Low
Elbow extension	High	High
Hand deviation angle	Moderate	Moderate
Hand flexion-extension angle	High	High
Hand pronation angle	Low	Low
Scapular elevation	High	High
Trunk torsion	High	High
Trunk anterior-posterior flexion	High	High
Trunk medial-lateral flexion	High	High

4.5 Real life scenarios

As already highlighted in the literature, the RGB-D devices can register upper-limb gestures having already been used in rehabilitative applications for physical assessment or training, like bi-dimensional movements in the sagittal plane (Scano A. et al. 2018), in the frontal plane (Capecci, M. et al. 2016), or even the three-dimensional range of motion of the upper limb (Bonnchere B. et al. 2016). In other cases, it has been used to assess the reachable workspace of patients with amyotrophic lateral sclerosis (ALS) (Oskarsson B. et al. 2016). Its use in this domain is a great advantage for both clinicians and patients alike. For example, ranges of motion provide accurate enough approximations of the joint position, providing clinicians with an objective indicator of the wellbeing of the patients. From a patient's point of view, it might lead to making home-based

rehabilitative treatments increasingly common. Additionally, it could also prove to be relevant for sport applications, such as the assessment the risks of anterior cruciate ligament injuries (ACL) (Mentiplay B. et al. 2018).

On the other hand, industrial applications are oriented towards workplace physical occupation, safety and injury prevention. Thus, movements on a workbench may include many simple movements, such as reaching for objects, or more complex ones, such as manipulating items on the table, or interacting with machines using simple and controlled movements, such as hand-over gestures (Pellegrinelli S. et al. 2016), (Glasauer S. et al. 2010), (Field M. et al. 2009). In a more general industrial context, it has been already used to study work environment safety. In the context of the recently started European H2020 Project "Mindbot" (https://cordis.europa.eu/project/id/847926), RGB-D technologies will be assessed while monitoring workers during interaction with collaborative robots. Moreover, the newly released Kinect Azure (https://azure.microsoft.com/it-it/services/kinect-dk/) will enhance the tracking capability of Kinect V2 and provide a more advanced tool to adopt the concepts proposed in this paper.

4.6 Limitations

The first limitation of this work is the limited number of workspace sectors. Real application scenarios might require the involvement of other sectors, such as shown in other upper-limb studies (Scano A. et al. 2019) simulating assembly scenarios that were excluded in this study due to limitations of the Kinect system tracking algorithms. Also, the number of movements could be expanded to mimic real scenarios, including other upper-limb gestures useful in industry (Pellegrinelli S. et al. 2016), (Jiang S. et al. 2017), (Miguez S. A. et al. 2016) and the tracking of other body segments, such as legs (Otte K. et al. 2016), (Bonnchere B. et al. 2016). A model incorporating the full human body would enable the inspection of a wider number of degrees of freedom and the comparison of the performance of full 3D movement. Moreover, other RGB-D solutions can be considered, both in the employed sensors and employed algorithms. For this study, a well-documented, commercial solution with wide diffusion was chosen.

Furthermore, only conditions in which the subjects obstruct the tracking were considered; in real scenarios, the environment might include further limitations. Lastly, it would be advised to consider an extended group of subjects in order to support a more solid statistical analysis.

Chapter 5 Conclusions

This study focused on the comparison of an RGB-D commercial sensor with a gold standard optoelectronic marker-based system. It was found that the RGB-D sensor with embedded human tracking algorithm could properly approximate the DoF computed with the marker-based system. However, it was found that the performance of the RGB-D sensor is less appropriate for the detection of specific DoF and that "wider" movements such as point-to-point are tracked with greater accuracy than those of exploration. In conclusion, RGB-D sensor is a potential candidate for motion analysis in rehabilitative and industrial settings where marker-based systems cannot be employed. These results could be of great interest to the scientific community and as such, they will be published in a scientific paper.

5.1 Future developments

Although RGB-D sensors have been studied in many contexts and used in many applications, there are still many areas in which they could be put to use. One could try and validate the use of these devices while extrapolating more complex kinematic variables such as kinematic synergies related to upper limb, lower limb or full body movements. One might also be interested in further assessing the performance of these devices in critical conditions, such as workplace environments with less favorable lighting conditions and obstructions other than the human body itself. Further tests should be performed on assessing the tracking capabilities of RGB-D devices of more demanding movements extrapolated from daily life and industry.

First Appendix

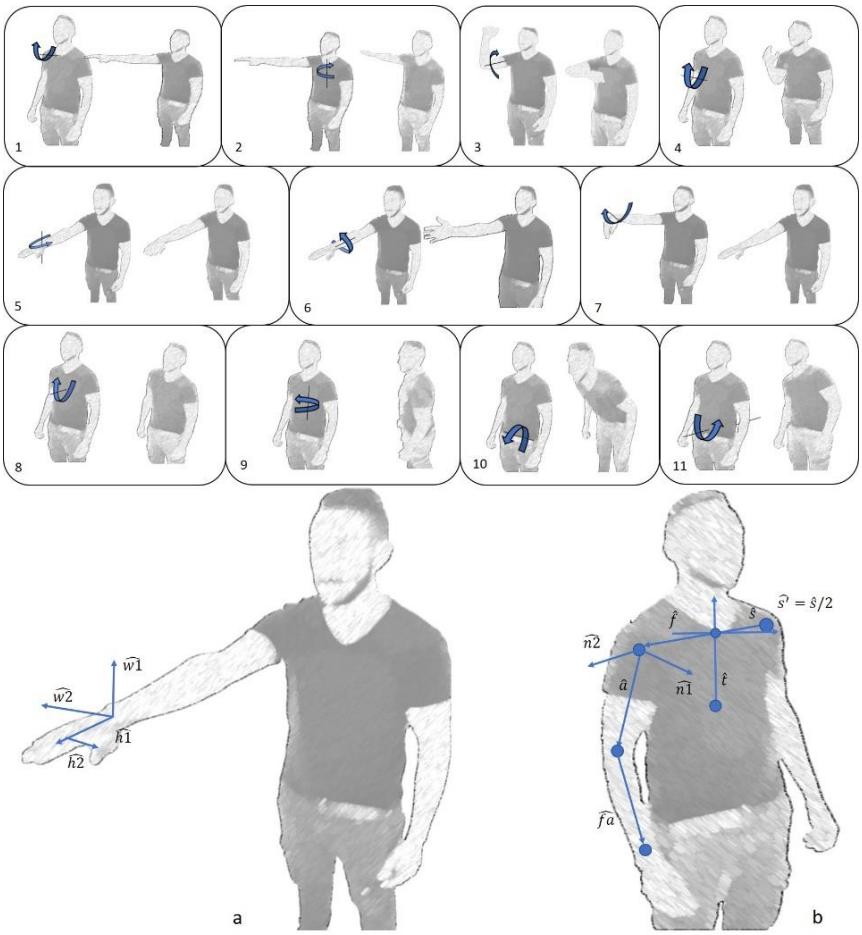

Figure 5.1. Graphical representation of the degrees of freedom computed with Vicon and Kinect V2.

In Figure 5.1 we have the comprehensive list of all degrees of freedom used which are in order:
1. Shoulder elevation; 2. Shoulder rotation along the vertical axis; 3. Shoulder internal-external rotation; 4. Elbow flexion-extension; 5. Hand flexion-extension; 6. Hand pronation-supination; 7. Hand deviation; 8. Scapular elevation; 9. Trunk torsion; 10. Trunk anterior-posterior flexion; 11. Trunk medial-lateral flexion; a. Hand reference vectors; b. Subject reference system.

$$Shoulder\ elevation = acos\ [\hat{a} * (-\hat{t})] \quad (5.1)$$

$$Shoulder\ rotation = acos\left[\widehat{ap} * (-\hat{f})\right] - 90 \quad (5.2)$$

$$Shoulder\ internal - external\ rotation = \text{acos}\ (\widehat{af\_p} * \widehat{n2}) - 90 \quad (5.3)$$

$$Elbow\ extension = acos\ (\hat{a} * \widehat{af}) \quad (5.4)$$

$$Scapular\ elevation = acos\ (\widehat{s'} * (\hat{s})) \quad (5.5)$$

$$Hand\ fexion\ and\ extension = acos\ (\widehat{u\_hand\_\Pi} * \widehat{w1}) - 90 \quad (5.6)$$

$$Hand\ deviation = acos\ (\widehat{u\_hand\_\Phi} * \widehat{w2}) - 90 \quad (5.7)$$

$$Hand\ pronation/supination = acos\ (\widehat{u\_hand2\_\Omega} * \widehat{w1}) - 90 \quad (5.8)$$

$$Trunk\ torsion = acos\left[\hat{s} * \left(-\hat{f}\right)\right] - 90 \quad (5.9)$$

$$Trunk\ antero/poesterior\ flexion = acos\ (\widehat{t_{sag}} * \hat{f}) \quad (5.10)$$

$$Trunk\ medio/lateral\ flexion = acos\left[\widehat{t\_front} * \left(-\widehat{s'}\right)\right] - 90 \quad (5.11)$$

Above are listed all the equations used in the extrapolation of the degrees of freedom.

Bibliography

Bagesteiro, L. B. and Sainburg, R. L. "Handedness: dominant arm advantages in control of limb dynamics," Journal of Neurophysiology, vol. 88, no. 5, pp. 2408–2421, 2002

Basso F. et al. Fast and robust multi-people tracking from RGB-D data for a mobile robot. In: Intelligent Autonomous Systems 12. Springer, Berlin, Heidelberg, 2013. p. 265-276.

Bonnechere B., Jansen, B., Salvia, P. et al., "Validity and reliability of the Kinect within functional assessment activities: comparison with standard stereophotogrammetry," Gait and Posture, vol. 39, no. 1, pp. 593–598, 2014.

Bonnechere B. et al. Three-dimensional functional evaluation of the shoulder complex using the Kinect™ sensor. In: Proceedings of the 4th Workshop on ICTs for improving Patients Rehabilitation Research Techniques. ACM, 2016. p. 5-8.

Brokaw E. B., Eckel, E. and Brewer B. R., "Usability evaluation of a kinematics focused Kinect therapy program for individuals with stroke," Technology and Health Care, vol. 23, no. 2, pp. 143–151, 2015.

Cai L, Ma Y, Xiong S, Zhang Y. Validity and Reliability of Upper Limb Functional Assessment Using the Microsoft Kinect V2 Sensor. Applied bionics and biomechanics. 2019;2019.

Caimmi M., Guanziroli E., Malosio M. et al., "Normative data for an instrumental assessment of the upper-limb functionality," BioMed Research International, vol. 2015, pp. 1–14, 2015.

Caimmi M., Carda S., Giovanzana C. et al., "Using kinematic analysis to evaluate constraint-induced movement therapy in chronic stroke patients," Neurorehabilitation and Neural Repair, vol. 22, no. 1, pp. 31–39, 2008.

Cameirão M. S., Smailagic A., Miao G., and Siewiorek D. P., "Coaching or gaming? Implications of strategy choice for home-based stroke rehabilitation", Journal of Neuroengineering and Rehabilitation, vol. 13, no. 1, p. 18, 2016.

Cameirão, M. S., Smailagic, A., Miao, G., and Siewiorek, D. P. (2016). Coaching or gaming? Implications of strategy choice for home-based stroke rehabilitation. Journal of Neuroengineering and rehabilitation, 13(1), 18.

Capecci M., Ceravolo M. G., Ferracuti F. et al., “Accuracy evaluation of the Kinect v2 sensor during dynamic movements in a rehabilitation scenario,” in 2016 38th Annual International Conference of the IEEE Engineering in Medicine and Biology Society (EMBC), pp. 5409–5412, Orlando, FL, USA, August 2016.

Cappozzo A. et al. Position and orientation in space of bones during movement: anatomical frame definition and determination. Clinical biomechanics, 1995, 10.4: 171-178.

Cappozzo A., Catani F., Leardini A., Benedetti M. G., and Della Croce U., “Position and orientation in space of bones during movement: experimental artefacts,” Clinical Biomechanics, vol. 11, no. 2, pp. 90–100, 1996

Carpinella I., Cattaneo D., and Ferrarin M., “Quantitative assessment of upper limb motor function in multiple sclerosis using an instrumented action research arm test,” Journal of Neuroengineering and Rehabilitation, vol. 11, no. 1, p. 67, 2014.

Chang Y. J., Chen S. F., and Da Huang J., “A Kinect-based system for physical rehabilitation: a pilot study for young adults with motor disabilities,” Research in Developmental Disabilities, vol. 32, no. 6, pp. 2566–2570, 2011.

Chang Y. J., Han W. Y., and Tsai Y. C., “A Kinect-based upper limb rehabilitation system to assist people with cerebral palsy,” Research in Developmental Disabilities, vol. 34, no. 11, pp. 3654–3659, 2013.

Chen X., Siebourg-Polster J., Wolf D. et al., “Feasibility of using Microsoft Kinect to assess upper limb movement in type III spinal muscular atrophy patients,” PLoS One, vol. 12, no. 1, article e0170472, 2017. Applied Bionics and Biomechanics 15.

Chen Y. C., Lee H. J., and Lin K. H., “Measurement of body joint angles for physical therapy based on mean shift tracking using two low cost Kinect images,” in 2015 37th Annual International Conference of the IEEE Engineering in Medicine and Biology Society (EMBC), vol. 2015, pp. 703–706, Milan, Italy, August 2015.

Chin J. H. and Vora N., “The global burden of neurologic diseases,” Neurology, vol. 83, no. 4, pp. 349–351, 2014.

(Christy) Du, Jinyan | Duffy, Vincent G. A methodology for assessing industrial workstations using optical motion capture integrated with digital human models Occupational Ergonomics, vol. 7, no. 1, pp. 11-25, 2007

Cicirelli, G., Attolico, C., Guaragnella, C., and D'Orazio, T. (2015). A kinect-based gesture recognition approach for a natural human robot interface. International Journal of Advanced Robotic Systems, 12(3), 22.

Clark R. A., Pua Y. H., Oliveira C. C. et al., “Reliability and concurrent validity of the Microsoft Xbox One Kinect for assessment of standing balance and postural control,” Gait and Posture, vol. 42, no. 2, pp. 210–213, 2015.

Colombo G., Regazzoni D., Rizzi C. (2013) Markerless Motion Capture Integrated with Human Modeling for Virtual Ergonomics. In: Duffy V.G. (eds) Digital Human Modeling and Applications in Health, Safety, Ergonomics, and Risk Management. Human Body Modeling and Ergonomics. DHM 2013. Lecture Notes in Computer Science, vol 8026. Springer, Berlin, Heidelberg

Colyer S. L., et al. A review of the evolution of vision-based motion analysis and the integration of advanced computer vision methods towards developing a markerless system. Sports medicine-open, 2018, 4.1: 24

Cruz L., Lucio, D., and Velho, L. (2012, August). Kinect and rgbd images: Challenges and applications. In 2012 25th SIBGRAPI Conference on Graphics, Patterns and Images Tutorials (pp. 36-49). IEEE.

D'Orazio, T., Marani, R., Renó, V., and Cicirelli, G. (2016). Recent trends in gesture recognition: how depth data has improved classical approaches. Image and Vision Computing, 52, 56-72.

Da Gama, Fallavollita P., Teichrieb V., and Navab N., "Motor rehabilitation using Kinect: a systematic review," Games for Health Journal, vol. 4, no. 2, pp. 123–135, 2015.

Darby J., M. B. Sánchez, P. B. Butler, and I. D. Loram, "An evaluation of 3D head pose estimation using the Microsoft Kinect v2," Gait and Posture, vol. 48, pp. 83–88, 2016.

Della Mea V., Simoncello A., "An ontology-based exploration of the concepts and relationships in the activities and participation component of the international classification of functioning, disability and health," Journal of Biomedical Semantics, vol. 3, no. 1, p. 1, 2012.

Diaz M. G., Tombari F., Rodriguez-Gonzalvez P., Gonzalez-Aguilera D., "Analysis and Evaluation Between the First and the Second Generation of RGB-D Sensors" IEEE Sensor Journal, vol 15, no 11, 2015, 10.1109/JSEN.2015.2459139

Dolatabadi E., Taati B., and Mihailidis A., "Concurrent validity of the Microsoft Kinect for Windows v2 for measuring spatiotemporal gait parameters," Medical Engineering and Physics, vol. 38, no. 9, pp. 952–958, 2016.

Eltoukhy M., Oh J., Kuenze C., and Signorile J., "Gait and Posture Improved Kinect-based spatiotemporal and kinematic treadmill gait assessment," Gait and Posture, vol. 51, pp. 77–83, 2017.

Fern'ndez-Baena, A., Susin, A., and Lligadas, X. (2012, September). Biomechanical validation of upper-body and lower-body joint movements of kinect motion capture data for rehabilitation treatments. In 2012 Fourth International Conference on Intelligent Networking and Collaborative Systems (pp. 656-661). IEEE.

Ferrarin M., Bovi G., Rabuffetti M. et al., “Reliability of instrumented movement analysis as outcome measure in Charcot–Marie–tooth disease: results from a multitask locomotor protocol,” Gait and Posture, vol. 34, no. 1, pp. 36–43, 2011.

Field M., Stirling D., Naghdy F. and Pan Z., Motion capture in robotics review IEEE International Conference on Control and Automation Christchurch, New Zealand, December 9-11, 2009

Galli, M., Cimolin, V., Crivellini, M., and Campanini, I. (2008). Quantitative analysis of sit to stand movement: experimental set-up definition and application to healthy and hemiplegic adults. Gait and posture, 28(1), 80-85.

Galli, M., Cimolin, V., Rigoldi, C., Tenore, N., and Albertini, G. (2010). Gait patterns in hemiplegic children with cerebral palsy: comparison of right and left hemiplegia. *Research in developmental disabilities*, *31*(6), 1340-1345.

Galna, B., Barry, G., Jackson, D., Mhiripiri, D., Olivier, P., and Rochester, L. (2014). Accuracy of the Microsoft Kinect sensor for measuring movement in people with Parkinson's disease. Gait and posture, 39(4), 1062-1068.

Geiselhart, F., Otto, M., and Rukzio, E. (2016). On the use of multi-depth-camera based motion tracking systems in production planning environments. Procedia CIRP, 41, 759-764.

Giancola S., Corti A., Molteni F., and Sala R., “Motion capture: an evaluation of Kinect V2 body tracking for upper limb motion analysis. Wireless mobile communication and healthcare,” in MobiHealth 2016. Lecture Notes of the Institute for Computer Sciences, Social Informatics and Telecommunications Engineering, vol. 192, Springer, Cham, 2017.

Glasauer, S., Huber, M., Basili, P., Knoll, A., and Brandt, T. (2010, September). Interacting in time and space: Investigating human-human and human-robot joint action. In 19th International Symposium in Robot and Human Interactive Communication (pp. 252-257). IEEE.

Gonzalez-Jorge, Higinio, et al. "Metrological evaluation of microsoft kinect and asus xtion sensors." Measurement 46.6 (2013): 1800-1806.

González-Ortega D., Díaz-Pernas F. J., Martínez-Zarzuela M., and Antón-Rodríguez M., “A Kinect-based system for cognitive rehabilitation exercises monitoring,” Computer Methods and Programs in Biomedicine, vol. 113, no. 2, pp. 620–631, 2014. 14 Applied Bionics and Biomechanics

Gotsis M., Lympouridis V., Requejo P. et al., “Skyfarer: design case study of a mixed reality rehabilitation video game,” In International Conference of Design, User Experience, and Usability, pp. 699–710, 2014.

Gu Y, Pandit S, Saraee E, Nordahl T, Ellis T, Betke M. Home-Based Physical Therapy with an Interactive Computer Vision System. InProceedings of the IEEE International Conference on Computer Vision Workshops 2019 (pp. 0-0).

Harrison J. K., McArthur K. S., and Quinn T. J., "Assessment scales in stroke: clinimetric and clinical considerations," Clinical Interventions in Aging, vol. 8, pp. 201–211, 2013.

Huber M. E., Seitz A. L., Leeser M., and Sternad D., "Validity and reliability of Kinect skeleton for measuring shoulder joint angles: a feasibility study," Physiotherapy, vol. 101, no. 4, pp. 389–393, 2015.

Kim, W. S., Cho, S., Baek, D., Bang, H., and Paik, N. J. (2016). Upper extremity functional evaluation by Fugl-Meyer assessment scoring using depth-sensing camera in hemiplegic stroke patients. PloS one, 11(7), e0158640.

Kim, S., Nussbaum, M. A., Esfahani, M. I. M., Alemi, M. M., Alabdulkarim, S., and Rashedi, E. (2018). Assessing the influence of a passive, upper extremity exoskeletal vest for tasks requiring arm elevation: Part I-"Expected" effects on discomfort, shoulder muscle activity, and work task performance. Applied ergonomics, 70, 315-322.

Kimura D., Kadota K., and Kinoshita H., "The impact of aging on the spatial accuracy of quick corrective arm movements in response to sudden target displacement during reaching," Frontiers in Aging Neuroscience, vol. 7, pp. 1–11, 2015.

Krakauer J. W., Latash M. L., and Zatsiorsky V. M., "Progress in motor control," Learning, vol. 629, no. 585, pp. 597–618, 2009.

Kutlu M., Freeman C., and Spraggs M., "Functional electrical stimulation for home-based upper-limb stroke rehabilitation," Current Directions in Biomedical Engineering, vol. 3, no. 1, pp. 25–29, 2017.

Kurillo G., Chen A., Bajcsy R., and Han J. J., "Evaluation of upper extremity reachable workspace using Kinect camera," Technology and Health Care, vol. 21, no. 6, pp. 641–656, 2013.

Lange B., Chang C. Y., Suma E., Newman B., Rizzo A. S., and Bolas M., "Development and evaluation of low cost gamebased balance rehabilitation tool using the Microsoft Kinect sensor," in 2011 Annual International Conference of the IEEE Engineering in Medicine and Biology Society, pp. 1831–1834, Boston, MA, USA, September 2011.

Lee, S. H., Yoon, C., Chung, S. G., Kim, H. C., Kwak, Y., Park, H. W., and Kim, K. (2015). Measurement of shoulder range of motion in patients with adhesive capsulitis using a kinect. PloS one, 10(6), e0129398.

Lee S. H., Yoon C., Chung S. G. et al., “Measurement of shoulder range of motion in patients with adhesive capsulitis using a Kinect,” PLoS One, vol. 10, no. 6, article e0129398, 2015.

Lu T. W. and O’connor J. J., “Bone position estimation from skin marker co-ordinates using global optimisation with joint constraints,” Journal of Biomechanics, vol. 32, no. 2, pp. 129–134, 1999.

Lu T. W. and O’connor J. J., “Bone position estimation from skin marker co-ordinates using global optimisation with joint constraints,” Journal of Biomechanics, vol. 32, no. 2, pp. 129–134, 1999

Miguez, Symone A.; Hallbeck, M. Susan; Vink, P., Work movements: balance between freedom and guidance on an assembly task in a furniture manufacturer. In: Advances in Safety Management and Human Factors. Springer, Cham, 2016. p. 503-511.

Mentiplay, B. F., Hasanki, K., Perraton, L. G., Pua, Y. H., Charlton, P. C., and Clark, R. A. (2018). Three-dimensional assessment of squats and drop jumps using the Microsoft Xbox One Kinect: reliability and validity. Journal of sports sciences, 36(19), 2202-2209.

Mobini, A., Behzadipour, S., and Saadat, M. (2015). Test–retest reliability of Kinect’s measurements for the evaluation of upper body recovery of stroke patients. Biomedical engineering online, 14(1), 75.

Morrow, K., Docan, C., Burdea, G., and Merians, A. (2006, August). Low-cost virtual rehabilitation of the hand for patients post-stroke. In 2006 International Workshop on Virtual Rehabilitation (pp. 6-10). IEEE.

Mosca, N., Renó, V., Marani, R., Nitti, M., D'Orazio, T., and Stella, E. (2017). Human Walking Behavior detection with a RGB-D Sensors Network for Ambient Assisted Living Applications. In AI* AAL@ AI* IA (pp. 17-29).

Mottura S., Arlati S., Fontana L., and Sacco M., “Enhancing awareness and personification by virtual reality and multimedia means in post-stroke patients during rehabilitation,” in 2014 5th IEEE Conference on Cognitive Infocommunications (CogInfoCom), pp. 179–184, Vietri sul Mare, Italy, November 2014.

Mousavi H. and Khademi M., “A review on technical and clinical impact of Microsoft Kinect on physical therapy and rehabilitation,” Journal of Medical Engineering, vol. 2014, pp. 1–16, 2014.

Moyà-Alcover G., Ayed I., Varona J., Jaume-i-Capó A. (2019) RGB-D Interactive Systems on Serious Games for Motor Rehabilitation Therapy and Therapeutic Measurements. In: Rosin P., Lai YK., Shao L., Liu Y. (eds) RGB-D Image Analysis and Processing. Advances in Computer Vision and Pattern Recognition. Springer, Cham

Bachynskyi, M., Oulasvirta, A., Palmas, G., and Weinkauf, T. (2014, April). Is motion capture-based biomechanical simulation valid for hci studies? study and implications. In Proceedings of the SIGCHI Conference on Human Factors in Computing Systems (pp. 3215-3224).

Nussbaum M. A. and Zhang X., "Heuristics for locating upper extremity joint centres from a reduced set of surface markers," Human Movement Science, vol. 19, no. 5, pp. 797–816, 2000.

Oskarsson, B., Joyce, N. C., De Bie, E., Nicorici, A., Bajcsy, R., Kurillo, G., and Han, J. J. (2016). Upper extremity 3-dimensional reachable workspace assessment in amyotrophic lateral sclerosis by Kinect sensor. Muscle and nerve, 53(2), 234-241.

Otte K., Kayser, B., Mansow-Model, S., Verrel, J., Paul, F., Brandt, A. U., and Schmitz-Hübsch, T. Accuracy and reliability of the kinect version 2 for clinical measurement of motor function. PloS one, 11(11), e0166532, 2016

Otte K., Kayser B., Mansow-Model S. et al., "Accuracy and reliability of the Kinect version 2 for clinical measurement of motor function," PLoS One, vol. 11, no. 11, article e0166532, 2016.

Ozturk A., Tartar A., Ersoz Huseyinsinoglu B., and Ertas A. H., "A clinically feasible kinematic assessment method of upper extremity motor function impairment after stroke," Measurement, vol. 80, pp. 207–216, 2016.

Pagliari D. and Pinto L., "Calibration of Kinect for Xbox One and comparison between the two generations of Microsoft sensors," Sensors, vol. 15, no. 11, pp. 27569–27589, 2015.

Pascual-Leone A., "Training modalities in robot-mediated upper limb rehabilitation in stroke: a framework for classification based on a systematic review," Journal of Neuroengineering and Rehabilitation, vol. 11, no. 1, p. 111, 2014.

Petuskey K., Bagley A., Abdala E., James M. A., and Rab G., "Upper extremity kinematics during functional activities: three-dimensional studies in a normal pediatric population," Gait and Posture, vol. 25, no. 4, pp. 573–579, 2007.

Pedraza-Hueso M., Martín-Calzón S., Díaz-Pernas F. J., and Martínez-Zarzuela M., "Rehabilitation using Kinect-based games and virtual reality," Procedia Computer Science, vol. 75, pp. 161–168, 2015.

Pellegrinelli, S., Moro, F. L., Pedrocchi, N., Tosatti, L. M., and Tolio, T. (2016). A probabilistic approach to workspace sharing for human–robot cooperation in assembly tasks. CIRP Annals, 65(1), 57-60.

Pfister A., West A.M., Bronner S, Noah J.A. Comparative abilities of Microsoft Kinect and Vicon 3D motion capture for gait analysis J Med Eng Technol. 2014 Jul;38(5):274-80

Pontonnier C., Dumont G., “Inverse dynamics method using optimization techniques for the estimation of muscles forces involved in the elbow motion,” International Journal on Interactive Design and Manufacturing, vol. 3, no. 4, pp. 227–236, 2009.

Pontonnier C., Dumont G., “Inverse dynamics method using optimization techniques for the estimation of muscles forces involved in the elbow motion,” International Journal on Interactive Design and Manufacturing, vol. 3, no. 4, pp. 227–236, 2009.

Potter K., Fulk G. D., Salem Y., and Sullivan J., “Outcome measures in neurological physical therapy practice: part I. Making sound decisions”, Journal of Neurologic Physical Therapy, vol. 35, no. 2, pp. 57–64, 2011.

Ramey, A., González-Pacheco, V., and Salichs, M. A. (2011, March). Integration of a low-cost RGB-D sensor in a social robot for gesture recognition. In 2011 6th ACM/IEEE International Conference on Human-Robot Interaction (HRI) (pp. 229-230). IEEE.

Rocha P., Choupina H., Fernandes J. M., Rosas M. J., Vaz R., and Cunha J. P. S., “Kinect v2 based system for Parkinson’s disease assessment,” in 2015 37th Annual International Conference of the IEEE Engineering in Medicine and Biology Society (EMBC), pp. 1279–1282, Milan, Italy, August 2015.

Roux E., Bouilland S., Godillon-Maquinghen A.-P., and Bouttens D., “Evaluation of the GO method within the upper limb kinematics analysis,” Journal of Biomechanics, vol. 35, pp. 1279–1283, 2002.

Santos C., Mehrsai, A., Barros, A. C., Araújo, M., and Ares, E. (2017). Towards Industry 4.0: an overview of European strategic roadmaps. Procedia Manufacturing, 13, 972-979

Scano A., Caimmi M., Malosio M. et al., “Upper limb robotic rehabilitation: treatment customization,” Gait and Posture, vol. 37, pp. S13–S14, 2013.

Scano A., Caimmi M., Malosio M., and Tosatti L. M., “Using Kinect for upper-limb functional evaluation in home rehabilitation: a comparison with a 3D stereoscopic passive marker system,” in 5th IEEE RAS/EMBS International Conference on Biomedical Robotics and Biomechatronics, pp. 561–566, Sao Paulo, Brazil, August 2014.

Scano A., Caimmi M., Chiavenna A., Malosio M., and Tosatti L. M., “Kinect One-based biomechanical assessment of upper-limb performance compared to clinical scales in poststroke patients,” in 2015 37th Annual International Conference of the IEEE Engineering in Medicine and Biology Society (EMBC), vol. 2015, pp. 5720–5723, Milan, Italy, 2015.

Scano A., Caimmi M., Chiavenna A., Malosio M., and Tosatti L. M., “A Kinect-based biomechanical assessment of neurological patients’ motor performances for domestic rehabilitation,” in Virtual Reality Enhanced Robotic Systems for Disability Rehabilitation, pp. 252–279, IGI Global, 2016.

Scano A., Chiavenna A., Malosio M., and Tosatti L. M., “Kinect V2 Performance Assessment in Daily-Life Gestures: Cohort Study on Healthy Subjects for a Reference Database for Automated Instrumental Evaluations on Neurological Patients” from 2017, Hindawi Applied Bionics and Biomechanics volume 2017 https://doi.org/10.1155/2017/8567084

Scano A., Chiavenna A., Malosio M., Tosatti L. M., Molteni F., Kinect V2 implementation and testing of the reaching performance scale for motor evaluation of patients with neurological impairment, Medical engineering and physics Vol 56 pag 54-58, 2018

Scano A., Molteni F. and Tosatti L. M., “Low-Cost Tracking Systems Allow Fine Biomechanical Evaluation of Upper-Limb Daily-Life Gestures in Healthy People and Post-Stroke Patients” from 2019, Sensor, doi: 10.3390/s19051224

Scano A., Dardari, L., Molteni, F., Giberti, H., Tosatti, L. M., and d'Avella, A. (2019). A comprehensive spatial mapping of muscle synergies in highly variable upper-limb movements of healthy subjects. Frontiers in physiology, 10, 1231.

Schaefer S. Y. and Hengge C. R., “Testing the concurrent validity of a naturalistic upper extremity reaching task,” Experimental Brain Research, vol. 234, no. 1, pp. 229–240, 2016.

Schmidt R., “A schema theory of discrete motor skill learning,” Psychological Review, vol. 82, no. 4, pp. 225–260, 1975.

Shengqian J., et al. A low-cost rapid upper limb assessment method in manual assembly line based on somatosensory interaction technology. In: AIP Conference Proceedings. AIP Publishing, 2017. p. 030010.

Sinclair, J.; Taylor, P. J.; Hobbs, S. J.. Digital filtering of three-dimensional lower extremity kinematics: An assessment. Journal of human kinetics, 2013, 39.1: 25-36.

Summa S., Pierella C., Giannoni P. et al., “A body-machine interface for training selective pelvis movements in stroke survivors: a pilot study,” in 37th Annual International Conference of the IEEE Engineering in Medicine and Biology Society (EMBC), pp. 4663–4666, Milan, Italy, August 2015.

Terkaj, W., and Tolio, T. (2019). The Italian flagship project: factories of the future. In Factories of the Future (pp. 3-35). Springer, Cham.

Vieira A., Gabriel J., Melo C., and Machado J., “Kinect system in home-based cardiovascular rehabilitation,” Proceedings of the Institution of Mechanical Engineers, Part H: Journal of Engineering in Medicine, vol. 231, no. 322, pp. 40–47, 2016.

Wiedemann L. G., Planinc R., Nemec I., and Kampel M., “Performance evaluation of joint angles obtained by the Kinect v2,” in IET International Conference on Technologies for Active and Assisted Living (TechAAL), London, UK, November 2015.

Wu, C., Quigley, A. and Harris-Birtill, D. Out of sight: a toolkit for tracking occluded human joint positions. Pers Ubiquit Comput 21, 125–135 (2017). https://doi.org/10.1007/s00779-016-0997-6

Yahya, M., Shah, J., Kadir, K., Warsi, A., Khan, S., and Nasir, H. (2019, May). Accurate Shoulder Joint Angle Estimation Using Single RGB camera for Rehabilitation. In 2019 IEEE International Instrumentation and Measurement Technology Conference (I2MTC) (pp. 1-6). IEEE.

Yang Y., Pu F., Li Y., Li S., Fan Y., Li D., Reliability and validity of Kinect RGB-D sensor for assessing standing balance. IEEE Sensors Journal. 2014 Jan 2;14(5):1633-8.

Zhou, H., and Hu, H. (2008). Human motion tracking for rehabilitation—A survey. Biomedical Signal Processing and Control, 3(1), 1-18.

https://cordis.europa.eu/project/id/847926

https://azure.microsoft.com/it-it/services/kinect-dk/